THESIS

SALT MOBILIZATION AND TRANSPORT IN AN UPLAND DESERT CATCHMENT OF THE LOWER ARKANSAS RIVER BASIN OF COLORADO

Submitted by

Carly Elizabeth Zimmer

Department of Civil and Environmental Engineering

In partial fulfillment of the requirements

For the Degree of Master of Science

Colorado State University

Fort Collins, Colorado

Fall 2021

Master's Committee:

Advisor: Ryan Bailey

Jeffrey Niemann
Stephanie Kampf

ABSTRACT

SALT MOBILIZATION AND TRANSPORT IN AN UPLAND DESERT CATCHMENT OF THE LOWER ARKANSAS RIVER BASIN OF COLORADO

Salt loading can significantly alter water quality in large river basins. Salt deposits occur naturally and anthropogenically and are transported to water bodies through overland flow and other environmental factors. The mobilization and transport of salt in high-desert regions can hinder the sustainability of crop production in downstream irrigated regions. Salinity transport and loading has been extensively investigated in regions of irrigation. However, little research has been conducted regarding salt mobilization in analogous regions with high-desert characteristics and little cultivation.

The goal of this thesis is to understand the mobilization of salt in predominantly undeveloped, uncultivated upland catchments in a semi-arid climate with sparse vegetation cover and steep gradients. The thesis is composed of two primary objectives. 1) Quantify the salt load contribution from the Purgatoire River Watershed, a high-desert watershed, to the Arkansas River, and 2) Identify possible major environmental factors that control the mobilization of salts in natural upland catchments.

A variety of field and computational methods were used to complete these two objectives. Electrical conductivity (EC) data loggers were placed at two locations along the Purgatoire River to quantify in-stream salt ion (SO_4, Ca, Na, Mg, HCO_3, K, Cl) loading. Daily in-stream loading (kg/day) of each salt ion was estimated using laboratory results of a set of

water samples (n = 10) at these sites and stochastic linear regression techniques. Results indicate that the overall mass loading of salt exported by the Purgatoire River to the Arkansas River, and the ratio of salt in the Arkansas River to the Purgatoire River, is significantly affected by annual rainfall. In 1990 (490 mm), the Purgatoire River exported approximately 64,600,000 kg of salt to the Arkansas River, accounting for 21.7% of the salt in the Arkansas River after merging. In 2020 (262 mm), the volume of annual precipitation fell by 47% and the Purgatoire River exported approximately 18,000,000 kg of salt, 72% less than 1990, to the Arkansas River accounting for 11.2% of the salt in the Arkansas River after merging. Results indicate that upstream desert catchments can have a large effect on salinity loads in irrigated river valleys such as the Arkansas River Valley.

For objective 2, environmental factors investigated for salt mobilization control include precipitation depths, land use type, topographic slope, percent calcium carbonate ($CaCO_3$) in soil, and percent calcium sulfate ($CaSO_4$) in soil. These factors were used to compute a spatial varying salt mobilization index throughout the Purgatoire River Watershed. The resulting index map shows hot spots of potential salt mobilization, which can be verified through additional research. Similar maps can be made for other high-desert regions to investigate potential sites of salt mobilization.

ACKNOWLEDGEMENTS

This work would not have been possible without the support, guidance, and collaboration of many people. First, thank you to my advisor Dr. Ryan Bailey for his dedicated guidance in the planning and implementation of field sites and statistical data interpretation. Thank you to the landowners and farmers who generously allowed the installation of field sites on their land. Thank you to the Colorado Department of Water Resources, the United States Geological Survey, and In-Situ Inc. for their cooperation, assistance, and expertise in equipment purchasing and large-scale data management. Thank you to my lab mates: Luke Flores, Pratikshya Neupane, Soheil Nozari, Pardis Hosseini, and Elle Henson, for their ingenuity, support, and unwavering assistance in the installation of field sites, ArcGIS management, and Python coding. Thank you to my committee members and the professors at Colorado State University for their guidance and inspiration. Finally, thank you to my family and friends for their steadfast participation in extensive field site visits and their enduring encouragement, love, and support.

TABLE OF CONTENTS

LIST OF TABLES

LIST OF FIGURES

CHAPTER 1: INTRODUCTION

1.1 Salt Pollution

The salinization of water and soil resources has been a constant concern for centuries. Impacting nations worldwide, salinization is a major hindrance of agricultural productivity and threatens water quality in large river basins (Vengosh, 2003). The excess concentration of soluble mineral salts in waters and soils occurs naturally and anthropogenically, within all climatic environments (Zaman, et al., 2018). Increasingly evident in semi-arid and arid zones, the salinization of water and soil resources is one of the most prominent issues in water-quality degradation (Vengosh, 2003).

There are two chief sources of soil salinity: primary/dryland and secondary. Primary soil salinity refers to naturally occurring saline soils. Shallow water tables, low soil permeability, and low levels of precipitation, occurring singularly or concurrently, lead to the salinization of soils (Zaman, et al., 2018). Groundwater dissolves soluble salts embedded within the soil and underlying geologic formations, and either discharges the salts to nearby surface waters (Vengosh, 2003) or evaporates upon reaching the surface, leaving behind the salt ions (Zaman, et al., 2018). Shallow water tables and low soil permeability increase the rate of evapotranspiration. As stated by Sparks (2003, p. 287), “It has been estimated that evaporation losses can range from 50 to 90% in arid regions, resulting in 2- to 20- fold increases in soluble salts.” Without enough precipitation to infiltrate the soil, salt accumulates, creating poor drainage and prolonging the issue of soil salinity (Sparks, 2003).

Secondary soil salinity refers to human-induced saline soils. The most common anthropogenic act influencing salinization is irrigation. Saline groundwater in semi-arid regions is often used as irrigation due to water scarcity (Zaman, et al., 2018). In congruence with primary soil salinity, the water quickly evaporates due to low soil permeability and inadequate drainage, leaving behind salt ions in the soil. Salinity affects an estimated 20-25% of irrigated land worldwide (Gates, et al., 2002) and nearly 7% of the global land area (Artiola, et al., 2019). Saline agricultural drainage waters, or return flows, produced with the intent of flushing salt ions, pollute surface waters (Williams, 2001). Clearing deep-rooted vegetation for agriculture purposes similarly leads to surface water salinization as regions of low plant density are prone to both wind and water erosion and subsequent salt transport (Cadaret, et al., 2016) (Williams, 2001).

There are numerous adverse effects of saline soils and waters. Plant growth is stunted by saline soils and salt-laden water impacting local vegetation and agricultural productivity. “High concentrations of soluble salts lower the pH and may limit plant growth, in some cases by more than 90%” (Kalev & Toor, 2018). Salinization leads to an increased risk of soil erosion due to loss of vegetation (Zaman, et al., 2018), as well as an increase in runoff due to decreased soil permeability and hydraulic conductivity (Sparks, 2003). Increased salinity in aquatic ecosystems negatively impacts the composition of freshwater biota, alters biogeochemical processes, and degrades potable water supplies for human consumption (Kerr, 2017).

1.1.1 Mobilization and Transport

Mobilization is the action of making something capable of movement, and transport is the action of moving something. Salt transport is the act of conveying suspended solids, typically containing organic and inorganic contaminants such as pesticides and metals, over a distance

(Sparks, 2003). Influenced by several factors, as previously discussed, salt mobilization is most common in semi-arid and arid regions (regions receiving between 25 and 500 mm of rainfall, annually) (Williams, 2001).

1.1.1a High-Desert Landscapes

Saline soils are common in high-desert landscapes as the average annual precipitation falls below the threshold of adequate water capable of leaching soluble salts from the soil (Sparks, 2003) and sustainable plant growth. As such, high elevation desert regions characteristically have low plant density, creating barren stretches of land subject to wind and water erosion and subsequent salt transport (Cadaret, et al., 2016). Intense, isolated, fleeting convective rain events are typical of high-desert regions over the summer months (Ponce & Hawkins, 1978).

1.1.1b Sources of Salt and Upland Catchments

Estimates from 1978 have divided sources of salt loading into three primary categories. Irrigation return flows are responsible for one-third of total salt load and represent the largest human-induced source of salinity. The second source of salinization responsible for one-third of global total salt load is natural point sources: evaporation-induced salinization, salt wells, springs, and groundwater seepage. The final source of salinization representative of one-third of total salt loading is nonpoint sources originating in vast regions of "wildland watersheds" (Ponce & Hawkins, 1978). Nonpoint sources differ from point sources because these sources of pollution typically occur by means of precipitation and snowmelt. As rainfall moves across the ground, pollutants are transported to other regions (United States Environmental Protection Agency, 2020).

Headwater upland catchments have been recognized as regions of high sediment generation. Yet, little research has been conducted in such settings (Warburton, 2009). The contributing factors to excess generation and transfer rates of sediment characteristic of upland catchments are steep slopes, high volumes of runoff, active geomorphic processes, and thin vegetation cover, predominantly during extreme precipitation/storm events (Warburton, 2009, p. 165). Steep, highly dissected slopes of weathered rock create prime zones of erosion and transport processes (Cadaret, et al., 2016).

1.1.1c Salt Load Parameters

The primary soluble mineral ions found in saline waters and soils are sodium (Na^+), calcium (Ca^{2+}), magnesium (Mg^{2+}), sulfate (SO_4^{2-}), potassium (K^+), chloride (Cl^-), carbonate (CO_3^{2-}), and bicarbonate (HCO_3^-) (Kerr, 2017). The primary sources of soluble salts in soils are: "weathering of primary minerals and native rocks, residual fossil salts, atmospheric deposition, saline irrigation and drainage waters, saline groundwater, seawater intrusion, additions of inorganic and organic fertilizers, sludges and sewage effluents, brines from natural salt deposits, and brines from oil and gas fields and mining" (Sparks, 2003). A grouping of soluble ions is described as total dissolved solids (TDS). Total dissolved solids are the organic and inorganic solids capable of passing through a filter with a pore size of 2 microns or less (Butler & Ford, 2018). The measurement of total dissolved solids is generally calculated as the summation of the measured concentrations of all salt components (Butler & Ford, 2018). Total suspended solids (TSS) are classified as larger particles that are incapable of passing through a 2-micron filter. TSS particles include clay, silt, and sand. Erosion of adjacent surface soils and stream banks typically generates high quantities of TSS in surface water (Butler & Ford, 2018). Inorganic TDS particles such as dissolved salt ions, metalloids, and metals, commonly originate from ions

present in atmospheric precipitation as well as the effects of precipitation such as the dissolution and desorption of ions attached to and in sediment (Butler & Ford, 2018).

To better understand the verbiage used throughout this thesis with respect to salt loading, the definitions are as follows: discharge is the volume of water that moves through a cross-section of a river over a measured period of time, flow/flowrate denotes the volume of water given a time increment, and salt load is the mass of salt that travels past a certain point along a river in a quantified amount of time. The salt load of a river is calculated as the product of the concentration of salt in the water and the discharge. When calculating the salt loading rate, the flowrate is used in place of discharge (Meals, et al., April 2013).

In stream electrical conductivity readings and other in-situ water quality parameters, are commonly used in conjunction with instantaneous solute concentrations and flow rate to estimate rates and quantities of in-stream salt (Gates, et al., 2018, p. 194). Electric conductivity measurements are used in water and soil testing based on the concept that the electrical current carried by a salt solution under standard conditions carries a positive correlation with the salt concentration of the solution, such that, as the salt concentration increases, so too does the electrical current (Sparks, 2003).

1.2 Previous Research: Precipitation Influenced Salt Transport in Semi-Arid Catchments

Covering one-third of the global land mass, semi-arid and arid regions are the archetypal locations for anthropogenic and natural salinization to occur. The future of accessible water for human consumption and agriculture in semi-arid and arid regions depends on the management of soil and water salinization, particularly as the fraction of semi-arid and arid regions expands due to global atmospheric warming (Williams, 2001, p. 330). There have been many studies conducted regarding agriculturally induced salinization and its effects on water and soil quality.

However, little research has been performed regarding the salinization impacts of naturally occurring basins with steep grades and high potential for salt mobilization.

Studies have been performed regarding precipitation and solute loading rates, although none in this literature review correlated precipitation with quantifying and identifying zones of salt transport from upland catchments. Langbein et al. (1958) investigated sediment yield with respect to annual precipitation, vegetation cover, and land use. Sediment yield is important when discussing salt loading because salts are transported via sediment, as further discussed through this literature review. An equation was developed to predict annual load in tons per square mile given the effective annual precipitation and the idea that vegetation opposes the influence of the erosive qualities of intense precipitation events. The erosive properties of precipitation increase as the quantity of precipitation increases, however, as the amount of effective annual precipitation increases, so does vegetation (Langbein & Schumm, 1958). Increased vegetation cover inversely affected the erosive impacts of precipitation increase. As such, sediment yield plateaus at a maximum of approximately 12 inches (305 mm) of annual precipitation, decreasing with increased annual precipitation. In conclusion, it was found that as precipitation decreased, the concentration of sediment per unit of runoff increased (Langbein & Schumm, 1958).

In an attempt to quantify the remaining one-third of the total salt load attributed to diffuse or nonpoint sources, Ponce et al. (1978) investigated salt transport via overland flow from the Mancos shale lands of the Price River basin via field investigation. After discovering a strong relationship between salt release via overland flow and rainfall intensity, a nonpoint source loading function was estimated to predict salinity associated with surface runoff. Prior to entering rills and other micro-channels, the salt concentrations in overland flow were relatively minor. However, the study found that as the water mass moved downstream the small shale

particles continued to dissolve and release greater quantities of salt to runoff. Following brief, intense rain events, water swiftly concentrates in channels, contributing to the mobilization of salt mass along arroyo channels (Ponce & Hawkins, 1978).

Cadaret et al. (2016) performed a precipitation analysis on the mechanisms driving sediment yield and the role of vegetation on soil chemistry in the Price-San Rafael River Basin. Similar to the study of Ponce et al. (1978), the analysis simulated varying intensities of rainfall on a range of slopes to identify salinity transport processes. The study found that vegetation played a protective role on the erosion of soils from increasing rainfall intensity. Concurrently, it was concluded that the "detachment and dissolution of sediment particles in runoff" was the primary process of salinity transport, however, most of the salt transported in runoff was likely still attached to suspended sediment particles, which affirmed the point previously made by Ponce et al. (1978) (Cadaret, et al., 2016).

For many decades, anthropogenic salinization has been a documented concern in Australia (Biggs, et al., 2013). Biggs et al. (2011) performed an analysis on artesian and sub-artesian bores in the Queensland Murray-Darling Basin in Australia, a heavily studied region with high levels of salt, to spatially recognize groundwater salt accessions. A catchment scale salt export/import ratio (E/I) was used to discern salt storage and mobilization progressions. The study found that 89% of groundwater salt additions originated from sub-artesian sources, with irrigation-intended bores contributing approximately half of the total salinized groundwater in the basin (Biggs A., 2011, p. 722). According to the ratio, the region is accumulating salt via atmospheric and groundwater accessions (Biggs A., 2011, p. 724). Although atmospheric accessions typically exceed groundwater salt accessions (Biggs A., 2011, p. 719), the analysis

performed by Biggs et al. (2011) illustrates the importance of groundwater contributions in salt mass balance analyses.

In a similar analysis, Biggs et al. (2013) attempt to quantify a salt mass balance across nine major catchments in the Queensland Murray-Darling Basin in Australia. Four factors of salt movement were considered: atmospheric inputs, streamflow exports, inter-basin inputs, and anthropogenic groundwater inputs (as previously discussed) (Biggs, et al., 2013, p. 105). In contrast to their previous report, they found that groundwater and inter-basin inputs were relatively equal to atmospheric inputs with similar spatial representation (Biggs, et al., 2013, p. 107). It was found that small upland catchment regions have a greater export/import ratio, indicating they readily export salt, than most larger catchments due to continual flow associated with groundwater discharge (Biggs, et al., 2013, p. 109). Concurrent with previous studies, Biggs et al. (2013) found that salt export via streamflow is greatly influenced by large, episodic precipitation events. Once more, it was found that the basin is accumulating salt due to stream water losses to floodplains, and surface water seepage and extraction (Biggs, et al., 2013, p. 104). Nevertheless, the inclusion of groundwater is of the utmost importance as it substantially alters export/import ratio (E/I) results, emphasizing its importance in salt mass balance analyses.

Relatively limited research has been done to understand the generation, transport, and fate of total dissolved solids within naturally occurring, dryland upland catchment landscapes of semi-arid regions. Naturally occurring salt afflicted basins are not as easily regulated as irrigated basins and may have greater influence over water salinization than anthropogenic factors, emphasizing the importance of this research.

1.3 Summary of Objectives

The goal of this thesis is to understand the mobilization of salt in predominantly undeveloped, uncultivated upland catchments in a semi-arid climate with sparse vegetation cover and steep grades. The report is composed of two primary objectives. The first objective is to quantify the salt load contribution from the Purgatoire River to the Arkansas River. This is important in recognizing the disparity in quantifying the relative contributions of highly irrigated and naturally barren basins to salt loads. The analysis is performed for a historical period (1990) and a current period (2020), with the latter using field methods as part of this project. The second objective is to understand the locations of salt mobilization in the Purgatoire River Watershed, and the environmental factors that control this mobilization of salts within the watershed. Factors include rainfall, topographic slope, land use type, and presence of salt minerals (calcium carbonate ($CaCO_3$), calcium sulfate ($CaSO_4$)) in the soil.

1.4 Thesis Organization

The remainder of this thesis is organized by chapter. Chapter 2 provides a detailed account of the implemented monitoring network throughout the study region and the procedures utilized to collect and interpret data. The primary results of this study are presented and discussed in detail in Chapter 3, and Chapter 4 summarizes key takeaways and offers avenues for future research.

CHAPTER 2: METHODOLOGY

2.1 Study Region

Originating in the southeast corner of Colorado in the Sawatch Range of the Rocky Mountains and traversing the states of Colorado, Kansas, Oklahoma and Arkansas, the Arkansas river spans 2,364 kilometers (1,469 miles) from West to East. The sixth longest river in the United States and the second longest tributary of the Mississippi River network, the Arkansas River drains an area of land nearly 416,000 square kilometers (160,500 square miles) (Stroud,

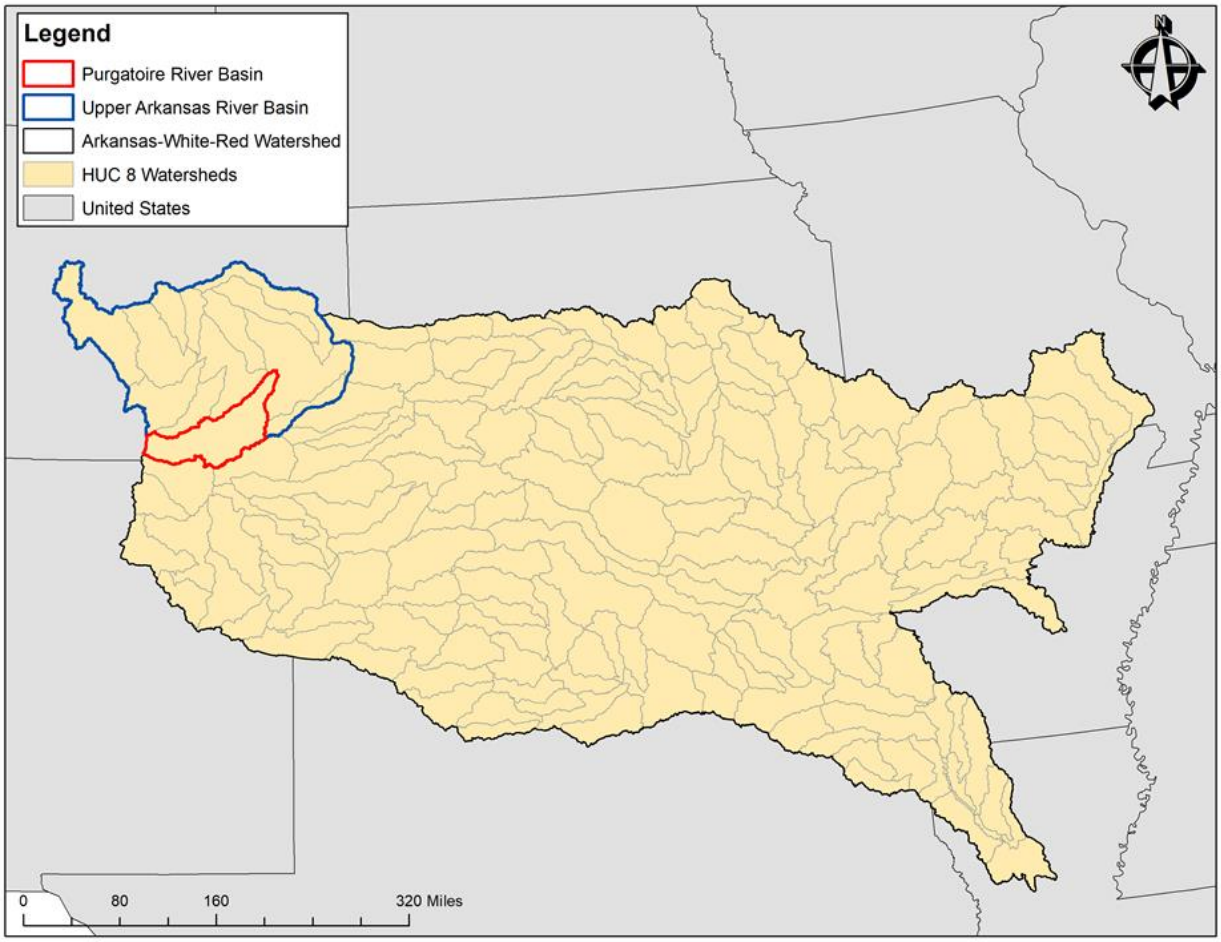

Figure 1. The Purgatoire River Basin with respect to the entire Arkansas-White-Red watershed in the United States (USGS).

2019). The Arkansas-White-Red watershed is one of 18 water resource regions (HUC2) in the contiguous United States. The watershed (HUC2) is broken into 14 basins (HUC4) and further dissolved into 173 subbasins (HUC8) that contribute flow to the Arkansas River. The Upper Arkansas River Basin is one of 14 (HUC 4) subbasins making up the Arkansas-White-Red water region in the US. The primary study region, the Purgatoire River Basin, is one of 13 (HUC 8) subbasins draining to the Upper Arkansas River Basin. The basins are illustrated in Figure 1.

The Upper Arkansas River Basin (UARB) contains an abundance of productive agricultural economies reliant on water. However, excess irrigation in the region has led to salinized and waterlogged soils and increased solute concentrations in the rivers (Gates, et al., 2006). Though undoubtedly linked to agriculture practices, salt transport can be concurrently linked to erosion and environmental factors in semi-arid regions (Cadaret, et al., 2016).

2.1.1 Purgatoire River Basin

The Purgatoire River in southeastern Colorado is a primary tributary of the Arkansas River within the Upper Arkansas River Basin as illustrated in Figure 2. After flowing 312 kilometers (194 miles), the river discharges into the Arkansas River near Las Animas, Colorado. It is one of the largest contributing subbasins (HUC8) of the Arkansas River within the Upper Arkansas River Basin, exporting large quantities of dissolved salt ion concentrations to the Arkansas River every year. Spanning the Colorado counties of Otero, Bent, Las Animas, Costilla and Huerfano and the New Mexico counties of Union and Colfax, the Purgatoire River Watershed has a contributing drainage area of 8,940 square kilometers (3,450 square miles or

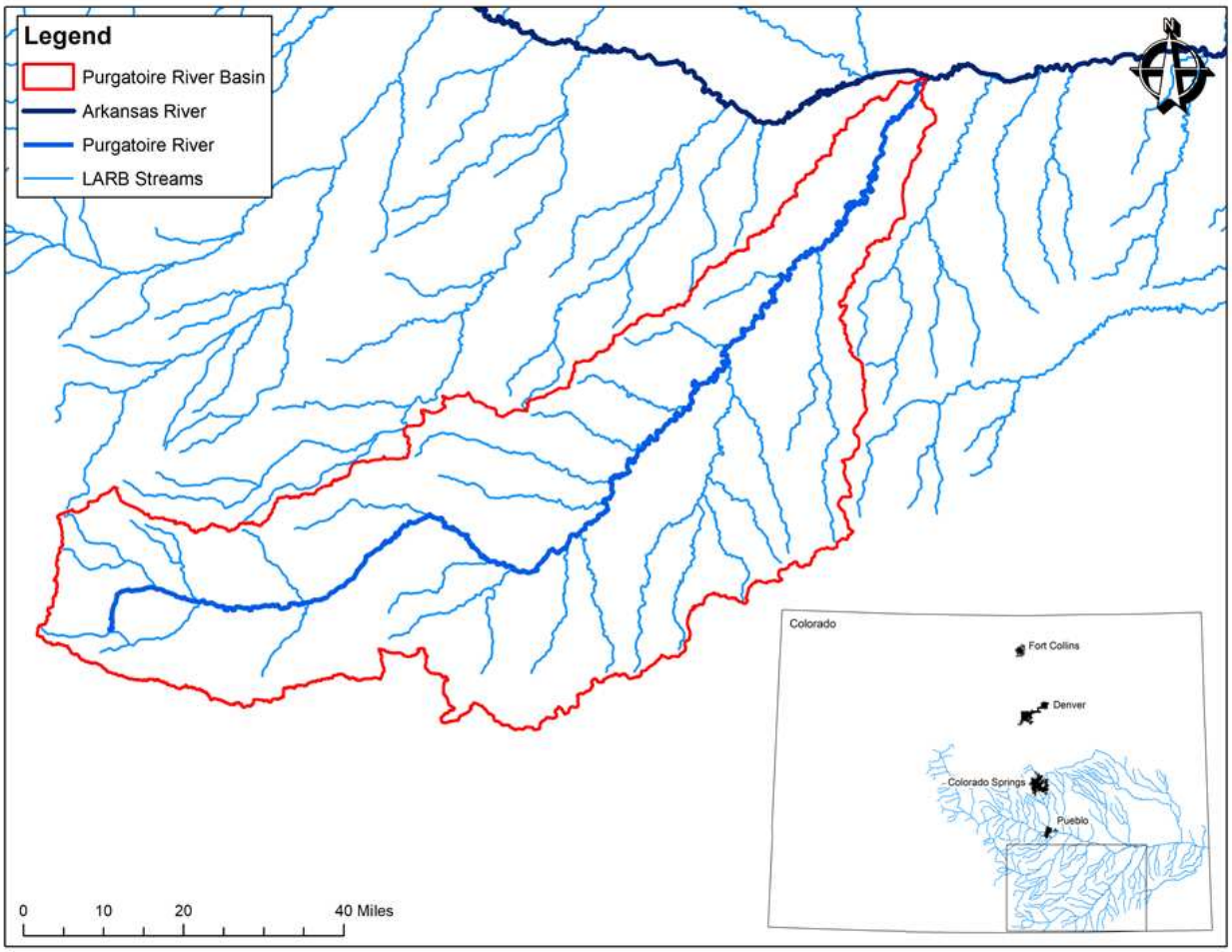

Figure 2. Map of the study region with respect to the state of Colorado and the Arkansas River Basin (USGS).

2,205,000 acres). The Purgatoire River is a fourth order perennial stream originating in the Sangre de Cristo Mountains near Weston, Colorado. The primary source of water comes from annual snowmelt (Purgatoire Watershed Partnership, 2014). For the purposes of this report, the Upper Arkansas River Basin will be referred to as the Lower Arkansas River Basin (LARB) as is its designation with reference to the state of Colorado.

The Purgatoire River Basin was chosen from 13 existing subbasins (HUC8) draining to the Upper Arkansas River basin because of its large drainage area, ongoing hydrologic flow

Figure 3. Images of the steep and scrub covered landscape within the Purgatoire Watershed.

monitoring, and undisturbed, high-desert landscape. The following six subsections clarify various components of the watershed.

2.1.1a Land Use

The Purgatoire River Basin is primarily undeveloped with steep grades as illustrated in Figure 3. Stretching from the Rocky Mountains to the Grasslands, it is in the Central Shortgrass Prairie Ecoregion of southern Colorado and has been identified as a priority conservation area by The Nature Conservancy in Colorado (Purgatoire Watershed Partnership, 2014, p. 33). According to the land cover map illustrated in Figure 4, less than 1.3% of the basin is developed or cultivated. The occupied land is predominantly used for livestock grazing. The remainder of the basin is largely unoccupied grassland with evergreen and mixed forests in the higher

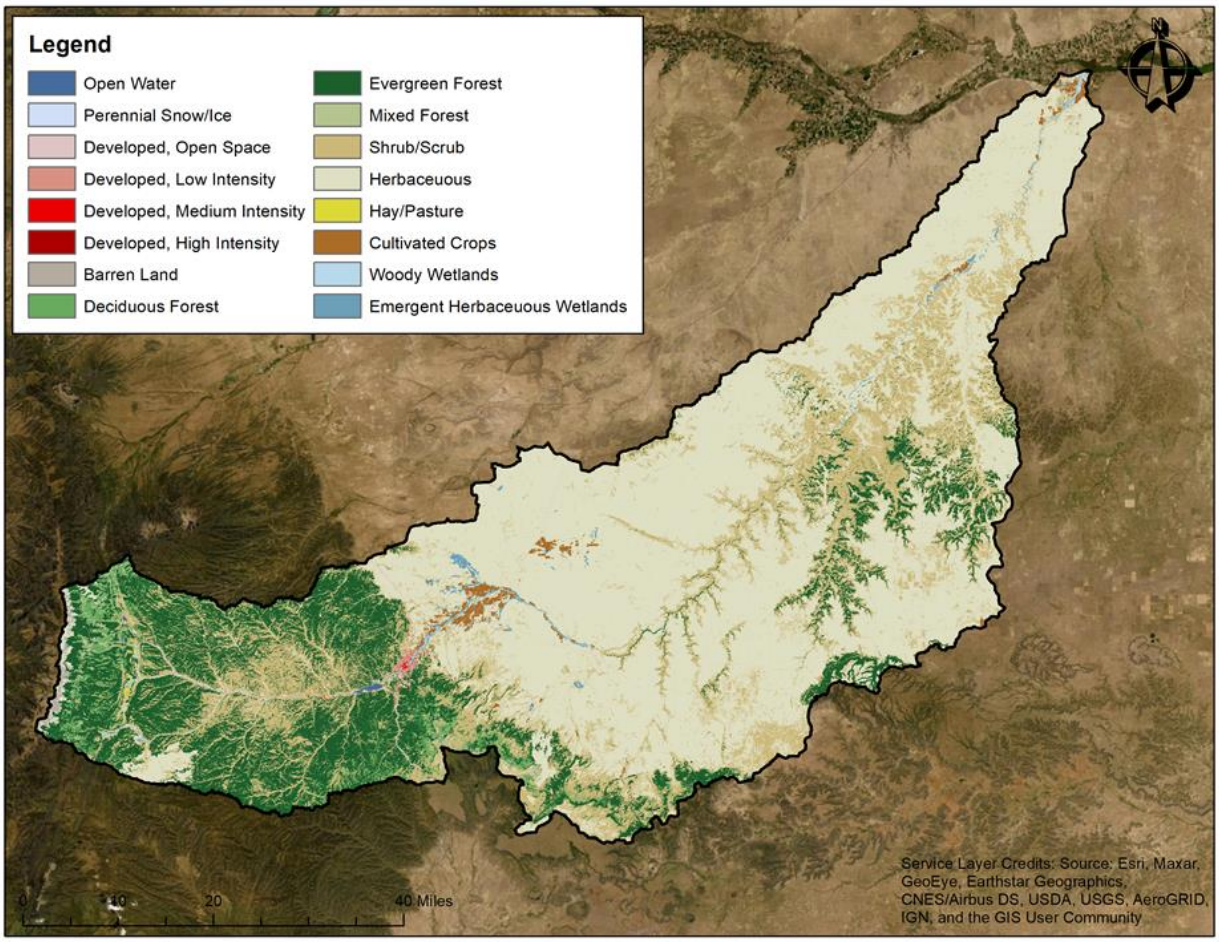

Figure 4. Map of land use in the Purgatoire River Basin based on data provided by the National Land Cover Dataset (USGS, 2016).

elevations of the watershed near the headwaters. Of the 53% and 23% herbaceous and shrub/scrub land cover, respectively, the vegetation in the eastern portion of the watershed is 46% piñon-juniper, 28% grassland, 21% shrubland, and 5% greasewood (Purgatoire Watershed Partnership, 2014). 61.3% of the watershed is privately owned and the remaining area is separated into National Grasslands and Forests, state owned land, and the U.S. Army base, Pinon Canyon Maneuvering site (Purgatoire Watershed Partnership, 2014).

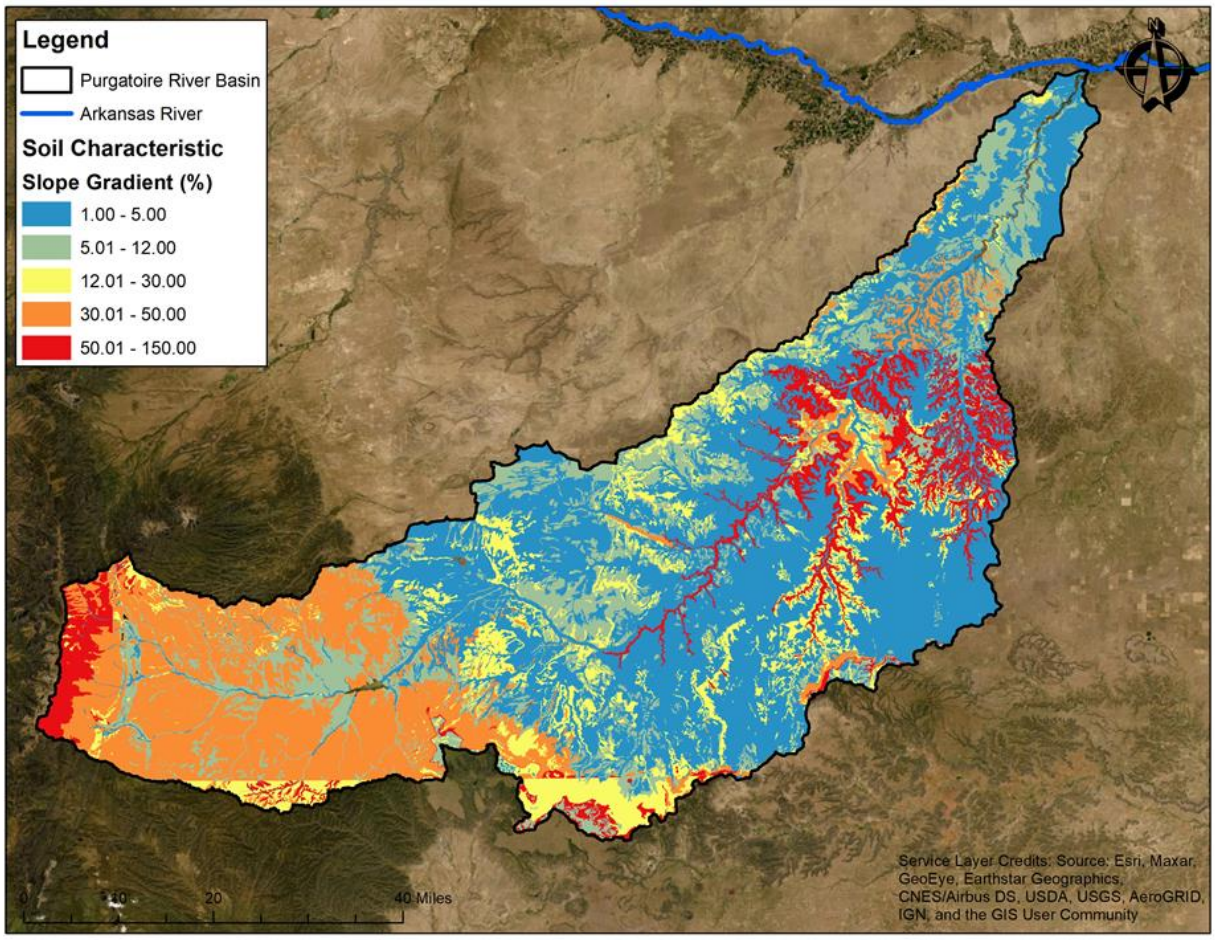

Figure 5. Spatial representation of the slope gradient represented as a percent throughout the Purgatoire River Basin (Web Soil Survey).

2.1.1b Elevation

The elevation of the study region gradually increases from east to west with a steep incline at the base of the Culebra Range of the Sangre de Cristo mountains, peaking at an elevation of 14,051 feet. The average slope gradient throughout the basin is 41% (Soil Survey Staff, et al.). Figure 5 illustrates the steep slopes in the central portion of the basin where heavy salt loading is hypothesized to occur. The mountains in the west give way to shrubland and elevated plateaus above the stream path in the east. Figure 3 illustrates the elevated plateaus that line the banks of the Purgatoire River in the central portion of the basin.

2.1.1c Climate

Precipitation is variable over summer months. The Purgatoire River Basin lies within a semi-arid climate receiving approximately 13 inches (330 mm) of rain per year. Most rainfall occurs between the months of April and October, with high-intensity precipitation events occurring between July and September. The ephemeral, concentrated storms of the summer months produce more runoff and streamflow than winter and spring precipitation even though they occur less frequently (Purgatoire Watershed Partnership, 2014, p. 95). Large storms (precipitation > 1.5 inch (38 mm)) represent roughly 20% of annual precipitation events, yet account for approximately 73% of annual sediment load (Purgatoire Watershed Partnership, 2014, p. 95). The average annual precipitation in the Purgatoire River Watershed varies spatially. The headwaters characteristically receive 43 inches (1,090 mm) of precipitation annually, whereas the eastern portion of the watershed receives 13 inches (330 mm) per year. Late spring and summer are the dominant season for rainfall, categorized as "torrential thunderstorms during the monsoon season" (Purgatoire Watershed Partnership, 2014, p. 50).

2.1.1d Soil Type

The soil within the Purgatoire watershed is predominantly hydrologic soil group C, covering 38 percent of the watershed, with soil group D accounting for 34 percent and group A and B covering 5 and 21 percent, respectively. Soils in hydrologic group C have slow infiltration rates when thoroughly wet (Soil Survey Staff, et al.). Soils with low infiltration rates have greater rates of runoff and subsequent sediment transport. The average sodium adsorption ratio (SAR) of a water extract from a saturated soil paste analysis is 0.91, and the average electric conductivity (EC) of an extract from a saturated soil paste analysis is 1,100 µS/cm at 25 °C. The average

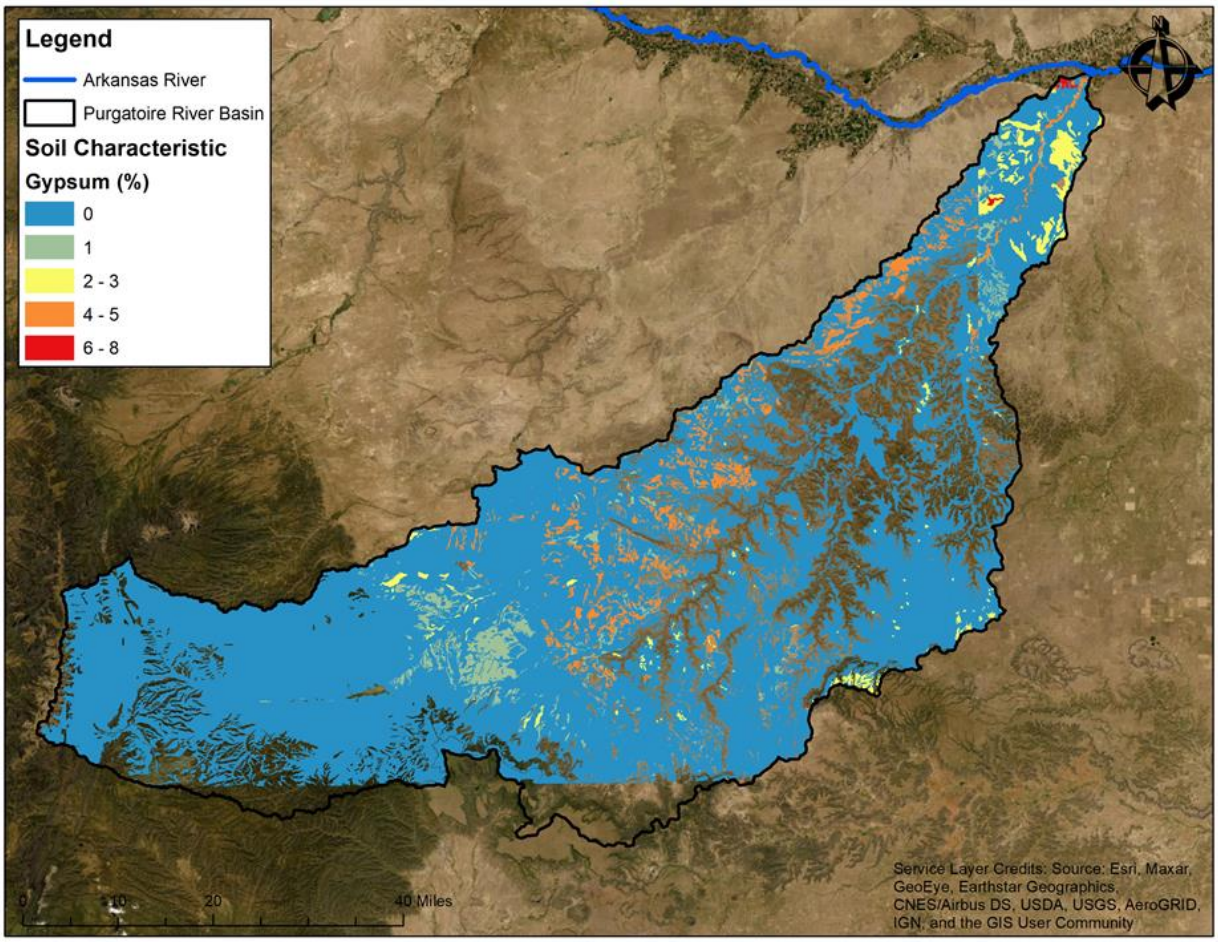

Figure 6. Spatial representation of the percent of calcium sulfate ($CaSO_4$), or "gypsum", in the soil of the Purgatoire River Basin (Web Soil Survey).

saturated hydraulic conductivity (K_{sat}) throughout the basin is 33 µm/s (2.9 m/day). Larger saturated hydraulic conductivity values represent soils that water easily flows through when saturated. The average percent of the expected values of the total sand, silt and clay throughout the basin are roughly: 35, 40 and 20, respectively.

Figures 6 and 7 illustrate the spatial variability of calcium sulfate ($CaSO_4$) and calcium carbonate ($CaCO_3$) within the basin, respectively. Web Soil Survey provided the soil characteristics used in this soil analysis (Soil Survey Staff, United States Department of Agriculture, Natural Resources Conservation Service). The average percent of gypsum in the soil

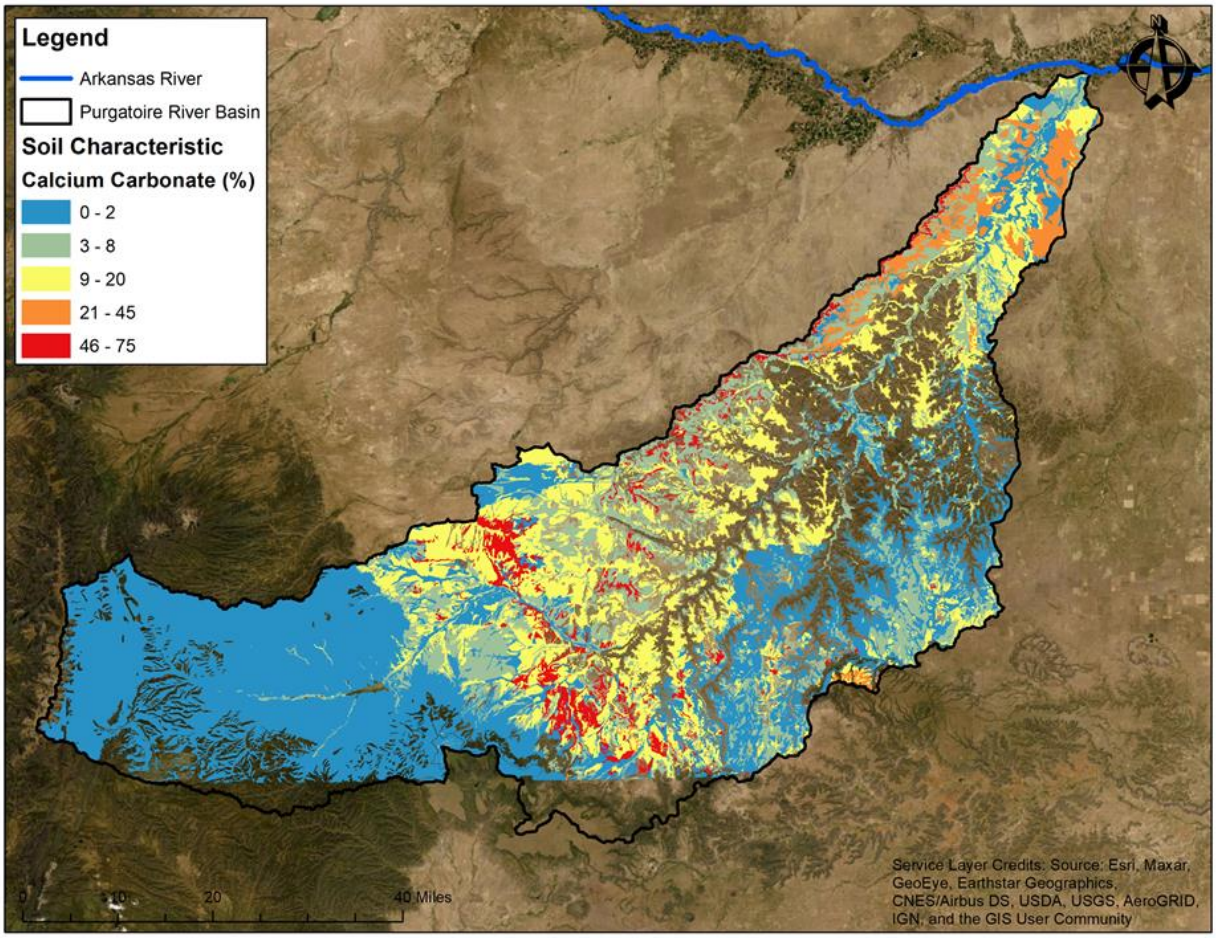

Figure 7. Spatial representation of the percent of calcium carbonate ($CaCO_3$) in the soil of the Purgatoire River Basin (Web Soil Survey).

in regions with some trace of the compound is 2.3 percent, and the average percent calcium carbonate in the soil throughout the basin in regions with some trace of the compound is 10.3 percent.

2.1.1e Geology

The western portion of the Purgatoire River Basin lies within the Central Raton Basin (Purgatoire Watershed Partnership, 2014). The basin overlays Trinidad Sandstone, Pierre Shale, and the Vermejo Formation. Similar to the Mancos Shale, a heavily studied prehistoric formation covering much of Utah and Colorado generating large deposits of salts in the unsaturated zone

due to 20,000 years of weathering (Bern, et al., 2020, p. 660), the Raton Basin consists of low permeability shale and siltstone throughout much of the formation (Purgatoire Watershed Partnership, 2014). The Mancos Shale formation has been linked to major sediment, salinity, and selenium transport in the Upper Colorado River basin (Cadaret, et al., 2016), a similar basin to the Upper Arkansas River basin.

2.1.1f Water Resources

The headwaters of the Purgatoire River are formed by the convergence of the North Fork stream and Middle Fork stream near Culebra Peak in the Sangre de Cristo Mountain Range. The flow of water in the river is largely controlled by the dam at Trinidad Lake implemented by the U.S. Army Corps of Engineers for irrigation storage, flood control, as well as recreation activities. The mean annual stream flow, in cubic feet per second, at the most upstream gage is 1.95 cubic meters per second (m^3/s) (68.5 cubic feet per second (cfs)) and the mean annual stream flow at the outlet is 1.70 cubic m^3/s (60.4 cfs) (Purgatoire Watershed Partnership, 2014, p. 48).

Approximately two-thirds of the Purgatoire River Watershed lies on top of the Cheyenne-Dakota aquifer (Purgatoire Watershed Partnership, 2014). The water table within the Cheyenne-Dakota aquifer is approximately 300 feet below the surface and is predominantly used for irrigation (Purgatoire Watershed Partnership, 2014, p. 47). The aquifer is recharged from local precipitation; however, the region receives limited precipitation annually and experiences high rates of evaporation. On average, more water is being extracted than returned since the middle of the 20^{th} century. (Purgatoire Watershed Partnership, 2014).

2.1.2 Previous Research in the Lower Arkansas River Basin

The Lower Arkansas River Basin in Colorado is one of the most salinity-affected irrigated regions in the United States (Gates, et al., 2002, p. 87). Increased agriculture in the region, made possible by thousands of miles of canals splintering off of the Arkansas River, has led to soil degradation and sediment enriched rivers (Gates, et al., 2006, p. 1). Many studies have been performed in the region regarding effects of irrigation on sedimentation and salinity primarily because of water rights and the high costs of salt-inflicted soils on crop production with the worldwide productivity losses estimated at $10 billion per year (Gates, et al., 2002, p. 87).

However, there is a gap in salinity research in the upland high-desert catchments of the Arkansas River Valley in Colorado. Natural, untilled, basins in semi-arid and arid regions often contribute high loads of salt to large river basins. This research is important in discerning the level at which naturally occurring basins export salt compared to irrigated basins, in addition to identifying environmental factors abetting such distribution. Understanding the salt contribution from untilled regions, and implementing management practices, could remedy the salinization of waters used downstream for agricultural purposes.

2.2 Objective One: Quantifying Salinity Loading from the Purgatoire River Watershed

2.2.1 Overview of Observation Network

The Purgatoire River Basin is an intensively monitored watershed. The existing monitoring network in place includes United States Geological Survey (USGS) and the Colorado Division of Water Resources (DWR) supervised sites. 29 observation points survey the river with the oldest site dating back to 1922. Most of the sites continuously monitor discharge, gage

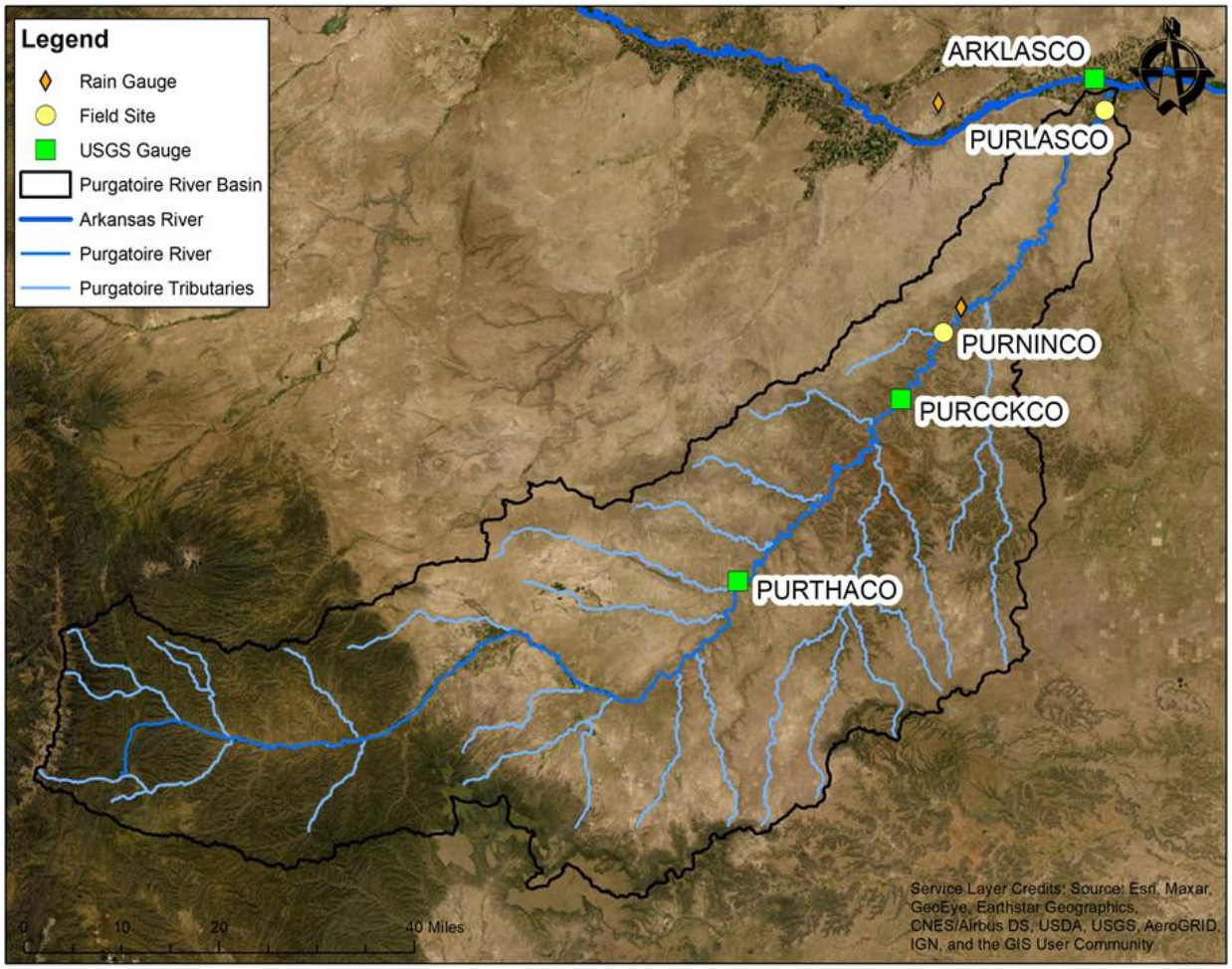

Figure 8. Overview of the observation network in the Purgatoire River Basin.

height, and temperature, with a few cataloging specific conductance and precipitation, as well. Data is available in 15-minute increments as well as daily, monthly, and annually.

Two sites were chosen from the catalog of 29 to launch additional sensors to monitor specific conductance: Ninemile Dam (PURNINCO) (see Figure 8), and the outlet of the river (PURLASCO). These sites were chosen based on previously available data provided by the monitoring organization and environmental factors of the drainage area. The monitoring network used in this report includes these two regularly monitored field sites, along with three United States Geological Survey (USGS) maintained sites. Due to missing or inconsistent data, the

timelines for each field site vary. The exact timeline of each site is detailed below. The monitoring network is operational as of the publication of this report and continues to provide specific conductance and discharge data. For this report, the primary timelines investigated will be for the years 1990 and 2020.

2.2.1a Purgatoire River near Las Animas, Colorado (PURLASCO)

The monitored outlet site of the Purgatoire River is stationed at 38°02'03.2", -103°12'05.1" in Bent County, Colorado. The contributing basin area upstream of this site is 8,880 square kilometers (3,429 square miles) (USGS). The site is under U.S. Geological Survey jurisdiction and provides ongoing discharge data in cubic feet per second. The site was initially chosen based on its proximity to the convergence of the Purgatoire River and the Arkansas River; a critical factor in understanding total salt load contributions to the Arkansas River, as well as salt mass balance analyses within the basin. Proving to be easily accessible after the initial field visit, an Onset HOBO freshwater conductivity data logger and an In-Situ Aqua TROLL multiparameter sonde were installed on September 14, 2019 and April 14, 2020, respectively. Figure 9 illustrates an aerial view of the stream and PVC encased loggers. Other important factors in the selection of this site were the consistent flow of water and the soil composition of the immediate drainage area. This site will be referenced as PURLASCO for the remainder of this report.

2.2.1b Purgatoire River at Ninemile Dam near Higbee, Colorado (PURNINCO)

The designated inlet site of the Purgatoire River, for the purpose of this analysis, is stationed at 37°42'53.4", -103°30'39.3" in Otero County, Colorado. The contributing basin area upstream of this site is 7,430 square kilometers (2,870 square miles) (USGS). The site, operated by the Colorado Department of Water Resources (DWR), provides continuous discharge,

precipitation, and air temperature readings. The site was chosen based on its proximity to alluvial valleys in the area with the intention of utilizing the specific conductivity data to examine the salt

Figure 9. Installation of specific conductance logger at Purgatoire River near Las Animas, Colorado.

disparities between the two monitored points to better understand overland flow and salt mobilization from upland catchments. Proving to be sufficiently accessible after consultation and two site visits, an In-Situ Aqua TROLL 600 electric conductivity logger was installed on April 14, 2020. Other important factors in the selection of this site were the consistent flow of water, soil composition and topographic slope of the immediate drainage area. There is a canal at the site that can divert the flow of water between the months of March 15 and November 15 if the combined flow of the river and canal is less than 0.25 cubic meters per second (m^3/s) (9 cfs). Figure 10 illustrates the diversion dam on the Purgatoire River. The canal will be referenced as

Figure 10. Purgatoire River at Ninemile diversion dam near Higbee, Colorado.

NMCHIGCO throughout the remainder of the report. As such, possible errors will be discussed further. This site will be referenced as PURNINCO throughout the remainder of the report.

2.2.1c United States Geologic Survey (USGS) Monitored Sites

Data from three additional sites monitored by the United States Geologic Survey (USGS) were used to conduct a mass balance analysis to calculate the total salt load exported by the Purgatoire River to the Arkansas River. Discharge and specific conductivity data from the USGS online log for the site on the Arkansas River (*Arkansas River at Las Animas, Colorado*, ARKLASCO) were used to calculate the percent of salt load in the Arkansas River originating from the Purgatoire River. This site has a contributing drainage area of 35,800 square kilometers (13,800 square miles) (USGS). Discharge, specific conductivity, and water quality data at two sites along the Purgatoire River (*Purgatoire River at Thatcher, Colorado*, PURTHACO and *Purgatoire River at Rock Crossing near Timpas, Colorado*, PURRCKCO) were used to emphasize the salt mobilization index, discussed in the next section, and discern the location of salt transport within the basin. PURTHACO has a contributing drainage area of 4,920 square kilometers (1,900 square miles) and PURRCKCO has a contributing drainage area of 7,120 square kilometers (2,750 square miles) (USGS).

2.2.2 Monitoring Network Installation and Procedures

This section describes the methodology for water quality sampling and equipment output readings. To examine the difference in salt mass between two points along the river, the two sites previously discussed were designated as an inlet and an outlet. The sites were chosen based on the landscape and environmental factors between them, such as steep upland catchments and high soil salinity. The two sites within the newly installed monitoring network were visited regularly, typically once a month, to download logged data, take water samples, and ensure

productivity. This section is broken into five subsections to further explain corresponding components of the monitoring network.

2.2.2a Continuous Surface Water Measurements

The primary achievement of the new monitoring system was the installation of electric conductivity logging equipment to monitor in-stream salt loading. To alleviate additional costs, the sites were chosen based on existing sites, monitored by federal or state agencies, with available supplementary data.

The Onset HOBO logger provided date and time, continuous actual conductivity (µs/cm) and temperature (°F) readings every 15-minutes. The data was downloaded using a HOBO Waterproof shuttle and a field laptop equipped with HOBOWare V3.7.22 software and converted to specific conductivity using the conductivity data assistant in HOBOWare Pro. The actual conductivity is converted to specific conductivity with Equation 1 where Y_e is the electrical conductivity, a is the 2.1 % / °C (temperature coefficient), and T is the water temperature in °C.

$$C_s = \frac{Y_e}{(1 - \frac{(25-T)*a}{100})} \quad [1]$$

The In-Situ Aqua TROLL 600 multiparameter sonde, equipped with electric conductivity and turbidity sensors, provided live water quality readings as well as continuous 15-minute readings, which were converted to daily values. The sonde provided the following parameters: date time, actual conductivity (us/cm), temp (°C), specific conductivity (µs/cm), salinity (PSU), total dissolved solids (ppt), resistivity (Ω·cm), density (g/cm^3), turbidity (NTU), total suspended solids (mg/L), barometric pressure (mm Hg), pressure (psi), depth (ft), external voltage (V), battery capacity (%). The accuracy of the conductivity sensor is +/- 0.5% plus 1 µS/cm from 0 to

Figure 11. Images of the field site at PURLASCO. In the left image, the Aqua TROLL 600 is shown held, and in the right image, the two casings for the sensors are displayed with the Onset HOBO logger hanging out of view in the left pipe and the Aqua TROLL 600 visible in the right pipe.

100,000 µS/cm and +/- 1.0% of reading from 100,000 to 200,000 µS/cm (In-Situ, 2016). The data files were downloaded via Bluetooth using the Vu-Situ app. The manual does not recommend routine calibration.

Sensors were installed within the major line of flow using a six-foot fence post hammered into the riverbed. A 3-foot polyvinyl chloride (PVC) pipe with 1-inch holes was attached to the fence post via 8-inch zip-ties and duct tape to house the data logger. Each data logger was dropped in and secured to the PVC pipe via fishing line for the Onset HOBO data logger and zip-

ties for the Aqua TROLL 600 multiparameter sonde as illustrated in Figure 11. An In-Situ telemetry system was at installed to transmit incremental data every 12 hours to effectively monitor salt load.

The Onset HOBO freshwater conductivity data logger at PURLASCO was utilized from September 15, 2019 through April 14, 2020 and then operated as a redundancy alongside the Aqua TROLL 600 multiparameter sonde for quality assurance. The Aqua TROLL 600 multiparameter sonde was installed at PURNINCO on April 14, 2020. The telemetry system was installed at PURLASCO on April 14, 2020 but was damaged in a large storm event in July.

2.2.2b Intermittent Surface Water Measurements

One water sample was taken at each sampling location during each visit and sent to Ward Laboratories, Inc. in Kearney, Nebraska for analysis of salt ion concentrations, total dissolved

Figure 12. Image of a set of water samples prepared to send to Ward Laboratories for analysis.

solids (TDS) and total suspended solids (TSS). The concentrations of the salt ions sodium (Na^+), calcium (Ca^{2+}), magnesium (Mg^{2+}), sulfate (SO_4^{2-}), potassium (K^+), chloride (Cl^-), carbonate (CO_3^{2-}), and bicarbonate (HCO_3^-) are commonly linked to the salinity of freshwater ecosystems (Kerr, 2017). The irrigation water quality analysis includes the following parameters and major ion concentrations: pH, sodium adsorption ratio (SAR), estimated total dissolved solids (ppm), electrical conductivity (mmho/cm), and the concentrations of sodium (Na^+), calcium (Ca^{2+}), magnesium (Mg^{2+}), potassium (K^+), chloride (Cl^-), sulfate as sulfur (SO_4^{2-}), carbonate (CO_3^{2-}), bicarbonate (HCO_3^-), nitrate and nitrogen (NO_3^-), boron (B), and total hardness as calcium carbonate ($CaCO_3$). Duplicates and one blank sample of distilled water were sent with every set of samples to ensure quality laboratory performance and sampling techniques.

Surface water samples were taken near the logging station to best relate water quality with real-time conductivity readings. The samples were labeled with the sample name, personal identification, time, date, and analysis type as illustrated in Figure 12. The writing was covered in clear packing tape to inhibit erasures caused by ice and water within the cooler. A chain of custody was prepared for all samples with the name of sample and the analysis type. Water samples were placed in a cooler with ice and the chain of custody form and shipped to the testing facility.

2.2.2c Soil Measurements

Soil samples were taken on three occasions at each sampling location and sent to Ward Laboratories, Inc. in Kearney, Nebraska for “saturated soil paste analysis (SAR)”. These samples were taken to provide a general representation of soil salinity in the region, particularly near streams where erosion runoff events occur. The saturated soil paste analysis includes the following parameters and major ion concentrations: saturation (%), saturated paste pH, saturated

Figure 13. Soil sampling site on the hillside near PURNINCO.

paste EC (mmho/cm), and the concentrations of bicarbonate (HCO_3^-), chloride (Cl^-), calcium (Ca^{2+}), magnesium (Mg^{2+}), sodium (Na^+), sulfate as sulfur (SO_4^{2-}), and the sodium adsorption ratio (SAR). The samples were gathered via hand or shovel and placed in small Ziploc bags for transport. Soil samples were taken to monitor runoff quality after large storm events. Figure 13 illustrates a hillside with distinct soil commonly found throughout the basin.

2.2.2d Discharge Measurements

The five sites within the monitoring network are currently equipped with continuous 15-minute streamflow readings through the DWR and USGS in cubic feet per second. Occasionally,

there were discrepancies in the data. When this occurred, neighboring values were used to estimate the daily streamflow values. The DWR streamflow gauge at PURNINCO measures the flow above the line of the constant flow bubbler and going over the wooden diversion dam. Flow going under or through the diversion dam is not measured. The USGS streamflow gauge at PURLASCO is affixed to the bridge above the stream to ensure discharge readings and deter damage from extreme flooding events. The other three sites were not visited and are exclusively monitored by the USGS.

2.2.2e Accuracy and Reliability

To provide accurate and reliable load patterns, sampling frequently is recommended. Due to the great distance between the university and the sites, sampling only occurred 12 times over the course of approximately 20 months. Meals et al. (2013) explains that monthly observations most likely will not yield reliable load estimates, however, error calculations are assessed later in this chapter. Additionally, some of the recorded samples were omitted from the analysis due to unreliable readings or equipment malfunction. Solute concentration and flow rate are substantially variable over time. Although the USGS flow rate log is revised before publication and the Aqua TROLL 600 does not require calibration for accurate results, probable error throughout this analysis was accounted for.

2.2.3 Unused Stations and Naturally Occurring Challenges

As with any field work, unanticipated challenges can, and usually, arise. Five monitoring sites were installed at the start of this study and two are operational at its conclusion. Initially, two tributaries of the Arkansas River were chosen as study areas and equipped with monitoring systems for quality and data assurance. An appointed inlet and outlet along each river were

designated as field sites for electric conductivity data logger installation. The tributaries were the Huerfano River and the Purgatoire River.

The equipment positioned at the assigned outlet of the Huerfano River (*Huerfano River near Boone, Colorado*, HUEBOOCO), which included an Onset HOBO freshwater conductivity data logger, an Aqua TROLL 500 multiparameter sonde, and an In-Situ telemetry system, was lost during an extreme storm event in July 2020 with streamflow values exceeding 2.8 cubic meters per second (m^3/s) (100 cubic feet per second (cfs)). The equipment installed at the designated inlet of the Huerfano River (*Huerfano River at I-25*, HUEI25CO), which included an Onset HOBO freshwater conductivity data logger, was lost during an extreme storm event in July 2020 with streamflow values reaching 8.5 cubic m^3/s (300 cfs). At the same time, beaver activity was visible in the area which could have led to the displacement of the equipment. This river was omitted from further research due to missing data. Subsequently, the installed site on the Cucharas River near Walsenburg, Colorado (*Cucharas River below Cucharas Reservoir*, CUCBCRCO) selected as the secondary inlet of the Huerfano River basin was not used in this study.

Illustrated in Figure 14, the equipment at PURLASCO and PURNINCO was severely damaged during an extreme storm event in June 2020 with streamflow's reaching estimated values of 28 m^3/s (990 cfs) and 88 m^3/s (3,100 cfs), respectively. The stations were reinstalled, however, the flow of water over the winter months was not large enough to reach the new downstream location of the equipment at PURNINCO, thus there is no available conductance data from September 2020 to January 2021 at this site. The site was reinstalled upriver and began collecting data January 14, 2021. Due to a dead battery, the equipment stationed at PURLASCO stopped cataloging data on January 17, 2021. Though serviced on February 11, 2021, there is

Figure 14. Images of the challenges faced throughout this research: large flows knocked out telemetry system and washed away one logger at PURLASCO (left image), and large flows caused irreversible damage and forced reinstallation at PURNINCO (right image).

three weeks of missing conductance data for this site due to maintenance. Additionally, due to an undetermined malfunction error, the equipment at PURLASCO stopped accurately logging turbidity on August 5, 2020. Although the equipment was repaired, the analyses of turbidity were consequently omitted from this study.

Rain gauges were originally installed at two sites (HUEBOOCO and PURLASCO) to monitor precipitation. These stations were monitored until the field laptop battery failed and could not be used to download data in the field any longer. The rainfall loggers provide data for September 14, 2019 through June 2, 2020. Daily precipitation data from the National Oceanic and Atmospheric Administration (NOAA) information center were used to analyze precipitation

for this report. The sites labeled *LA JUNTA MUNICIPAL AIRPORT, CO US* (38.04949°, -103.51335°) and *LA JUNTA 20 S, CO US* (37.75144°, -103.47671°) were used for analysis of ARKLASCO and PURLASCO, respectively. The Arkansas River is a large river basin spanning hundreds of miles prior to ARKLASCO; thus, the precipitation analysis should be interpreted as such.

2.2.4 Linear Regression Analysis

The *Statistical Methods in Water Resources* handbook defines linear regression estimation as "the process of estimating the line that minimizes some measure of the distance between the line and the observed data points." Ordinary least squares (OLS) regression was used in this analysis to minimize the sum of the squared vertical distances between the observed data and the line (Helsel, et al., 2020). The main objective of the monitoring network was to create a relationship between electric conductivity (as specific conductance at 25 °C) and individual salt ion concentrations, pulled from intermittent surface water samples, to estimate daily in-stream concentrations (g/m^3) and loadings (kg/day) of salt ions. These relationships were developed using linear regression. This section has been broken into four subsections to further clarify each component of the analysis.

2.2.4a Specific Conductivity and Total Dissolved Solids

Solute concentrations provided by instantaneous water samples are commonly related to in-stream water quality parameters via linear regression. The relationship is developed to predict solute concentrations when data from water samples are not available via continuous water quality parameters (Gates, et al., 2018). The dissociation of salts and minerals in water leads to the formation of positively and negatively charged particles. These particles create an electric current in the water. The measure of water's ability to carry an electric current is known as

electric conductivity (In-Situ, 2016, p. 127). The measure of electric conductivity can be used as a surrogate for salinity because it is directly related to the concentration of salt ions in the water. As such, the more salt ions that are present, the higher the conductivity of the water, and the higher the salinity (Fondriest Environmental, Inc., 2014). The salt ions represented in the analysis of PURLASCO, PURNINCO and ARKLASCO were sodium, calcium, magnesium, sulfate, bicarbonate, potassium, and chloride. The salt ions represented in the analysis of PURRCKCO and PURTHACO were identical except for the omission of bicarbonate.

2.2.4b Salt Ion Concentration Equations

Each salt ion concentration equation calculated for PURLASCO was estimated using ten water samples taken between September 14, 2019 and May 16, 2021. The data retrieved between January 17, 2021 and February 22, 2021 were not used in the estimation of the equations because they harshly skewed the equations due to inaccurate specific conductivity readings taken live instead of continuous because the battery had failed a month prior. These equations were used to estimate continuous salt ion concentrations given specific conductivity for the years 1990 and 2020. These years were chosen due to limited continuous specific conductivity data. The U.S. Geological Survey retains daily specific conductivity for PURLASCO between 1990 and 1995.

For PURNINCO, each salt ion concentration equation was estimated using the analysis of nine water samples taken between April 14, 2020 and April 2, 2021. These equations were used to estimate continuous salt ion concentrations given specific conductivity for the summer of 2020: April 16, 2020 to July 16, 2020. The summer months contained the only viable specific conductivity and discharge data given low flows and offline equipment due to agency affiliated calibrations. However, the summer months are of the most interest as most high-intensity storms

occur during these months. No agency retains historic or current daily specific conductivity data for this site.

Taken between the years 1960 and 2010, data from 40 water samples were used in conjunction with specific conductivity values at parallel points in time to calculate the salt ion concentration equations for ARKLASCO. The equations were used to predict salt ion concentrations given specific conductivity values for the years 1990 and 2020. These years were chosen due to limited continuous specific conductivity data. The U.S. Geological Survey retains continuous daily specific conductivity data for ARKLASCO from 1986 through present day.

Forty-five water samples were used to calculate the salt ion concentration equations for PURRCKCO, taken between 1983 through 1990. The equations were used to predict salt ion concentrations given specific conductivity values for the year 1990. The U.S. Geological Survey retains continuous daily specific conductivity data for PURRCKCO from 1984 through 1992. Taken between the years of 1983 and 1990, 46 water samples were used to calculate each salt ion concentration equation for PURTHACO. The equations were used to predict salt ion concentrations given specific conductivity value for the year 1990, for comparison with salinity concentrations and loadings during the year 2020. The U.S. Geological Survey retains continuous daily specific conductivity data for PURTHACO from 1983 through present day.

2.2.4c Linear Regression Calculation

Ordinary least squares regressions were performed to model the relationship between specific conductivity and salt ion concentrations. A strong relationship between specific conductivity and salt concentration is common as discussed in previous sections. Accordingly, linear regression can be highly effective in estimating total salt load from continuous specific conductivity and intermittent concentration data (Meals, et al., April 2013). Linear regression

equations were calculated for data from all five study sites. The coefficient of determination (R^2) will be used to determine how well the two variables are related. In regression, an R^2 value of 1 indicates an equation that perfectly predicts the value of the dependent variable given the value of the independent variable. To avoid sole reliance on R^2, further uncertainty estimations were assessed.

Specific conductance from continuous sensors was compared to salt ion concentration values from intermittent surface water sampling. The individual salt ion concentrations for seven salt ions, sodium, calcium, magnesium, sulfate, potassium, bicarbonate, and chloride, were organized by date and associated with the corresponding specific conductivity value in the water at that exact time to retain accuracy. On sampling days when the water did not reach the logger, live readings were taken using the Aqua TROLL 600 in the stream at the same location where water samples were taken. Equations used to predict salt ion concentration for seven individual salt ions were calculated. An example of observed values gathered from the continuous logger and intermittent water samples used in the linear regression is shown in Table 1.

Table 1. Example set of specific conductivity and salt ion concentration values used in linear regression calculation.

Date	Specific Conductivity (µS/cm)	Sodium Concentration (ppm)
9/13/19 15:10	2,998	278
1/18/20 13:55	3,174	333
4/15/20 12:10	3,224	429
6/2/20 9:25	3,505	384
7/17/20 10:25	909	67

The method used in this OLS regression analysis was an error estimation using Solver in Excel where salt ion concentration was estimated using random regression coefficient values (m and b) and the corresponding specific conductivity. The variability between this estimated value

and the actual salt ion concentration was calculated and the sum of these values was taken and minimized by Solver by modifying the linear regression coefficients, the slope (m) and y-intercept (b). To verify the Solver results, the line of best fit was estimated by graphing the independent, specific conductivity, and dependent, salt ion concentration, variables. This method accurately calculated the equation of the line between conductivity and salt ion concentration according to a comparison to the line of best fit.

Equation 2 represents a base equation for calculating salt ion concentration where c(t) is the salt ion concentration in parts per million (ppm) at some point in time, m and b are the linear regression coefficients, and SC is the specific conductivity in micro siemens per centimeter per day (µS/cm/day) at the same point in time. Each salt ion (Na^+, Ca^{2+}, etc.) has varying linear regression coefficients: the slope and y-intercept. These equations were used to predict salt ion concentrations at times water samples were not taken.

$$c(t) = (m \times SC) + b \quad [2]$$

2.2.4d Load Calculation

The flux is the product of instantaneous flow and instantaneous concentration and has units of mass over time. When integrated through time, the flux becomes a mass, as illustrated by Meals et al. in Equation 3, where M is the mass of salt in kilograms per day, k is a unit conversion factor to convert cubic meters to liters, c(t) is concentration in ppm and q(t) is flowrate in cubic meters per day (m^3/day) (Meals, et al., April 2013).

$$M = k \int_t c(t) \times q(t)\, dt \quad [3]$$

The load was calculated daily at each site using the salt ion concentration equation and the flow rate, converted from cubic feet per second to m^3/day. For the 15-minute SC data points

provided by the Aqua TROLL 600 and used in the salt ion concentration equation, a VBA code was written to calculate total daily load. The summation of the daily values was taken to calculate the total mass of salt passing each of the sites over a given time period in kilograms. Equation 3 represents the equation for total salt load per day by combining Equation 2 and Equation 3. The flow rate provides the time interval when converted from a discharge value by giving the mass of water passing a specified point over a given time interval.

$$M = \frac{1}{1000} \times \int_t ((m \times SC) + b) \times q(t)\, dt \quad [4]$$

2.2.5 Statistical Analysis

After the total salt load was estimated using the equations provided by the linear regression for PURLASCO and ARKLASCO for the years 1990 and 2020, the associated uncertainty was assessed through residual/random error estimation. The residual value is an estimation of the error in a result; it is the difference between the observed value and the measured value (Helsel, et al., 2020).

A confidence interval evaluation was assessed for each linearly regressed relationship and each site's salt load over the entire year. To evaluate uncertainty, a probability limit of 95 percent, equivalent to two standard deviations, was set for the analysis. Specific conductivity represented the independent variable and individual salt ion concentration was the dependent variable. These two topics are discussed in depth in the following two subsections.

2.2.5a Solute Concentration Uncertainty

The general guidelines laid out in Gates et al. (2018) and the *Statistical Methods in Water Resources* handbook for residual error estimation/error around the linear model were implemented to assess the variability in the relationship between SC and salt ion concentration.

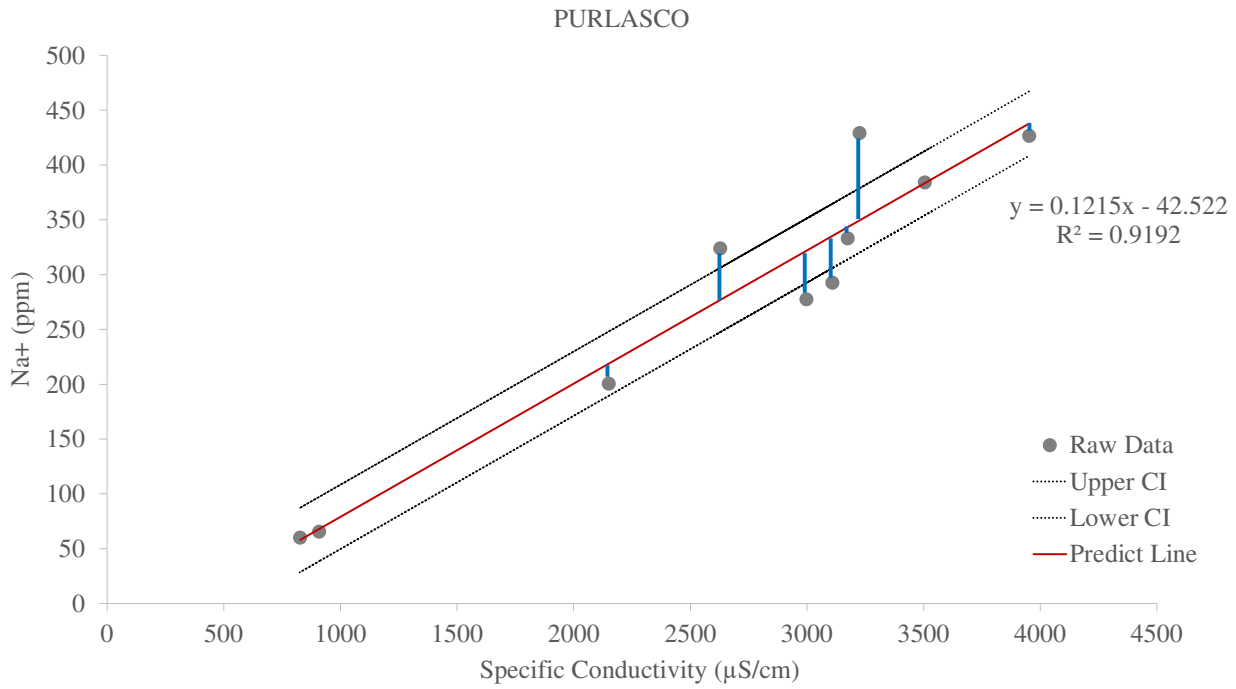

Figure 15. Graphical representation of the linear relationship between raw salt concentration data of sample salt (sodium, Na^+) and specific conductivity for the outlet, PURLASCO. The blue lines represent the residuals calculated and used in the error estimation. The equation of the line and the R^2 value are displayed on the graph.

The error associated with the linear model is a random variable, $\varepsilon_{C_{i,j}}$. Its magnitude is the unexplained variability in the data, and it is independent of the explanatory variable (Helsel, et al., 2020).

First, the estimated regression coefficients were used alongside the corresponding specific conductivity value to calculate the predicted salt ion concentration. To generate the residual of each point, the observed concentration value was subtracted from the predicted concentration value, as seen in Equation 6. An illustration of residual values is shown in Figure 15 as blue lines.

$$y = (m \times SC) + b \quad [5]$$

$$\varepsilon_{C_{i,j}} = y - y_0 \quad [6]$$

where *y* is the predicted salt ion concentration (ppm), y_0 is the observed salt ion concentration (ppm), $\varepsilon_{C_{i,j}}$ is the estimated residual of the concentration C of salt ion *i* at location *j*, *c(t)* is the estimated salt ion concentration with respect to the error (ppm), *m* and *b* are the linear regression coefficients and *SC* is specific conductivity (µS/cm/day).

Residuals were calculated for each of the seven salt ion equations for each of the two sites, PURLASCO and ARKLASCO. The residual values were assumed to have a mean of zero, a constant variance independent of the explanatory variable, and be normally distributed (Helsel, et al., 2020). The standard deviation and mean of the residuals were calculated and used alongside the Excel function NORM.INV to generate iterations of the inverse of the normal cumulative distribution for the specified mean and standard deviation. The Excel RAND function was used as the input for the probability input, a probability corresponding to the normal distribution. This function returns an evenly distributed random real number greater than or equal to 0 and less than 1. The random error was added to the concentration equation as seen in Equation 8. The error adjusted concentration equation was then multiplied by the flow rate to provide an estimate of salt ion loading (kg/day), as illustrated in Equation 9. The random error within the concentration equation was altered for each day and iteration as illustrated by Equation 8. Any negative and null values were omitted from the analysis.

$$\Delta\varepsilon_{C_{i,j}} = NORM.INV(RAND(), r_{\bar{x}}, r_{\sigma}) \quad [7]$$

$$c_{\varepsilon}(t) = ((m\ x\ SC) + b) + \Delta\varepsilon_{C_{i,j}} \quad [8]$$

$$M_{\varepsilon} = \frac{1}{1000} \times \int_t c_{\varepsilon}(t) \times q(t)\ dt \quad [9]$$

where $r_{\bar{x}}$ is the mean of the residuals, r_{σ} is the standard deviation of the residuals, $c_{\varepsilon}(t)$ is the error adjusted concentration and $\Delta\varepsilon_{C_{i,j}}$ is the regression error and M_{ε} is the error adjusted mass of salt, in kilograms.

2.2.5b Confidence Intervals

Alongside the linear regression uncertainty analysis, confidence intervals were fit to each linearly regressed equation and the subsequent total salt load at each site for each year. Confidence intervals are commonly evaluated alongside linear regression analysis. First, observed data is used to calculate a range of values for an unknown parameter. Then, a confidence interval defines the probability of the true value of a parameter falling within that estimated interval. Common probability limits for confidence interval analysis are 95% and 99%, however, a confidence interval does not indicate that 95% of the data will fall between the bounds, rather that there is a 95% certainty that the range will contain the population mean (Hayes, 2021).

The 95% confidence interval of the linear relationship between specific conductivity and salt ion concentration was calculated using the Excel LINEST function and equations 10, 11, 12 and 13. Given the independent and associated dependent variables, the LINEST function outputs the slope (m), y-intercept (b), standard error of the slope (Se_m), standard error of the y-intercept (Se_b), the R^2 value, the standard error of the y-predicted value (Se_y), and the degrees of freedom (df). To find the uncertainty in the regression coefficients, the t-value was calculated using Equation 10 and 0.05, to signify 95 percent interval, and the computed degrees of freedom from the LINEST output. The TINV function in Excel returns the two-tailed inverse of the users t-distribution. Using the t-value, the certainty of the slope and y-intercept are calculated as illustrated by Equation 11 and 12. The standard error of the predicted y is used to calculate the

confidence interval for the y data points (dependent variable). This linear approximation is the constant uncertainty of y for each of the dependent values predicted and is illustrated in Equation 13. After these values are calculated, the first of three new columns of data are computed. The predicted y values are generated using the estimated linear equation and corresponding specific conductivity. Then, the confidence interval of y (Δy_{CI}) is added to or subtracted from the predicted y to achieve the 95% upper and lower confidence interval bounds (Adams, 2010).

$$t_{\propto,v} = TINV(0.05, df) \quad [10]$$

$$\Delta m = t_{\propto,v} \times Se_m \quad [11]$$

$$\Delta b = t_{\propto,v} \times Se_b \quad [12]$$

$$\Delta y_{CI} = \frac{t_{\propto,v} \times Se_y}{\sqrt{df+2}} \quad [13]$$

where $t_{\propto,v}$ is the t-value, *df* is the degrees of freedom, *Se* is the standard error of the associated regression coefficient, and Δy_{CI} is the confidence interval of y.

Given the error adjusted load equation, an ensemble of 1,000 daily salt loads were simulated over the course of one year for each salt ion, river, and year. The standard deviation of the daily loads of each year was calculated and used to analyze the 95 percent confidence interval. The 95 percent confidence interval was assumed to be two standard deviations. A Python code was used to graph the annual load iterations.

2.2.6 Final Load Estimation

The total annual load was calculated using three methods. The first approach computed the total annual load in Excel with no residual correction factor, as described in section 2.2.4. The second variation was also calculated in Excel but accounted for the residual error correction

factor as described in section 2.2.5. The third process computed the total annual load using a Python script using integration and interpolation to account for missing data. The results from the third method are reported.

2.2.7 Missing Data

There are periods of time with missing discharge and specific conductivity data throughout the study periods. Missing data was accounted for in the analysis of quantifying salinity loading from the Purgatoire River Watershed via interpolation which is described in more depth in the next section. However, missing data was not accounted for when calculating individual percentages of each salt ion. A list of the dates with missing data per site are reported in Appendix C.

There were no missing data for PURLASCO in 2020. However, there were 25 missing daily specific conductivity data points for PURLASCO in 1990, but no missing flow rate data. There were 47 missing daily specific conductivity data points for ARKLASCO in 1990, but no missing flow rate data. 15 out of 366 specific conductivity readings were null at ARKLASCO in 2020, but there were no missing flow rate data. Further, there were a number of missing specific conductivity values at PURRCKCO in 1990, with 39 out of 365 null values, representing 10.7% of the dataset. As compared to 13 out of 365 null values for PURTHACO, representing 3.6% of the dataset. There were nine null daily discharge values for PURTHACO and 10 null daily discharge values for PURRCKCO occurring over the same time period. These data may have been lost due to extreme storm events. Without specific conductivity readings, the salt load remained null. The error associated with missing data and comparative loads is discussed in the results. Missing data have been removed from graphical representations reported in the results.

2.2.8 Code Generation

A Python code was written to generate the annual individual and total salt loads and visual representations. The code was programmed to read each of the 1,000 iterations and plot them on a linear or log scale. The program calculated the mean, first, and second standard deviation of each daily value, producing a time series. Each of the five statistics for each salt ion were added daily to get the total. The program interpolated empty cells and integrated over the data set using the trapezoidal rule to produce the mean total load of salt for each site along with the first and second standard deviations.

2.3 Objective Two: Assessing Controls on Salt Transport

This objective assesses the location of and control on salt mobilization in the Purgatoire River Watershed. This assessment uses two methods: first, a spatial analysis of watershed characteristics to indicate potential locations of salt mobilization from the landscape; and second, a brief salinity mass balance between multiple locations in the Purgatoire River, to determine where salt mass enters the river system.

2.3.1 Landscape Analysis: Salt Mobilization Index

This section describes the methodology for identifying zones within the watershed with a high probability of transporting high levels of salt mass to the Purgatoire River network (tributaries + major stream). To pinpoint these zones, landscape characteristics believed to promote salt mobilization were identified. The four watershed attributes utilized for determining the salt mobilization index were 1) topographic slope, 2) calcium carbonate presence in soil, 3) calcium sulfate presence in soil, and 4) land use and are illustrated in Figure 16.

Three of the four basin attributes were gathered from the Web Soil Survey database. Within the Web Soil Survey database, each attribute is separated into three ranges: low,

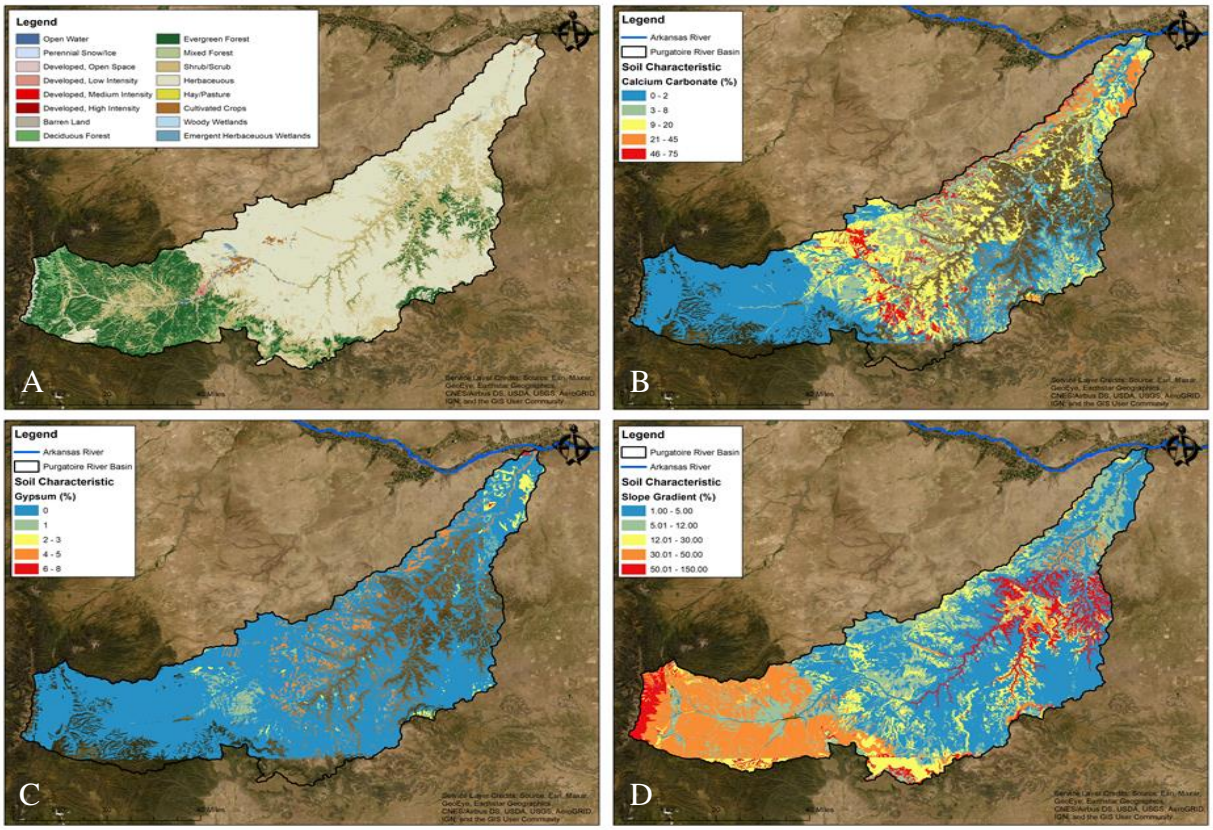

Figure 16. Spatial references used in the calculation of the salt mobilization index including (A) land use, (B) percent of calcium carbonate ($CaCO_3$) in the soil, (C) percent of calcium sulfate ($CaSO_4$)/gypsum in the soil, and (D) slope gradient as a percent (USGS) (Web Soil Survey).

representative, and high. The low and high values cap the probable range of this attribute whereas the representative value is an estimated expected value. The high value was used in this analysis for the topographic slope gradient, calcium carbonate, and calcium sulfate.

Expressed as a percentage, the slope gradient is the difference in elevation between two points. Calcium carbonate is a common substance found in minerals and rocks, such as limestone. The chemical formula for calcium carbonate is $CaCO_3$. High levels of calcium carbonate in soil can lead to heightened soil pH and increased soil salinity. The value assigned for calcium carbonate to each polygon via Web Soil Survey is expressed as a percent: “the percent of carbonates, by weight, in the fraction of the soil less than 2 millimeters in size” (Soil

Survey Staff, et al.). The calcium carbonate values in the database are separated into three ranges similar to the slope gradient: low, representative, and high. The high value was used in this analysis. The chemical formula for calcium sulfate, or gypsum, is $CaSO_4$. Gypsum is commonly found in the soil of semi-arid regions due to insufficient precipitation. Significantly contributing to loading, gypsum dissolution is a primary contributor to total dissolved solids in water systems. "In an irrigation district in Spain, 82% of the exported TDS resulted from gypsum dissolution" (Bern, et al., 2020, p. 660). The gypsum values in the database are expressed as the total percent, by weight, of hydrated calcium sulfates in the fraction of the soil less than 20 millimeters in size (Soil Survey Staff, et al.). The data are separated into three ranges: lower, representative, and high. The high value was used in this analysis. Data for the fourth basin attribute, land use/land cover, was collected from the Multi-Resolution Land Characteristics Consortium (MRLC) National Land Cover Database (NLCD). Recognizing the type of land cover in regions of the basin is important in analyzing the probability of salt mobilization as the type of land cover may influence erosion and infiltration rates (Cadaret, et al., 2016).

ArcMap in ArcGIS by ESRI was utilized as the platform for the landscape analysis. To begin, a shapefile of the Purgatoire River Basin was gathered from StreamStats and projected to the coordinate system UTM NAD83 Zone 13N, the zone that covers most of Colorado. The land use map from 2016 was downloaded from the Multi-Resolution Land Characteristics Consortium (MRLC) National Land Cover Database (NLCD) and clipped to the basin boundary. Then, the land use raster was converted to a feature class polygon. The Digital Elevation Model (DEM) was gathered from The National Map provided by the USGS. DEM tiles with a spatial resolution of 1/3 arc-second were mosaiced together and extracted to the basin boundary. As previously mentioned, soil characteristics were downloaded from Web Soil Survey monitored by the United

States Department of Agriculture (USDA) Natural Resources Conservation Service (NRCS). The attribute table containing the data for each soil component (slope gradient, calcium carbonate, gypsum, hydrologic soil group, etc.) was joined to the given shapefile. After all necessary layers were downloaded and analyzed, the land use polygon feature class was intersected with the soil characteristics polygon feature class to attain a master polygon feature class with analyzable data of all four attributes.

To estimate the salt mobilization index, the table of attributes of the intersected polygon feature class was analyzed. The table of attributes lists all the thousands of disseminated polygons within the basin and their assigned value for each characteristic, such as slope gradient, percent calcium carbonate, etc. The range of values assigned to each attribute characteristic, shown in Table 2, were distributed evenly quarterly to analyze all four attributes uniformly and simplify calculations. Different variations of the salt mobilization index may be produced by altering these ranges to emphasize one characteristic over others or by simply smoothly varying quantities to weight all values equally. Once each range was designated, they were assigned an index multiplier based on which range of values the attribute value fell. The higher the index multiplier, the more weight that characteristic carried and the higher the salt mobilization index became indicating a high probability of salt transport. After every attribute value had a corresponding index multiplier, the sum of all four attribute (% slope, % $CaCO_3$, % $CaSO_4$, land use code) index multipliers was taken and multiplied by a weighting factor of one over the number of attributes, in this case four. This equation is shown in Equation 14, where SMI is the salt mobilization index, and n is the number of characteristics being analyzed, and n_x is the index multiplier assigned to the range of values that the given polygon value falls into for each characteristic.

Polygons assigned a land use value of 52 (Shrub/Scrub, see Figure 4) were given index multiplier values of 1 because barren land with little vegetation increases salt transport (Cadaret, et al., 2016). No other land use was used in this analysis, so all other index multipliers were assigned a value of zero. Polygons with a soil composition containing above 5 percent gypsum were assigned an index multiplier of 1. Polygons with an overall soil composition containing greater than 35 percent calcium carbonate were assigned an index multiplier of 1, as well. The highest ranges were assigned index multipliers of 1 for these soil characteristics because gypsum and calcium carbonate are commonly found in the soil of semi-arid regions and are readily mobilized (Bern, et al., 2020). Polygons within the basin with a slope gradient greater than 49 percent were given an index multiplier value of 1 because the primary region of study displayed slopes greater than 49 percent. All other assigned ranges are illustrated in Table 2. If both calcium carbonate and gypsum had percentages of 0, the final index was given a value of 0 because soil salinity is a key factor in salt mobilization. By overlaying areas of high slope, high sodic soil level (calcium carbonate and gypsum), and shrub/scrub land cover, a salt mobilization index map was created.

Table 2. Index multiplier based on environmental characteristic in the Purgatoire River Basin.

	Slope (%)	Calcium Carbonate (%)	Gypsum (%)	Land Use Code	Index Multiplier (n_x)
Low	1 – 5	1 – 4	1	–	0.25
Medium	6 – 19	5 – 9	2 – 3	–	0.50
High	20 – 49	10 – 35	4 – 5	–	0.75
Maximum	50 – 150	36 - 75	6 – 8	52	1.00

$$SMI = \frac{1}{n} \times (n_{Slope} + n_{CaCO3} + n_{CaSO4} + n_{Land}) \quad [14]$$

2.3.2 Mass Balance Analysis

After calculating the total salt load of each site, a mass balance was performed to evaluate salt movement within the basin and support the findings of the salt mobilization index. Two sites were selected for mass balance analysis through the summer of 2020 and three sites were selected for a historic mass balance analysis for the year 1990. The percent of each salt ion with respect to the total mass of dissolved solids at each site was calculated, as well.

An identical approach to objective one was taken throughout this analysis to quantify the salt load at various points along the Purgatoire River to estimate the variance in salt load and hypothesize its point of generation. Current and historic conditions were examined to highlight environmental factors that may be linked to high loading rates. Residual error correction factors were not utilized for the current salt load analysis of PURNINCO, PURLASCO, or the historic annual total salt load analysis of PURRCKCO or PURTHACO. Although there is error in each site's corresponding linear regression equations, it was not evaluated as the emphasis of this objective is not salt load quantity but landscape and environmental factors leading to transport.

2.3.2a Present Mass Balance Analysis

To evaluate salt movement within the basin, a mass balance between the designated inlet, PURNINCO, and outlet, PURLASCO, was performed. The regression equations along with the corresponding discharges were used to compute the total salt load passing through each site. Residual error estimations were not performed for this assessment. The length of stream between the two points is roughly 48 kilometers (30 miles) with 116 meters (380 feet) of elevation loss. The salt exported by the active canal near PURNINCO was calculated with the same method.

2.3.2b Historic Mass Balance Analysis

Historic loads from 1990 at three points along the river, PURTHACO, PURRCKCO, and PURLASCO (see Figure 8) were compared to examine precipitation effects and environmental factors on discharge and salt loading. Historic daily precipitation data was gathered from the National Oceanic and Atmospheric Administration (NOAA) information center. The USGS provided all necessary discharge values for the analysis. The purpose of the historic analysis was to discern the variability of the quantity of salt in the river as it moved downstream. The key principle was to distinguish which section, if any, contributed more salt than others; therefore, identifying environmental factors of that section that could have led to an increased salt input.

The total loads of each site were calculated using the first method of total annual flow estimation along with flow data from the USGS and the linearly regressed equations developed in this thesis from the USGS water sample and SC data. The environmental factors were distinguished using the landscape analysis explained in the next section.

CHAPTER 3: RESULTS AND DISCUSSION

3.1 Salinity Loading from the Purgatoire River Watershed

The goal of objective one was to analyze the extent of salt mobilization and transport in a region of the LARB with sparse cultivation. Ultimately, the total percent of salt load in the Arkansas River originating from the Purgatoire River was calculated.

3.1.1 Analysis of Observed Data

Bar plots of SO_4 concentrations for each sample set at PURLASCO and ARKLASCO are shown in Figure 17. The remainder of the salt ion concentration bar plots are provided in Appendix A. Daily flow rates were collected from the USGS's website for both sites. Specific

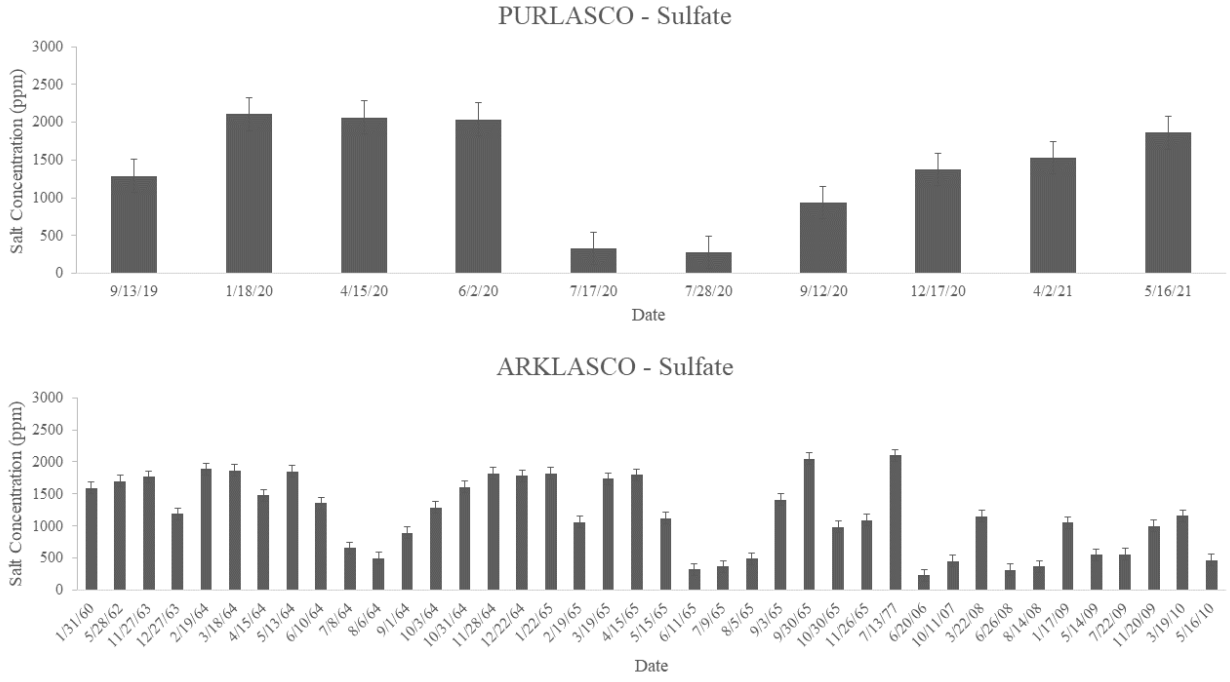

Figure 17. Bar plots of sulfate (SO_4) concentrations at PURLASCO and ARKLASCO organized by the date of extraction with corresponding standard error bars.

conductivity and flow rate have an inverse relationship, as is evident in Figure 18. Large flows dissipate salt ion concentrations, lowering the specific conductivity.

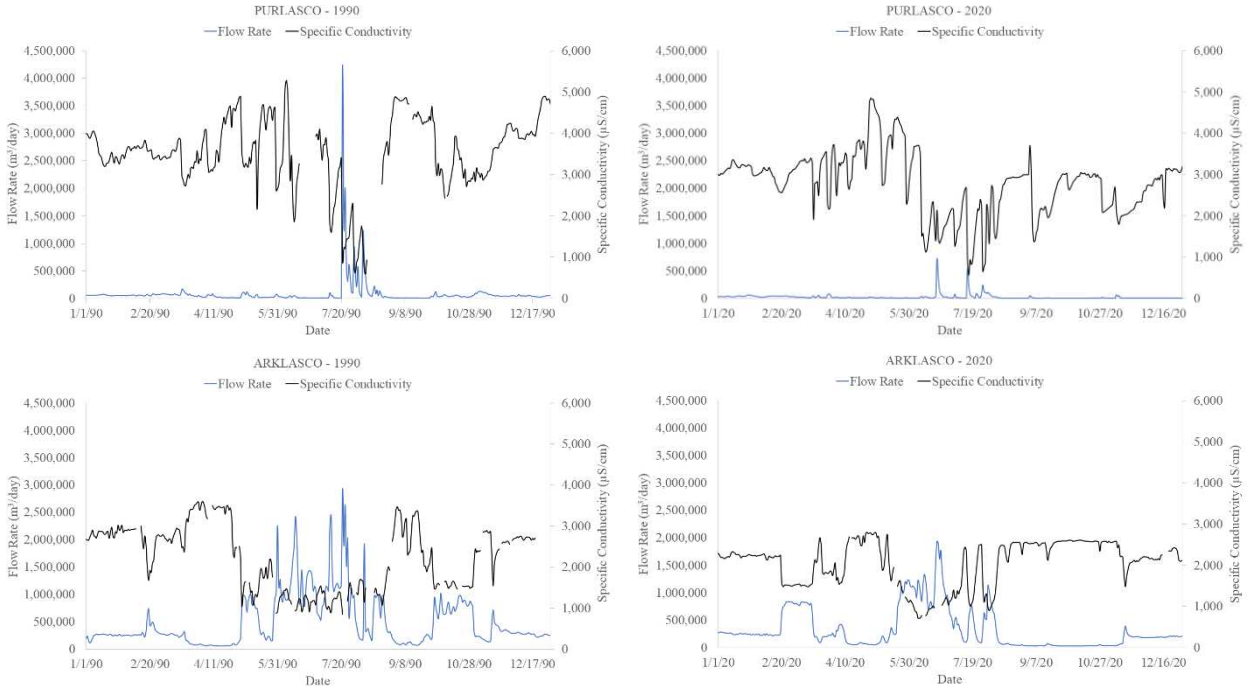

Figure 18. Time series of flow rate (blue) and specific conductivity (black) at PURLASCO in 1990, PURLASCO in 2020, ARKLASCO in 1990, and ARKLASCO in 2020 (USGS).

3.1.2 Statistical Analysis of Linear Regression Methods

Flow rate and solute concentration vary significantly over time (Meals, et al., April 2013). By creating a relationship between specific conductivity and individual salt ion concentrations, salt loading can be predicted through time given continuous specific conductivity and flow rate data. The linear regression analysis performed influences objectives one and two because salt loads were calculated for both objectives. As such, objective two will be briefly discussed in this section. For objective one, linear regression was performed on two sets of water sample and specific conductivity data, PURLASCO and ARKLASCO. The two sets of linear equations were used to predict salt ion concentrations, and subsequent salt loads, for 2020. For

objective two, in addition to the two sets of data used for objective one, linear regression was performed on an additional three sets of water samples and specific conductivity data, PURNINCO, PURTHACO, and PURRCKCO. The additional three sets of linear equations were used to predict salt ion concentrations, and subsequent salt loads, for two different time intervals, 1990 and the summer of 2020.

3.1.2a Relationship of Specific Conductivity and Salt Concentration

Instantaneous water samples (solute concentration) and continuous water quality parameters (electric conductivity) are often related via regression equations to estimate in-stream solute concentrations when water sample data are not available (Gates, et al., 2018, p. 194). As such, instantaneous solute concentration data for each site were related to the corresponding specific conductivity data point. Graphical representations of the linear equation estimated for mass of sulfate at each of the five sites analyzed are illustrated in Figure 19. The remaining graphs representing the salt concentration relationships are provided in Appendix B. As illustrated by the graphs, the relationship between sulfate and specific conductivity is largely linear as evident by the coefficient of determination (R^2). Upon site comparison, the salt ion with the lowest average coefficient of determination was potassium with a mean R^2 value of 0.100. After comparing data from all the sites, the salt ion with the highest mean coefficient of determination was sodium with a mean R^2 value of 0.948. Table 3 provides the coefficient of determination of each salt ion/SC relationship with respect to the location, along with an average of the site's coefficient of determinations and an average of the salt ion's coefficient of determination.

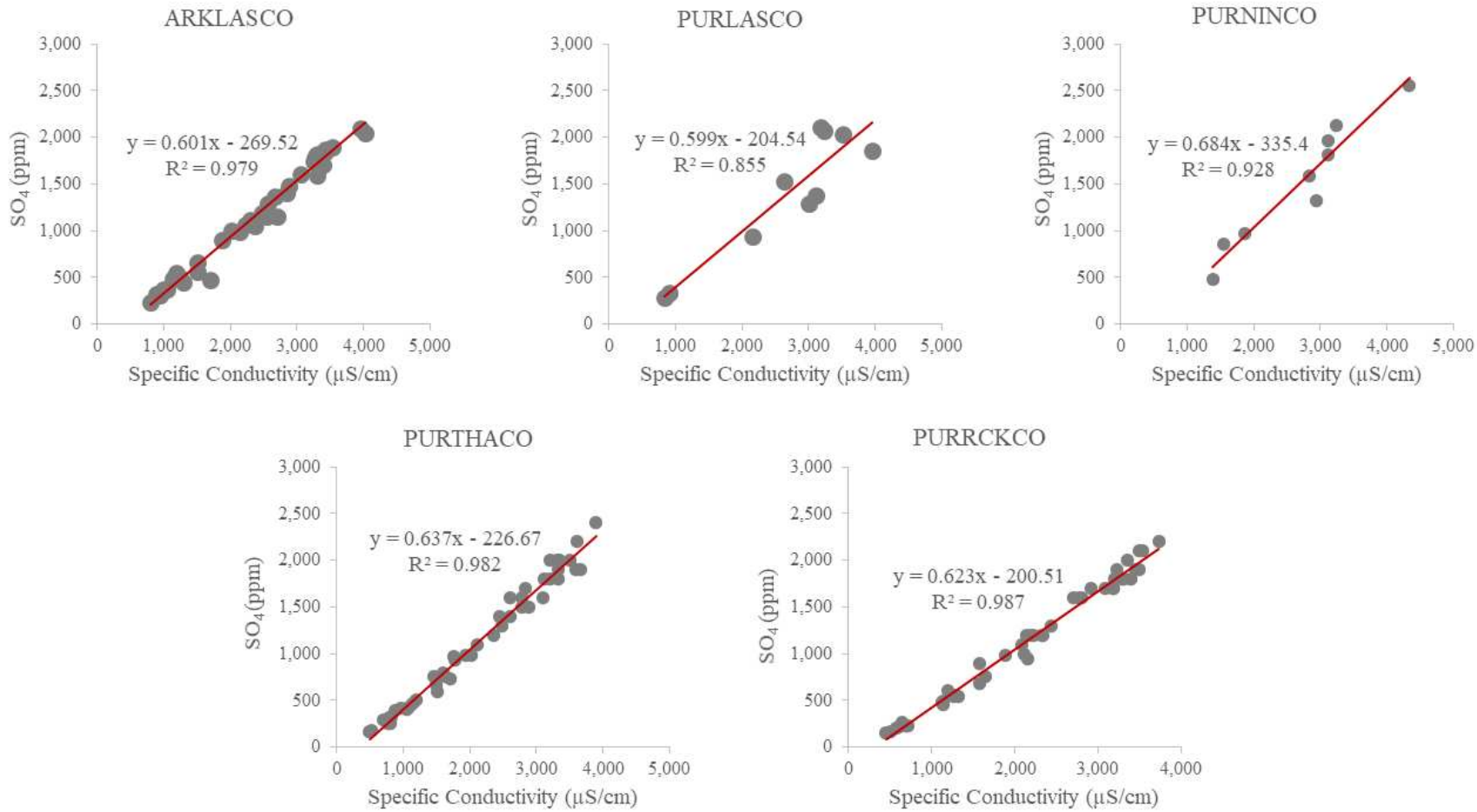

Figure 19. Graphical representation of the linear relationship between specific conductivity and a sample salt ion (sulfate, SO_4) for each monitored field site. Each relationship is titled with the corresponding field site. The equation of the line and the coefficient of determination (R^2) appear on each graph.

Table 3. Coefficient of determination of relationship between solute concentration and specific conductivity for each field site.

	# of Samples	Na	Ca	Mg	SO_4	K	Cl	Mean R^2
PURTHACO	46	0.974	0.953	0.976	0.987	0.017	0.870	0.796
PURRCKCO	45	0.945	0.867	0.970	0.982	0.067	0.645	0.746
PURNINCO	9	0.931	0.931	0.917	0.928	0.119	0.706	0.755
PURLASCO	10	0.919	0.894	0.815	0.855	0.005	0.937	0.737
ARKLASCO	40	0.969	0.938	0.964	0.979	0.291	0.957	0.850
Salt Mean	-	0.948	0.916	0.928	0.946	0.100	0.823	

Table 4. Individual salt ion concentration equations calculated using linear regression for the outlet, PURLASCO.

Salt Ion	Equation	R^2
Sodium	y = 0.122x - 42.510	0.919
Calcium	y = 0.083x + 42.795	0.894
Magnesium	y = 0.063x - 26.276	0.815
Sulfate	y = 0.599x - 204.525	0.855
Potassium	y = -0.0002x + 8.507	0.005
Bicarbonate	y = 0.051x + 211.907	0.279
Chloride	y = 0.025x - 1.031	0.937

Table 5. Individual salt ion concentration equations calculated using linear regression for the station, ARKLASCO.

Salt Ion	Equation	R^2
Sodium	y = 0.134x - 78.700	0.969
Calcium	y = 0.099x + 5.873	0.938
Magnesium	y = 0.0417x - 10.882	0.964
Sulfate	y = 0.601x - 269.508	0.979
Potassium	y = 0.0007x + 3.452	0.291
Bicarbonate	y = 0.045x + 128.286	0.591
Chloride	y = 0.037x - 15.183	0.957

Table 6. Example calculation of salt load (sodium, Na) given continuous flow rate and specific conductivity, the linear regression equation from Table 3, and the residual error correction factor for PURLASCO in 2020.

Date	Flow Rate (m^3/day)	Specific Conductivity (µS/cm)	Na (ppm)	Random Residual Factor	Na (kg/day)
1/1/2020	25,200	2,999.5	322.0	36.3	9,030
1/2/2020	34,990	2,979.0	319.5	-2.4	11,090
1/3/2020	33,270	3,025.2	325.1	-24.2	10,010
1/4/2020	31,810	3,010.0	323.3	-38.7	9,050
1/5/2020	30,090	3,031.2	325.8	-30.6	8,890

3.1.2b Residual Calculation

Although strong relationships can be created through linear regression, the error around the regression must be evaluated (Helsel, et al., 2020). After the linear equations were generated and the residuals of each were calculated, the final loads were estimated. Figure 18 illustrates the estimated linear relationship between sodium and specific conductivity along with the 95 percent confidence interval bounds estimated using the confidence interval of y in Equation 13 (Adams, 2010). To estimate the error around the linear regression, residual values were calculated. The residual value of one point is the difference between the predicted (calculated) concentration and the observed (raw) concentration. The mean and standard deviation of each set of residuals was calculated and used as the input for random variable generation. The random variable function was utilized to further assess uncertainty as the residuals were assumed to display a normal distribution. The random residual variable was added to the base linear concentration equation to estimate load. The daily equation for load was iterated through 1,000 times for the entire year, such that one year of data points was one iteration, producing 365,000 data points per salt per site per year totaling 10,220,000 load data points.

3.1.3 Analysis of Salt Load Export from the Purgatoire River to the Arkansas River

The Purgatoire River exports large quantities of salts to the Arkansas River every year. The purpose of objective one was to quantify the total annual salt load of the Purgatoire River in 2020 and evaluate how this value compares to the total annual load of the Purgatoire River in 1990. It was hypothesized that the total load relies heavily on environmental factors, however, the salt load may have decreased due to years of previous surface erosion. Understanding the spatiotemporal variability of salt loading is important when comparing basins of various uses.

The total annual salt load exported by the Purgatoire River to the Arkansas River in 2020 was 18,000,000 kg with a 95% confidence interval between 25,600,000 and 10,600,000 kg. The total annual salt load exported by the Purgatoire River to the Arkansas River in 1990 was 64,600,000 kg with a 95% confidence interval between 90,200,000 and 39,100,000 kg. In this analysis, the total salt load was composed of seven individual salt ions, sodium, calcium, magnesium, sulfate, potassium, bicarbonate, and chloride. When reporting the total load values, the first and second standard deviations are reported. Dependent on how much data is available, normally distributed observed data will fall within four standard deviations of the mean. The first standard deviation holds 68% of all data, the second standard deviation will hold 95% of all data, and the third standard deviation will hold 99.7% of all data, with 0.3% falling outside of these thresholds. The second standard deviation will be referred to as the 95% confidence interval. The following four subsections discuss the contribution of each individual salt ion, the total salt load exported by the Purgatoire River, and the influence of precipitation.

3.1.3a Graphical Representation of Individual Salt Ions

Three base graphs were generated: a graph on a log scale with visible iteration lines and colored lines representing the mean, first and second standard deviations, a graph on a log scale

with colored lines representing the mean, first and second standard deviations and color blocking in between those bounds, and finally, a graph of the daily load on a linear scale.

When graphing the iterations on a logarithmic (log) scale, the minimum allowable value for the second standard deviation was set to 1.05 to eliminate undefined values. In standard deviation analysis, when the value produced by subtracting the second standard deviation was omitted, the positive second standard deviation was omitted, as well. This omission created some blank second standard deviation regions on the log graphs of some salt ions. However, when reporting the daily maximum mean, first, and second standard deviations of the mean in the following tables, the values were not restricted. Graphically, the log scale was set to the same proportion for each salt to demonstrate the differing levels of each salt throughout the year. In some instances, there may be some iterations that fall below the visible threshold; however, none fall below zero. The lowest value on the scale necessary to capture all iterations is 0.001. However, for visibility purposes, the log scale for all individual salt ion loads was set to 1 to 10^7. The linear scale was automatically adjusted by Python to best illustrate the annual salt load. Setting the linear scale to the same proportion for each salt ion diffused the comprehensive details necessary to recognize the variability of each salt load.

Representing the spatiotemporal variability of individual salt ion loads, Figures 20 and 21 permitted the individual analysis of load variance through space and time. The data were fit to a linear scale to better visualize the contribution of each salt ion to the total load, as well as a logarithmic scale to better visualize the detailed variability of each salt ion by omitting disproportionately high data points. In either figure, the column on the left depicts different salt ions on a linear scale from four different scenarios: PURLASCO in 1990, PURLASCO in 2020, ARKLASCO in 1990, and ARKLASCO in 2020. The column on the right depicts the

corresponding salt ion from the left on a logarithmic scale. Sulfate is a primary salt ion and as such, the graphical representation of its contribution is enlarged in Figure 22. Across all seven salt ions, most of the inconsistency occurred during the summer months; it can be hypothesized that environmental factors occurring during these months lead to increased salt loading. Additionally, at PURLASCO daily loading rates in 1990 were significantly higher than those of 2020. The annual total quantity of flow passed through PURLASCO in 1990 changed by 72% in 2020. Subsequently, the in-stream salt loading was altered by the same degree, as well. The daily loading rates at ARKLASCO were additionally higher in 1990, but not by a large margin. Similar to the flow at PURLASCO, the annual quantity of flow passed through ARKLASCO in 1990 had changed by a degree of 33% in 2020.

Figure 20 showcases three of the seven salt ions that had the largest contributions, apart from sulfate. Loading rates are heavily dependent on flow rates as evident by the comparison of Figure 18 and the instantaneous increase in the load of bicarbonate (HCO_3) at PURLASCO in 1990 and 2020 illustrated in Figure 20 (C). The daily loading rate increased from 2,800 kg/day to approximately 1,090,000 kg/day on day 201. The region experienced 3.2 inches (80 mm) of precipitation within two weeks of the large loading event. The flow rate spiked on day 201 at 4,230,000 m^3/day increasing from the previous days flow rate of 7,340 m^3/day; the specific conductivity in the water fell from 3,390 µS/cm to 887 µS/cm.

Figure 21 showcases three of the seven salt ions that had the lowest contributions, evident by the almost invisible daily loads on the linear scale in the left column. Figure 21 (A) depicts a time series of the daily mean of potassium (K) loading rates in 1990 and 2020 at ARKLASCO. In 1990, the day of maximum solute loading was concurrently day 201 with a spike of approximately 12,000 kg/day jumping from 5,050 kg/day on the previous day. The flow rate

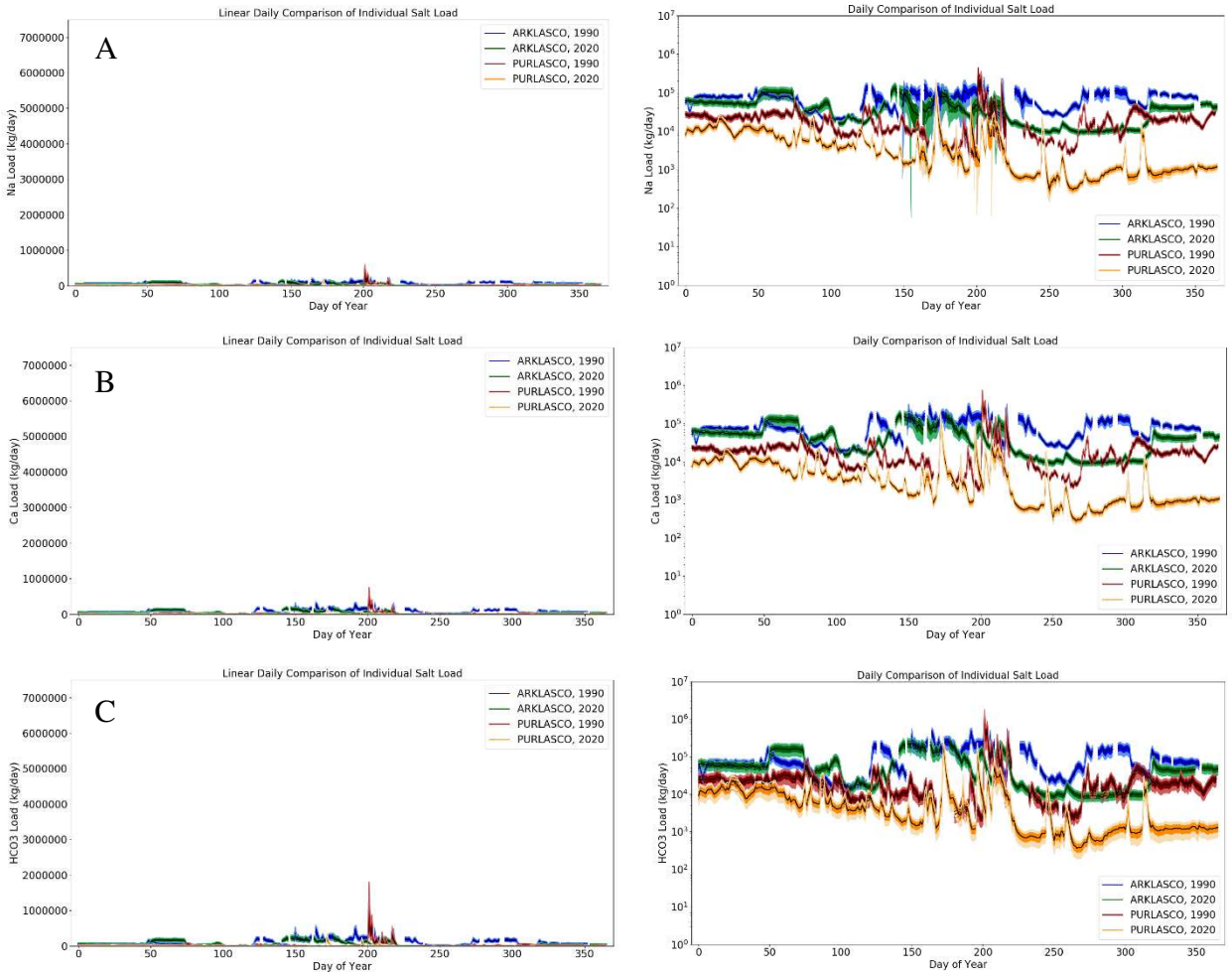

Figure 20. Comparative annual time series of (A) sodium, (B) calcium, and (C) bicarbonate on a linear (left column) and logarithmic (right column) scale. The scenarios are organized by color, with red illustrating PURLASCO in 1990, orange representing PURLASCO in 2020, blue depicting ARKLASCO in 1990, and green representing ARKLASCO in 2020. The darker shade represents the first standard deviation of the mean, whereas the lighter shade depicts the second standard deviation of the mean.

concurrently increased from 1,170,000 m^3/day to 2,940,000 m^3/day. Like PURLASCO in 1990, there was substantial precipitation in the days leading up to the event. The area received approximately 4.60 inches (120 mm) of precipitation within two weeks of the event.

Figure 21 (B) illustrates a time series of the daily ensemble mean of magnesium (Mg) loads in 2020 at PURLASCO. The daily load of magnesium increases from 1,780 kg/day to 79,100 kg/day within one day. Though there was not much precipitation leading up to the event,

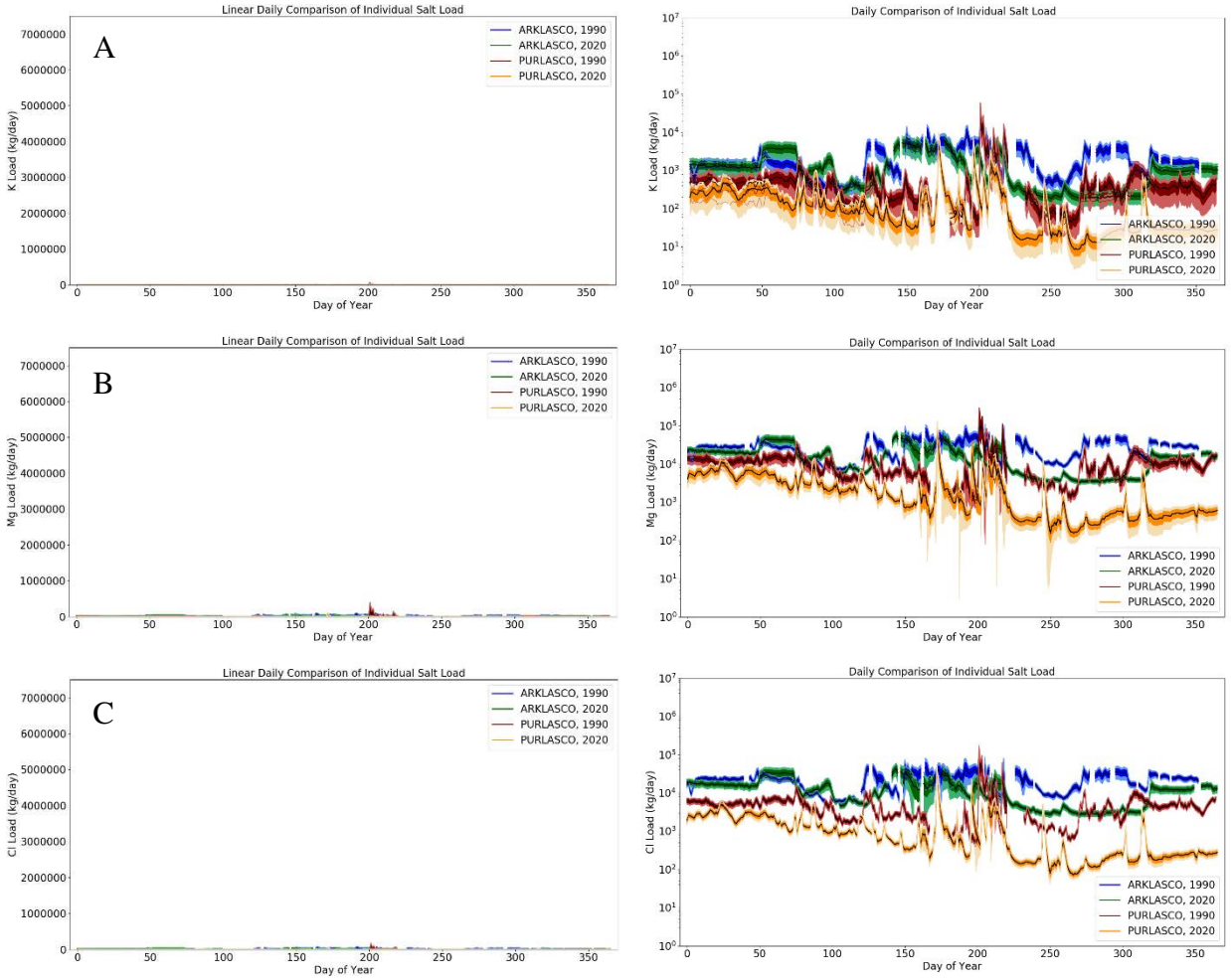

Figure 21. Comparative annual time series of (A) potassium, (B) magnesium, and (C) chloride on a linear (left column) and logarithmic (right column) scale. The scenarios are organized by color, with red illustrating PURLASCO in 1990, orange representing PURLASCO in 2020, blue depicting ARKLASCO in 1990, and green representing ARKLASCO in 2020. The darker shade represents the first standard deviation of the mean, whereas the lighter shade depicts the second standard deviation of the mean.

the flow rate additionally escalated, increasing from approximately 27,900 m^3/day to 719,000 m^3/day. The sudden changes in flow rate, and subsequent loading, may stem from upstream factors such as releasing flows from the Trinidad Reservoir. Information regarding agency affiliated release flows would need to be investigated.

Figure 21 (C) showcases a time series of the daily mean of chloride (Cl) loading rates in 2020 and 1990 at ARKLASCO. The daily mean loading rates of chloride at ARKLASCO in

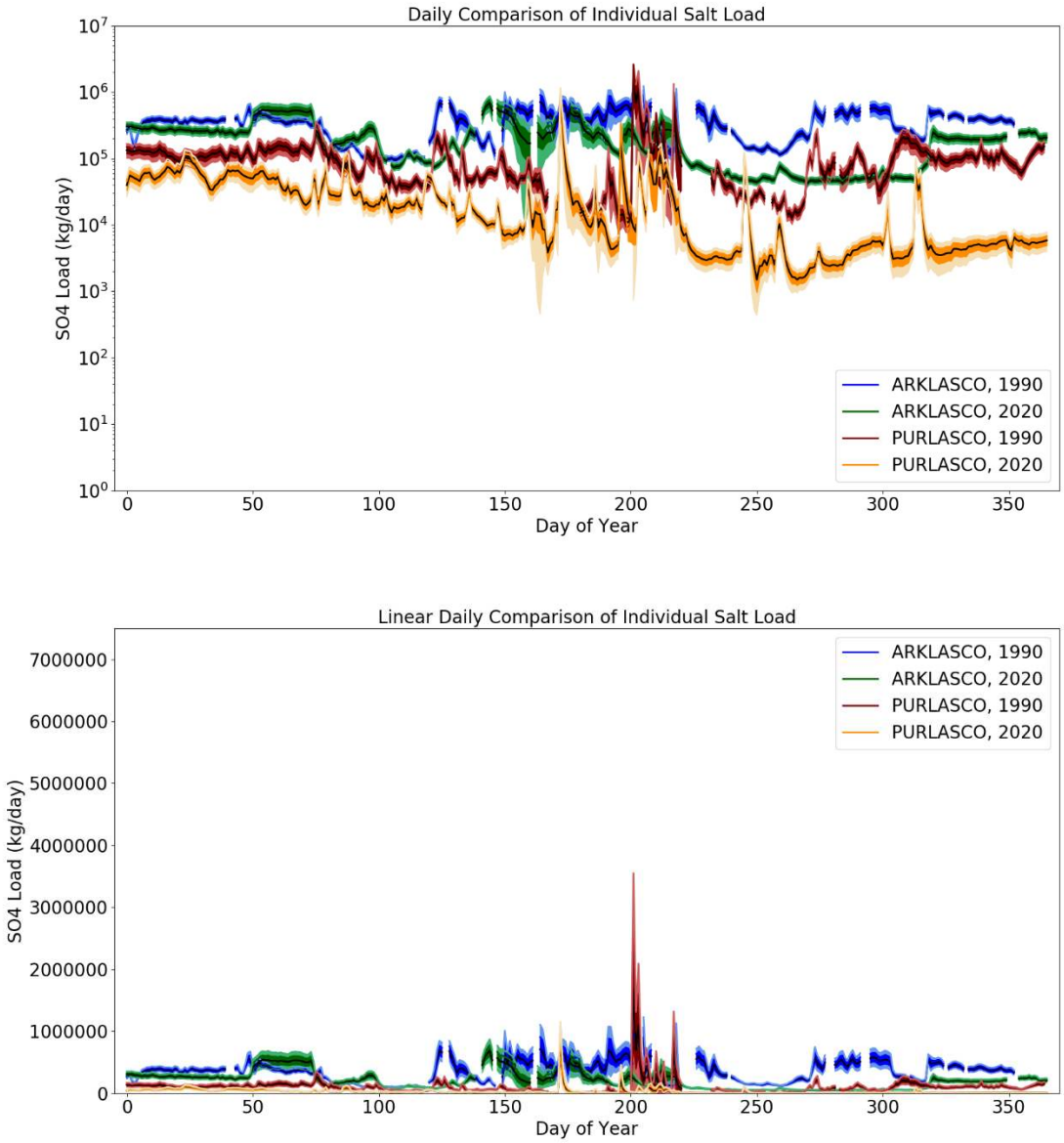

Figure 22. The top image illustrates the sulfate load over time for 1990 and 2020 at PURLASCO and ARKLASCO on a log scale. The bottom image illustrates the sulfate load over time for 1990 and 2020 at both sites as well, on a linear scale with the same dimensions as the TDS in Figure 25. The second standard deviation on day 201 at PURLASCO in 1990 is 3,550,000 kg/day.

2020 were relatively consistent. There was not one major loading event as seen at PURLASCO in 2020. The maximum daily loading rate at ARKLASCO for chloride was 43,000 kg/day. The flow rate correspondingly increased from approximately 913,000 m^3/day to 1,125,000 m^3/day, and the region received 0.35 inches (9 mm) of rain within the previous two weeks. These salts

were chosen to best showcase the ensembles as these four salts have some of the lowest coefficient of determination values associated with their linear regression equations. Figure 20 (A and B) have similar loading events to the previously discussed salt ions and do not require further discussion.

Due to the extreme flow event at PURLASCO in both years, the maximum mean daily load of each dissolved salt ion is provided in Table 7. Although there was not one large flow event, the maximum mean daily load of each dissolved solid at ARKLASCO are provided in Table 8 for consistency. Tables 7 and 8 represent the mean salt load on one day at each site during each year to better discern the large salt loading that occurs during intense, brief storm events. The total represents the summation of all salt ions, indicating the total mean daily salt load on that day of the year.

Table 7. Maximum of the mean daily individual salt load (kg/day) over the course of one year at PURLASCO. In 1990, the maximum load occurred on day 172 and in 2020, the maximum load occurred on day 201.

	Na	Ca	Mg	SO_4	K	HCO_3	Cl	Total
1990								
+2 SD	596,000	754,000	400,000	3,550,000	59,000	1,800,000	170,000	6.73 E6
+1 SD	447,000	624,500	288,000	2,620,000	47,000	1,444,000	131,000	5.16 E6
Mean	297,000	495,000	175,000	1,690,000	35,000	1,089,000	92,500	3.88 E6
-1 SD	147,000	366,000	62,500	764,000	23,000	734,000	54,000	2.00 E6
-2 SD	60,000	237,000	15,500	177,000	11,500	379,000	23,000	0.84 E6
2020								
2 SD	213,000	206,000	128,000	1,150,000	9,700	350,000	50,600	1.90 E6
+1 SD	185,000	183,000	104,000	963,000	8,000	291,000	44,300	1.59 E6
Mean	157,000	160,000	79,000	774,000	5,700	231,000	37,900	1.44 E6
-1 SD	129,000	137,000	55,000	584,000	3,800	172,000	31,500	0.98 E6
-2 SD	101,000	114,500	30,000	395,000	1,900	113,000	25,000	0.68 E6

Table 8. Maximum of the mean daily individual salt load (kg/day) over the course of one year at ARKLASCO. In 1990, the maximum load occurred on day 201 and in 2020, the maximum load occurred on day 144.

	Na	Ca	Mg	SO_4	K	HCO_3	Cl	Total
1990								
+2 SD	250,000	407,000	117,000	1,230,000	18,500	696,000	88,900	2.55 E6
+1 SD	205,000	337,000	94,500	1,060,000	15,000	591,000	70,000	2.17 E6
Mean	159,000	267,000	77,600	891,000	12,000	486,000	55,200	1.95 E6
-1 SD	114,000	200,000	61,800	724,000	8,700	380,000	40,400	1.42 E6
-2 SD	91,000	153,000	46,000	557,000	5,440	275,000	28,500	1.07 E6
2020								
+2 SD	180,000	223,000	74,300	870,000	9,000	346,000	59,000	1.58 E6
+1 SD	156,000	196,000	65,500	778,000	7,500	295,000	50,900	1.39 E6
Mean	132,000	169,000	56,700	687,000	6,000	244,000	42,700	1.34 E6
-1 SD	107,000	141,000	47,900	595,000	4,400	193,000	34,500	1.02 E6
-2 SD	88,000	114,000	39,100	504,000	2,900	141,000	26,900	0.828 E6

3.1.3b Ratio Representation of Individual Salt Ions

Each of the seven individual salt ions is some percent of the total quantity of dissolved solids. Figures 23 and 24 illustrate a time series overlay of all seven individual salt ion loads on a log scale. The sulfate load is consistently the highest contributor, while potassium is habitually the lowest. Sulfate is a naturally occurring compound in water and soil. Semi-arid regions with high levels of calcium sulfate in the soil may transport higher levels of sulfate to water bodies. Figure 22 illustrates the temporal variability of sulfate at PURLASCO and ARKLASCO. The load peaks throughout the summer months. The maximum daily mean loading rate of sulfate at each site for each year is reported in Tables 7 and 8. A detailed analysis on the environmental factors influencing loading rates is discussed in the next section.

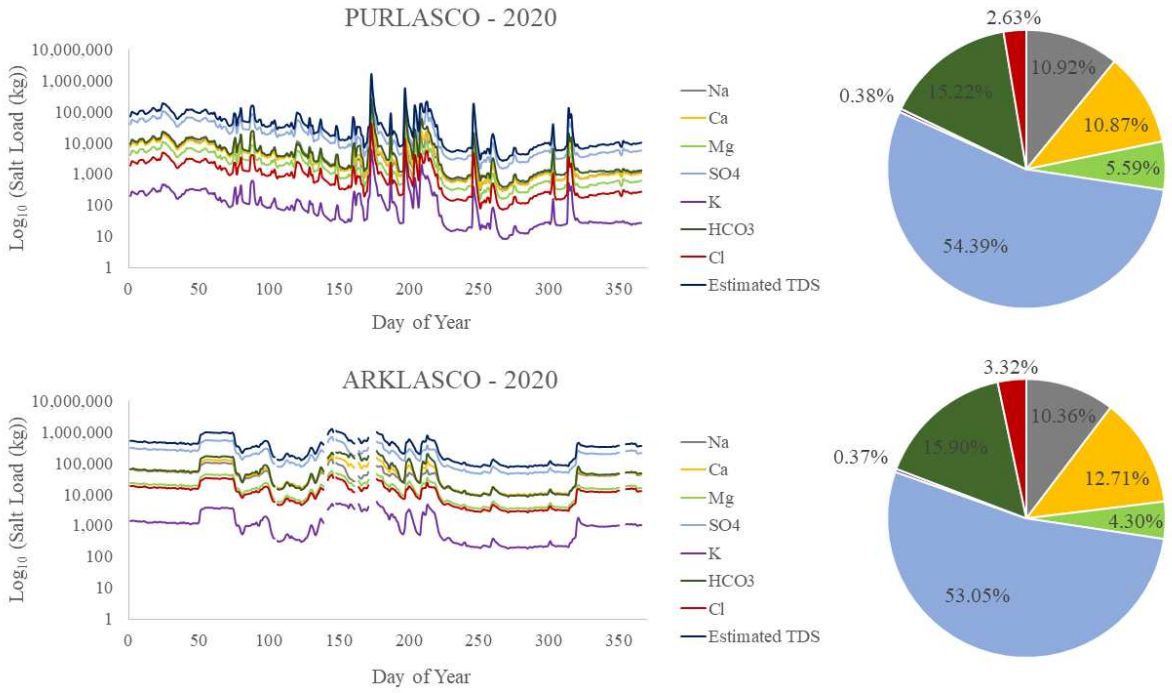

Figure 23. Time series of daily salt loads of individual salt ions of PURLASCO and ARKLASCO in 2020. The pie charts symbolize the percent of each salt ion of the total and is positioned to the right of the corresponding river's log scale.

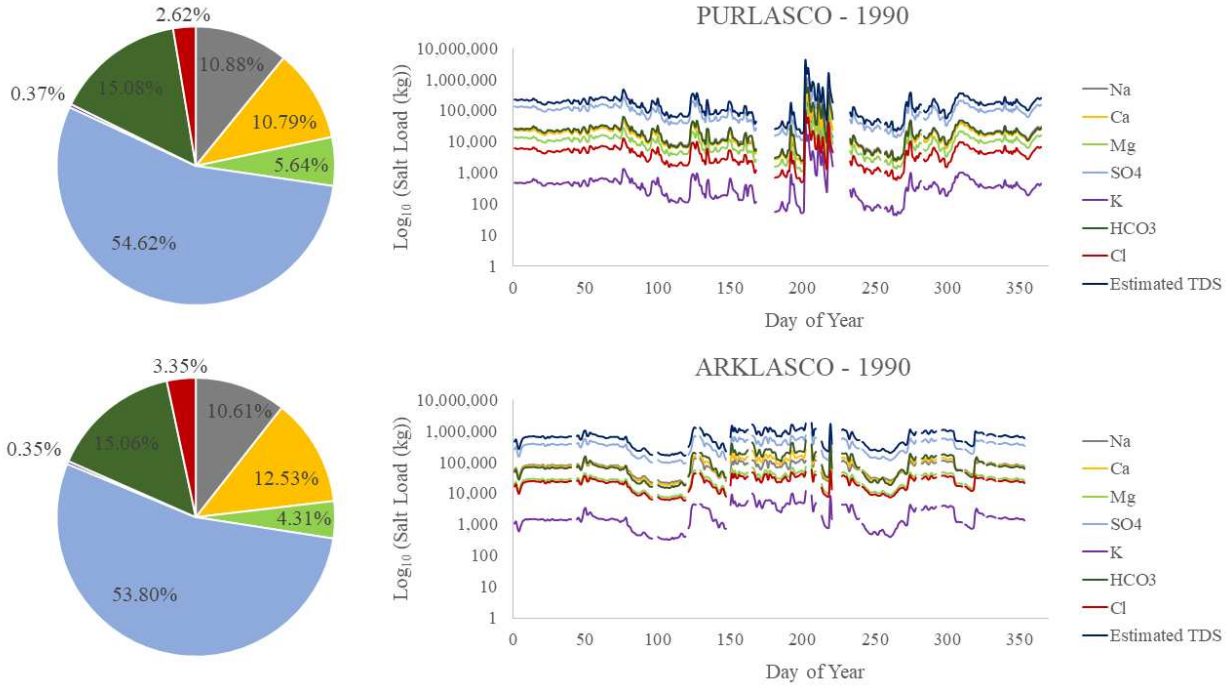

Figure 24. Time series of daily salt loads of individual salt ions of PURLASCO and ARKLASCO in 1990. The pie charts symbolize the percent of each salt ion of the total and is positioned to the left of the corresponding river's log scale.

3.1.3c Total Annual Load Calculation

The values in Table 10 were calculated using the second total annual load estimation method. One year of values is considered one iteration. Thus, the mean of all 1,000 iterations was taken daily for each salt, providing one set/year of values for each salt. The sum of those values was taken to attain a mean daily salt load per salt ion. Each individual salt summation was combined to attain one total annual salt load. Table 11 illustrates the total annual load estimation calculated using a Python script using interpolation and integration. The total mean daily salt load (TDS) is illustrated in Figure 25, on logarithmic and linear scales. The percent contribution of salt load in the Arkansas River originating from the Purgatoire River Watershed, along with the range of percentages based on the uncertainty analysis, is reported in Table 12. The percent was calculated by taking the summation of the two total annual salt loads representing the point in time after the Purgatoire River enters the Arkansas River and dividing the Purgatoire River salt load from that summation.

The Purgatoire River supplied 6.55% of the flow in the Arkansas River in 2020 after their junction. Of the total combined flow, 11.2% of the total salt in the Arkansas River originated from the Purgatoire River. In 1990, the Purgatoire River supplied 14.47% of the combined total flow in the Arkansas River and 21.7% of the combined total salt load. There is a 48% change in the percent of salt exported by the Purgatoire River between 30 years, with the percent of flow shifting by 54%. Load is highly dependent on flow. It is evident that the comparative years had a significant difference in precipitation; 1990 was a wet year and 2020 was a dry year. Chosen due to limited daily specific conductivity data, the years had varying precipitation levels, thus making it difficult to draw temporally relevant conclusions. The flow export changed by a

greater percent than the exported quantity of salt, insinuating that although flow and salt load are related, salt is still reaching the Arkansas River when flow is decreasing.

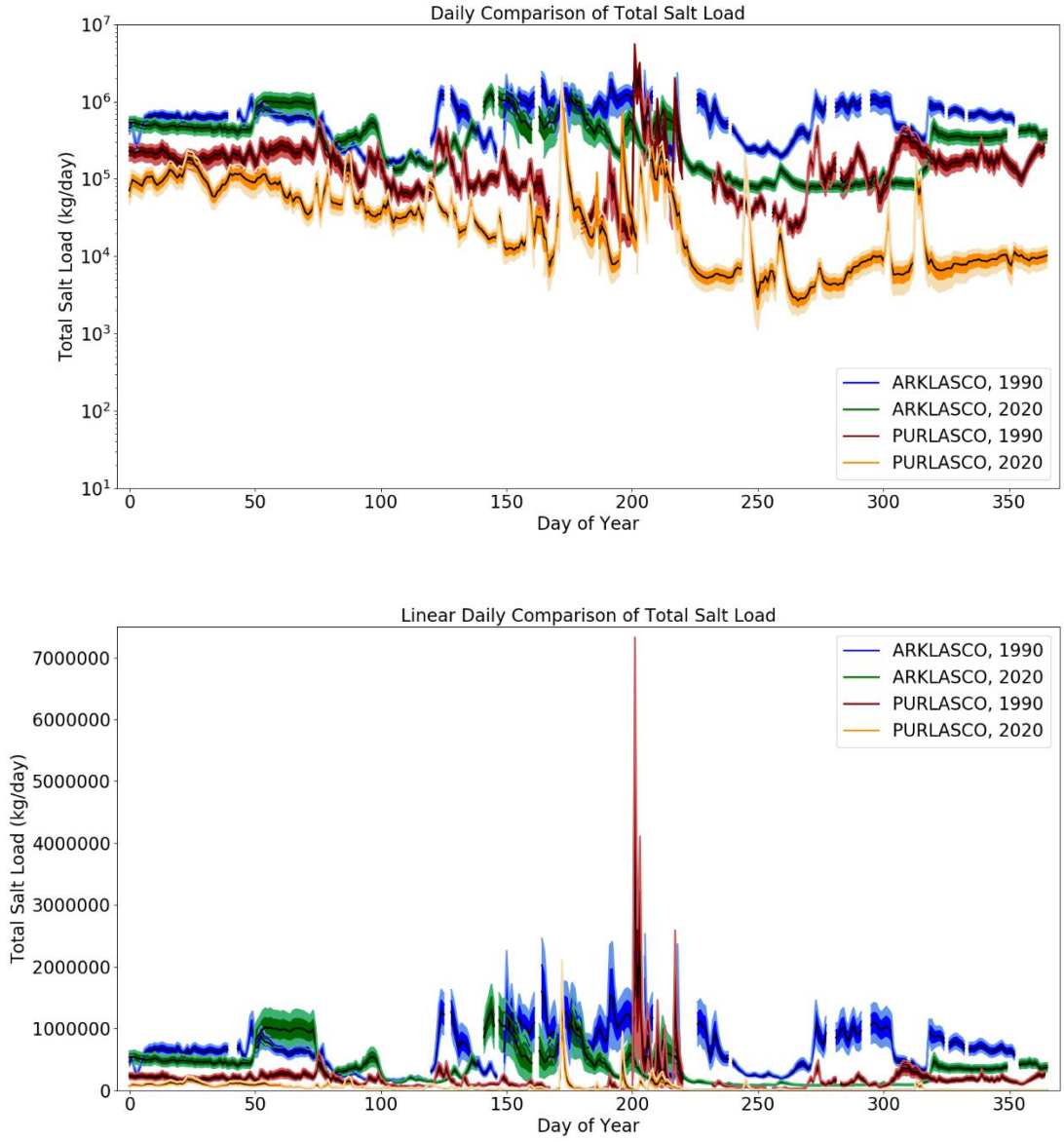

Figure 25. The top image illustrates an overlay of the combined total salt load (TDS) at each site with respect to time on a log scale for increased visibility. The bottom image illustrates an overlay of the combined total salt load (TDS) of each site with respect to time on a linear scale. The maximum daily salt load clearly visible in the bottom image are reported in Table 9.

The daily maximum salt load at ARKLASCO in 1990 and 2020 accounted for 0.71% and 0.91% of the total annual salt load, respectively. The daily maximum salt load at PURLASCO in 1990 and 2020 accounted for 6% and 8% of the total annual salt load, respectively. A temporal trend cannot be assumed due to insufficient annual data. Two years on opposite sides of the spectrum of precipitation were unintentionally chosen for this study. Table 9 details the variability in the daily maximum load. The values in this table correspond to the *Total* column in Tables 7 and 8. The Arkansas River may have had larger export quantities of salt in the river, but the Purgatoire River exported a significant amount in a shorter time frame. There is an estimated 95% probability that the total annual mass loadings reported in Table 11 lie within a range equivalent to 59% to 142% of the temporally averaged ensemble mean load values, depending on the river and year (Gates, et al., 2018).

Table 9. Estimated maximum daily salt load (kg/day) corresponding to high points in Figure 25 and the totals from Tables 7 and 8.

	PURLASCO		ARKLASCO	
	1990	2020	1990	2020
2 SD+	7,330,000	2,110,000	2,760,000	1,710,000
1 SD+	5,600,000	1,780,000	2,240,000	1,510,000
Mean Daily Load (TDS)	3,880,000	1,440,000	1,800,000	1,310,000
1 SD-	2,150,000	1,110,000	1,440,000	1,110,000
2 SD-	643,000	780,000	1,070,000	904,000
% of Total Load	6%	8%	0.71%	0.91%

Table 10. Estimated annual salt load (kg/year) of each salt ion and the corresponding percent of the total.

	PURLASCO				ARKLASCO			
	1990	%	2020	%	1990	%	2020	%
Na	6,930,000	11	1,970,000	11	22,100,000	11	13,800,000	10
Ca	6,870,000	10	1,970,000	11	26,000,000	13	17,000,000	13
Mg	3,590,000	6	102,000	6	8,960,000	4	5,740,000	4
SO_4	34,800,000	55	9,830,000	54	112,000,000	54	70,800,000	53
K	238,000	0	68,400	0	718,000	0	490,000	0
HCO_3	9,610,000	15	2,750,000	15	31,300,000	15	21,200,000	16
Cl	1,670,000	3	476,000	3	6,960,000	3	4,420,000	3
Annual Load (TDS)	63,700,000		17,200,000		208,000,000		133,000,000	

Table 11. Estimated salt load (kg/year) for 1990 and 2020 at the Purgatoire River outlet (PURLASCO) and the Las Animas site of the Arkansas River (ARKLASCO).

	PURLASCO		ARKLASCO	
	1990	2020	1990	2020
+2 SD	90,200,000	25,600,000	298,300,000	186,000,000
+1 SD	77,500,000	21,800,000	265,900,000	165,000,000
Mean Annual Load (TDS)	64,600,000	18,000,000	234,000,000	143,000,000
-1 SD	51,800,000	14,300,000	201,000,000	122,000,000
-2 SD	39,100,000	10,600,000	169,000,000	100,000,000
Discharge (m^3)	30,700,000	8,440,000	181,000,000	120,000,000

Table 12. Yearly salt load contribution from the Purgatoire River Watershed represented as a percent of the combined total annual salt load after junction with Arkansas River.

	1990	2020
+ 2 SD	23.2%	12.1%
+ 1 SD	22.6%	11.7%
Mean	21.7%	11.2%
- 1 SD	20.5%	10.5%
- 2 SD	18.8%	9.6%
% Contribution of Total Flow	14.5%	6.55%

3.1.3d The Role of Precipitation

Precipitation plays a key role in salt transport. As Ponce et al. (1978) discussed, precipitation provides the energy to separate soil particles and the means of transportation by

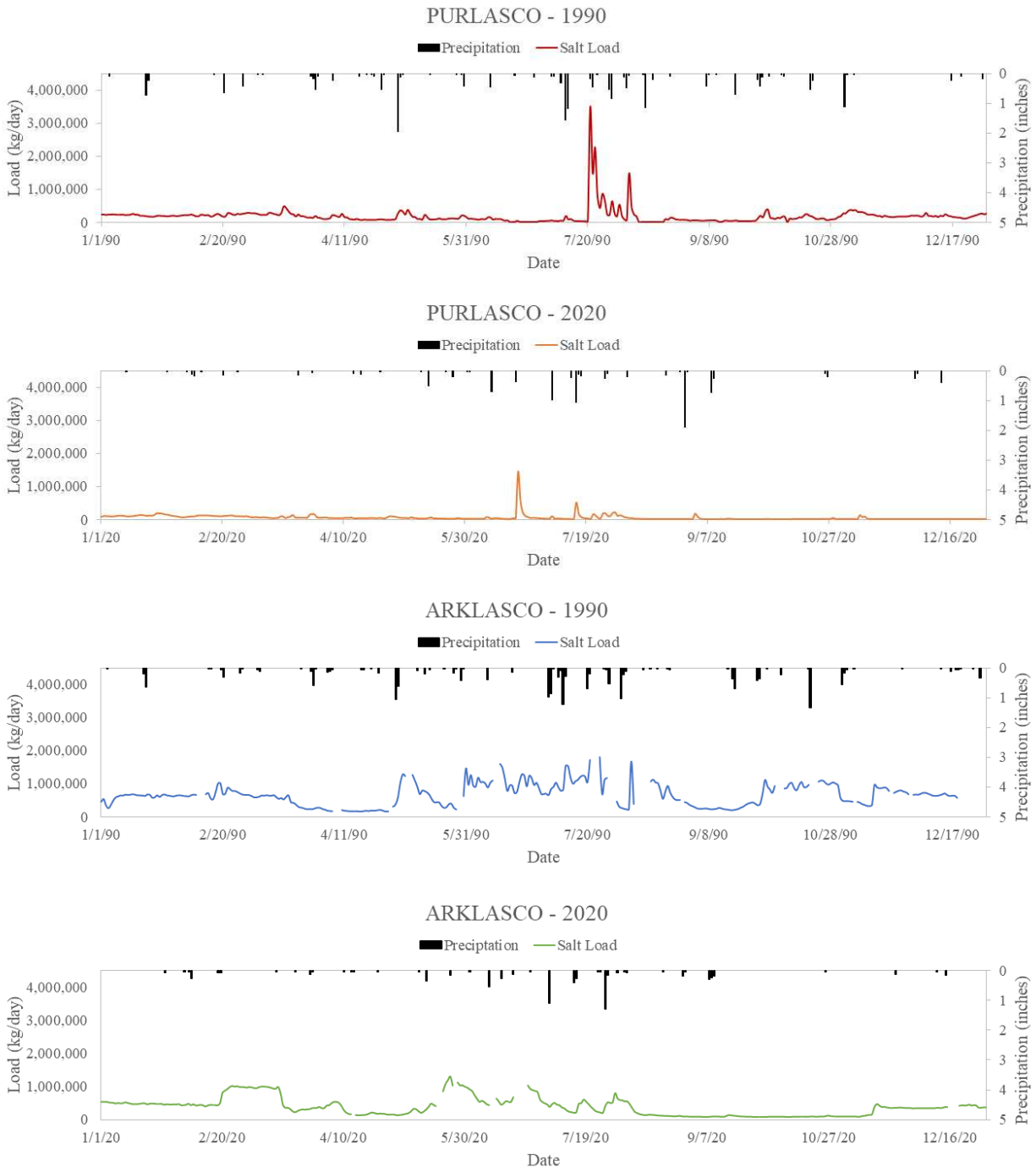

Figure 26. Time series of daily salt loading with respect to space and time and the corresponding annual precipitation events (NOAA).

which eroded particles and salt mass mobilize from the site of origination (Ponce & Hawkins, 1978). The total annual precipitation at ARKLASCO in 1990 was 17.40 inches (440 mm) and 6.68 inches (170 mm) in 2020. The total annual precipitation at PURLASCO in 1990 was 19.30 inches (490 mm) and 10.31 inches (262 mm) in 2020. The variance in salt load between the two years can perhaps be linked to the 62% and 47% difference in total annual precipitation at ARKLASCO and PURLASCO, respectively. Figure 26 illustrates a time series of flow rate and precipitation for each year and site. The time series of total daily mean salt load in this figure was calculated via the second variation, without interpolation. The actual quantities of salt load were calculated via the third method which accounts for the missing data visible in the graphs. 64,600,000 kg of salt were transported through the outlet of PURLASCO in 1990. This amount is correlated to 19.3 inches (490 mm) of precipitation. In contrast, 18,000,000 kg of salt were

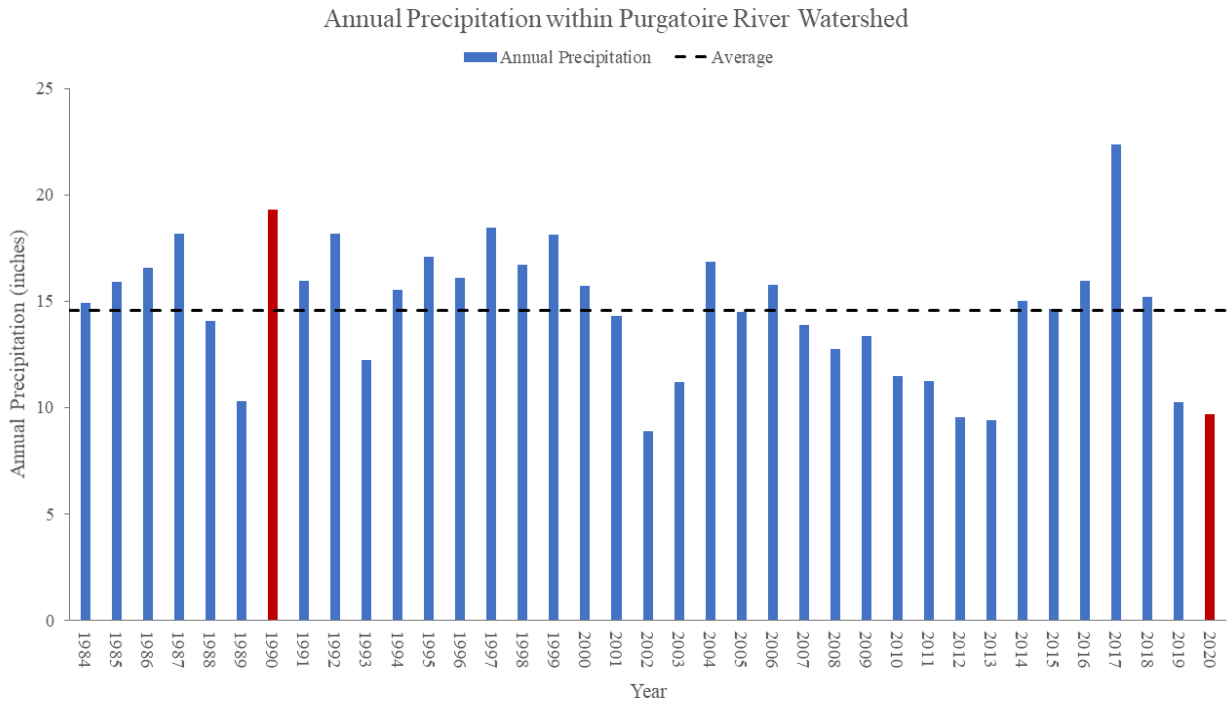

Figure 27. Bar chart of annual precipitation within the region along with the average noted by the black dashed line (NOAA).

transported through the outlet of the Purgatoire River in 2020, associated with 10.3 inches (262 mm) of precipitation. With just two years of data, it is difficult to confidently correlate precipitation with salt load; however, by monitoring the total annual salt load of the outlet and the annual quantity of precipitation over several years, a relationship between total annual salt load and total annual precipitation could be generated, providing forecasting opportunities. As such, Figure 27 illustrates the annual precipitation received by the region over 37 years.

To conclude, the percentages in Figures 22 and 23 were calculated using the total quantity of dissolved solids generated in Excel, via total annual load calculation variation two, which did not include interpolated values. In all scenarios, sulfate is the highest contributor to the total quantity of dissolved solids. The soil surrounding the tributary may be highly saturated with sulfate minerals such as calcium sulfate. The soil samples taken on three occasions confirm high levels of sulfate in the riparian soil. The percentages of sodium and calcium were similar in all cases and bicarbonate was the second most abundant salt ion in the total quantity of dissolved solids. Heightened levels of in-stream bicarbonate can be linked to calcium carbonate in the soils of draining tributaries as bicarbonate ions are created when carbon dioxide from rainwater interacts with calcium carbonate laden soils (Sparks, 2003, p. 287). The same equations were used for both time series, as such, there was not much variability from year to year or site to site, except for a few minor additions or subtractions due to changing specific conductivities and flow rates.

3.2 Controls on Salt Mobilization

3.2.1 Analysis of Salt Mobilization Index

Salt mobilization is prevalent in semi-arid regions with little plant growth and high-intensity precipitation events (Cadaret, et al., 2016). Upland catchments in the Purgatoire River

Basin provide extreme slopes for high-intensity overland flow as illustrated in Figure 5. Figure 26 illustrates the salt mobilization index calculated to predict regions within the basin with a high probability of salt mobilization. A salt mobilization index value of 1 indicated that the area had a soil composition of 36% or greater of calcium carbonate and 6% or greater of calcium sulfate, a slope greater than 50%, and a land use cover of Shrub/Scrub (land use code 52). The highest salt mobilization index value in this scenario was 0.8125, which indicated the area had a slope of 50%, the land cover was Shrub/Scrub (land use code 52), and the soil composition was comprised of greater than 36% calcium carbonate and between 4 and 5 percent calcium sulfate. There were no instances of simultaneous maximum degree for all parameters (salt mobilization index of 1). Besides 0, the lowest estimated salt mobilization index value of 0.1354 indicated the area had a slope of 25%, was not Shrub/Scrub land cover (land use code 52) and had a soil composition of either 0% calcium carbonate and 1% gypsum or 1-4% calcium carbonate and 0% gypsum. The fraction of each index is reported in Table 13.

The southwest portion of the basin is predominantly deciduous and evergreen forests. This region has mainly 0 index readings because of the land use type and low percentage of the corresponding soil components. Unfortunately, there are large regions of the soil characteristic maps with null values (no soil survey data) showcased in Figures 6 and 7. Although these regions are extremely steep and are covered by Shrub/Scrub (land use code 52) as illustrated in Figures 4 and 5, the null soil percentages cause the index value to be 0.

The purpose of the salt mobilization map was to pinpoint regions within the Purgatoire River Basin that have a high probability of generating and transporting solute to surface water. As illustrated in Figures 28 and 29, there are zones between the two field sites with high index values. The regions of yellow and red were of the most interest because they likely generate

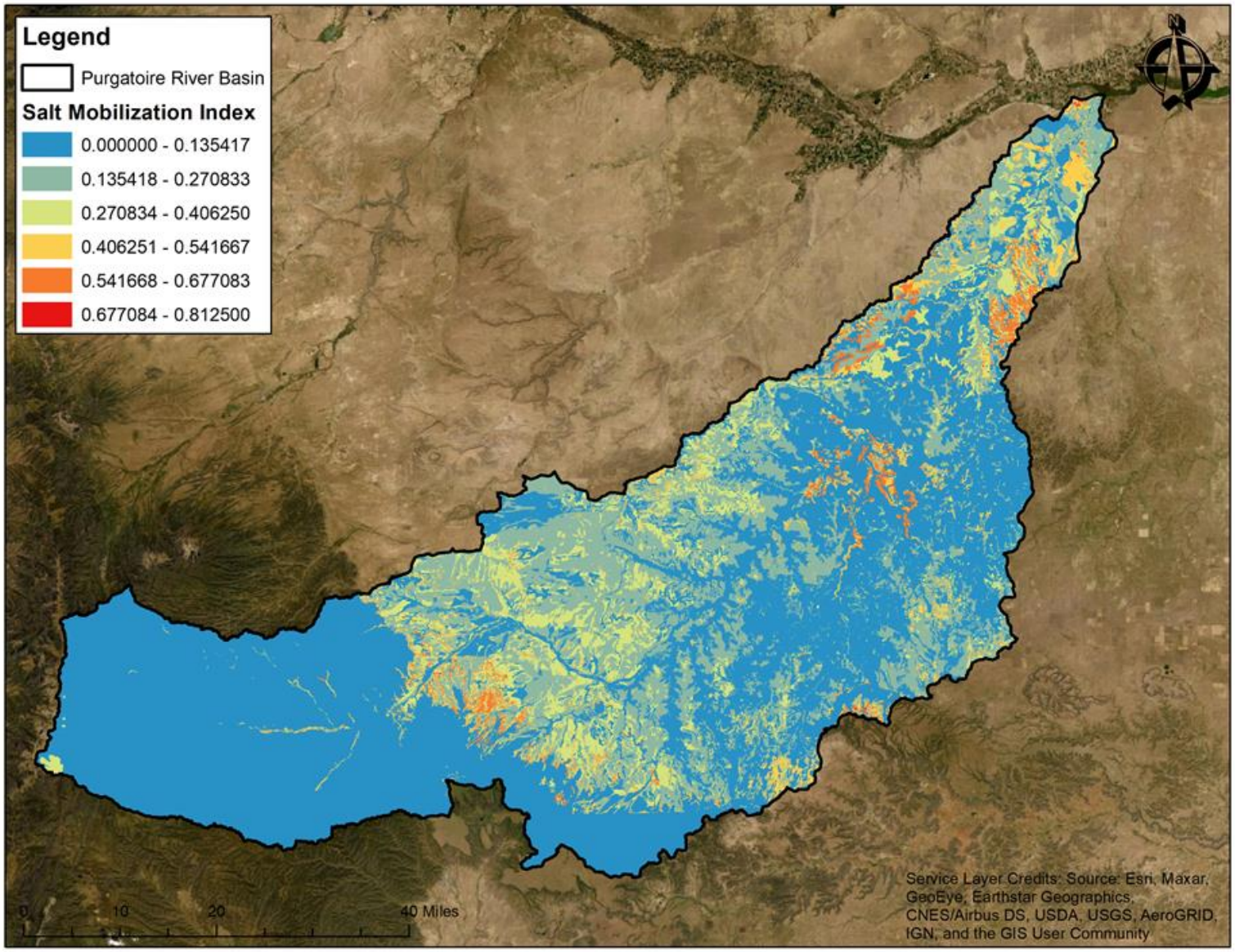

Figure 28. Spatial representation of the salt mobilization index calculated using different soil characteristics.

large salt loads. Hypothetically, the variance in the solute loads between the two sites would have captured the salt loading generated at these sites. However, due to naturally occurring adversities, the only applicable data for comparison was three months. The results of the salt mass balance are discussed in the next section.

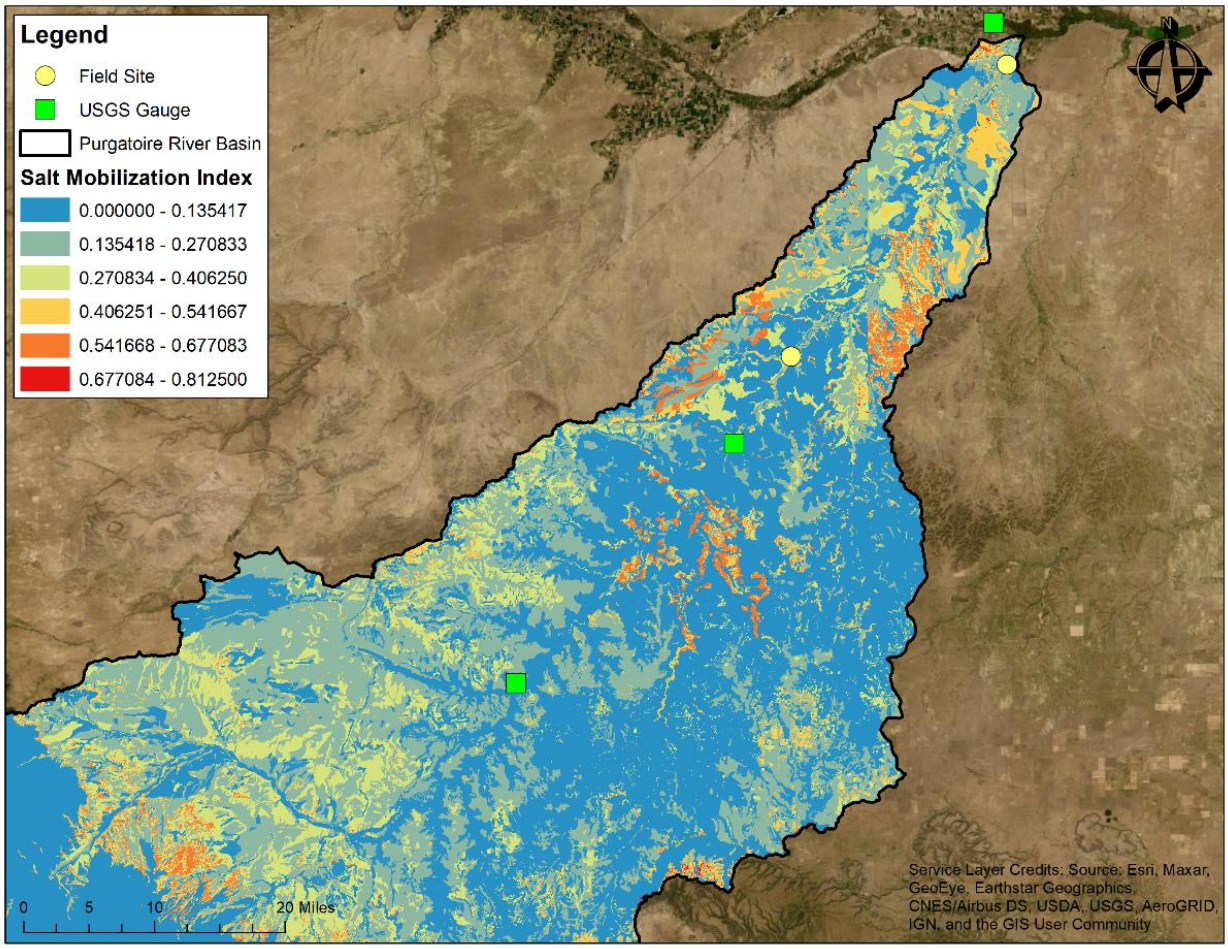

Figure 29. Magnified representation of the salt mobilization index map with respect to implemented field sites.

As an additional piece of evidence of high salt ion mass in the soils in areas near the Purgatoire River channel corridor, soil samples were taken three times over the course of this study. The riparian soil sampled at the PURNINCO site contained high levels of sodium and sulfate with one sample of sodium and sulfate representing 33% and 60% of the soil sample, respectively. The soil sampling site is illustrated in Figure 30. The upland catchments

surrounding the site at PURNINCO contain high percentages of calcium carbonate and gypsum, as detailed in Figures 6 and 7. The percent of each salt ion for the summer months of 2020 for the river and canal are illustrated in the next section in Figure 32. Unlike the salt composition of PURLASCO and ARKLASCO, PURNINCO has a higher quantity of sulfate. This is the result of high volumes of gypsum in the soil alongside steep grades. The salt mobilization index is relatively high in the tributaries draining to the Purgatoire River before reaching PURNINCO. The Purgatoire River picks up a sizeable percentage of bicarbonate (HCO_3) between the two sites. This may be linked to the high volumes of calcium carbonate in the soils of the tributaries draining to the river between the two sites. Bicarbonate ions are created as the result of carbon dioxide in water with calcium carbonate. Rainwater and respiration from plant roots or other soil organisms are typically the source of the carbon dioxide in water (Sparks, 2003, p. 287).

Table 13. The percent of each index value with respect to the entire watershed.

Index Value	Percent of Total Basin (%)
0.0000	67.65
0.1250	2.58
0.1875	3.53
0.2500	4.55
0.3125	2.97
0.3750	5.03
0.4375	3.12
0.5000	5.82
0.5625	2.64
0.6250	1.49
0.6875	0.31
0.7500	0.29
0.8125	0.02

Figure 30. Soil sampling site at PURNINCO representative of the highest measurements of sodium and sulfate.

3.2.2 Analysis of Mass Balance

A mass balance was used to support the results shown in section 3.2.1. Mass balance estimates have been used by several investigators when analyzing solute mass loading along the lengths of rivers (Gates, et al., 2018).

3.2.2a Analysis of Present Salt Mass Balance

Two sites were analyzed to better understand the impacts of summer storms on salt loading, PURNINCO and PURLASCO. These sites were installed for the purpose of this research. Specific conductivity and flow rate data between April 16, 2020, and July 16, 2020 were analyzed using linear relationships between specific conductivity and salt ion concentrations created using water quality data from April 15, 2020 through April 2, 2021. Similar to objective one, the water samples were analyzed for seven salt ions and related to

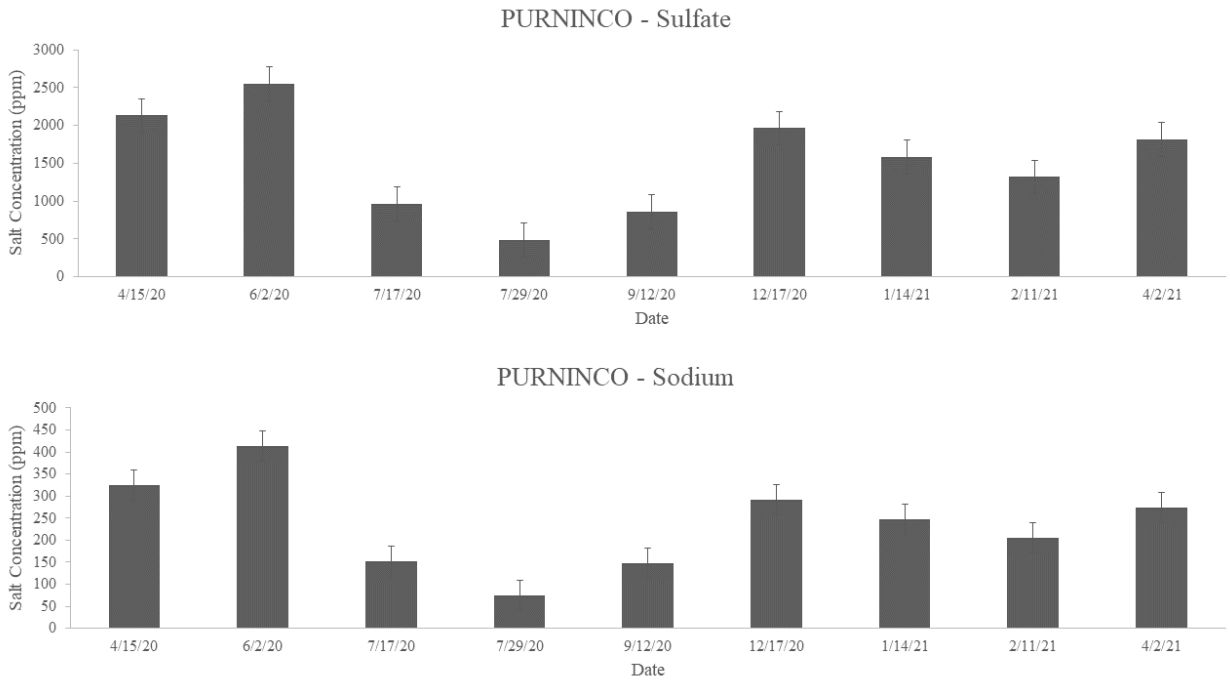

Figure 31. Bar plots of sodium and sulfate concentrations at PURNINCO organized by the date of extraction with corresponding standard error bars

specific conductivity. The concentration readings of sodium and calcium from the water samples are provided in Figure 31. Each salt ion concentration equation for PURNINCO is provided in Table 14. The total salt loads for PURLASCO, PURNINCO and NMCHIGCO are reported in Table 15.

Table 14. Individual salt ion concentration equations calculated using linear regression for the station, PURNINCO.

Salt Ion	Equation	R^2
Sodium	y = 0.134x - 78.700	0.931
Calcium	y = 0.0986x + 5.873	0.931
Magnesium	y = 0.042x - 10.882	0.917
Sulfate	y = 0.601x - 269.508	0.928
Potassium	y = 0.0007x + 3.452	0.119
Bicarbonate	y = 0.045x + 128.286	0.512
Chloride	y = 0.037x - 15.183	0.706

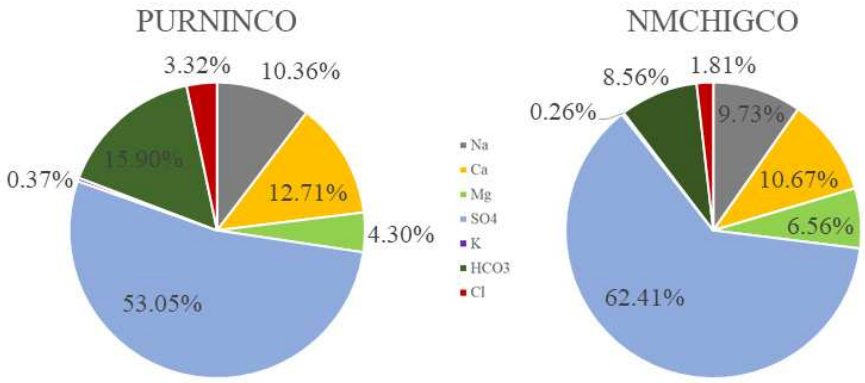

Figure 32. The percent of each salt ion in the total dissolved solids with respect to location.

As previously discussed, there is a canal diversion at the Purgatoire River dam near Higbee, Colorado where this station is located. It is important to discuss the loads and flow that the canal diverts from the river. Used predominantly for agriculture and livestock in the surrounding area, the canal can divert the flow of water between the months of March 15 and November 15 if the combined flow of the river and canal is less than 0.25 m^3/s (9 cfs). The canal transferred 11% of the total flow and 11% of the salt load from the river over the specified three months. At the same rate, annually, that equates to 44% of the salt loading.

PURNINCO experienced a large storm event on June 20, 2020, with the daily flow rate reaching 1,786,000 m^3/day (740 cfs) and the daily salt loading reaching 7,260,000 kg/day. According to the NOAA rain gauge located at *LA JUNTA 20 S, CO US* (37.75144°, -103.47671°), the area received 0.36 inches (9 mm) on June 20, 2020; no water was released from Lake Trinidad. The storm was presumably large in extent rather than in quantity of rainfall due to the magnitude of flows produced by such a low capacity of precipitation. This large storm event accounted for 96% of the sites salt loading over three summer months. Over the summer, the area received 1.72 inches of rainfall (44 mm), which was approximately 17% of the annual

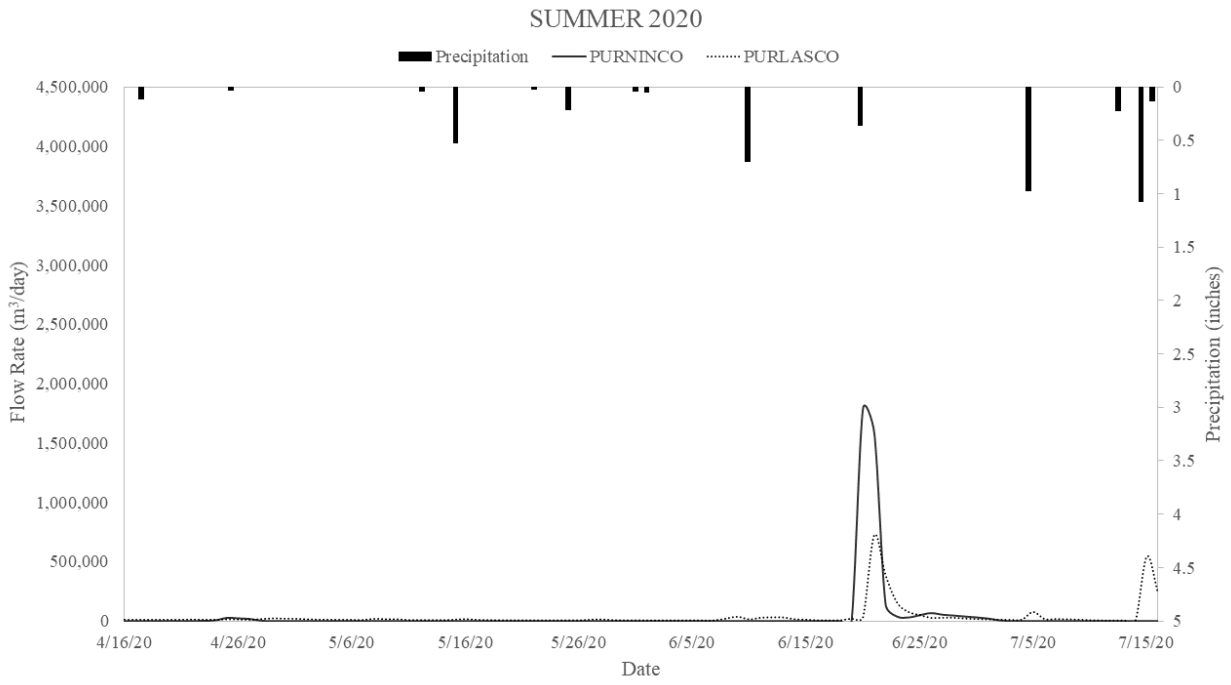

Figure 33. Time series of precipitation events and flow rates with respect to site location through the summer of 2020 (USGS) (NOAA).

precipitation in 2020. Figure 33 illustrates the relationship between flow rate and precipitation with respect to site location. This figure showcases the flow passing by PURNINCO and not the flows diverted to the canal. As explained in the Purgatoire Watershed Partnership Report (2014), "larger, less frequent storms generally contribute much more to sediment transport than smaller, more frequent storms. Storms where precipitation exceeded 1.5 inches (38 mm) accounted for about 73 percent of the suspended sediment load from 1983 through 2006. Storms where precipitation was 0.5 inch or less accounted for less than 3 percent of the sediment load, even though the small storms accounted for 79 percent of the storms."

Over 48 kilometers, the salt load decreased by roughly 40 percent over the summer of 2020. The discrepancy over the summer of 2020 in salt loading could have been influenced by a variety of environmental factors. The variance is most likely from exports by the canal or groundwater seepage. The canal exports a sizeable portion of the salt load from PURNINCO.

Additionally, there could be other unmarked diversions that export some of the salt load before reaching PURLASCO, as well. The primary cause of the large salt export passed through PURNINCO is the large storm event on June 20, 2020, accounting for 96% of the entire salt load over the summer months. Confirmed by a Colorado DWR hydrographer, the flow event was corroborated by three upstream gauges and was not the result of a release out of Lake Trinidad.

Table 15. The total salt load in kilograms passed through each site between April 16, 2020, and July 16, 2020, beginning from the most upstream site on the left.

	NMCHIGCO	PURNINCO	PURLASCO
Load (kg)	1,200,000	9,330,000	5,480,000
Annual Discharge (m^3/day)	470,000	3,990,000	3,160,000

To provide additional precipitation analysis, the region's soil moisture content should be examined. Soil that is already saturated, or becomes saturated quickly after a rain event, has no available capacity within the pores for additional water, thus increasing infiltration-excess overland flow and erosion and subsequent solute transport (George & Conacher, 1993). "If a soil has high quantities of Na^+ and the EC is low, soil permeability, hydraulic conductivity, and the infiltration rate are decreased due to swelling and dispersion of clays" (Sparks, 2003, p. 296). A more thorough analysis of runoff and sediment mobilization could be performed by understanding the basin's soil moisture content during the rainy season.

3.2.2b Analysis of Historic Salt Mass Balance

In addition to the historic analysis of PURLASCO and ARKLASCO in objective one, the USGS monitored sites PURTHACO and PURRCKCO were analyzed for the year 1990. Unfortunately, there was no current data to complete a current analysis for 2020 at both sites. The USGS gathered water samples were analyzed for multiple parameters including six of the

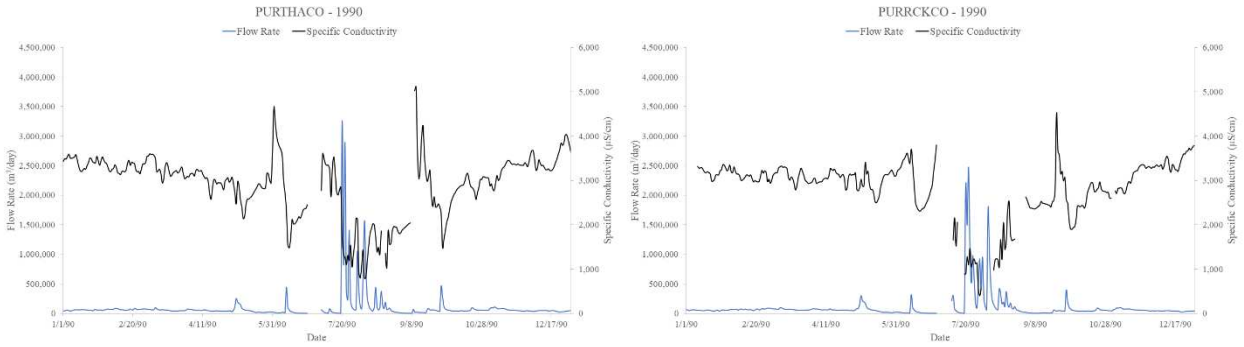

Figure 34. Time series of flow rate and specific conductivity at field sites PURTHACO (left) and PURRCKCO (right) (USGS).

seven analyzed salt ions, sodium (Na^+), calcium (Ca^{2+}), magnesium (Mg^{2+}), sulfate (SO_4^{2-}), potassium (K^+), and chloride (Cl^-). Each of the salt ion concentration equations for PURTHACO and PURRCKCO are provided in Tables 16 and 17. The time series of flow rate and specific conductivity for each site is illustrated in Figure 34. As is typical, there is an inverse relationship between specific conductivity and flow rate.

The total salt loads for PURLASCO, PURTHACO and PURRCKCO are reported in Table 18. Unfortunately, specific conductivity data for many summer days, when large storm events occur, was missing at PURTHACO and PURRCKCO. As such, the results are presented but should be interpreted accordingly. Additionally, there are zero reported canal diversions between PURTHACO and PURRCKCO and four monitored contributing tributaries. There is one reported canal diversion between PURRCKCO and PURLASCO, and five monitored stations. As such, it is difficult to be overly confident with the results and the following analysis regarding salt mobilization should be interpreted accordingly.

Table 16. Individual salt ion concentration equations calculated using linear regression for the station, PURTHACO.

Salt Ion	Equation	R^2
Na	y = 0.085x - 26.378	0.945
Ca	y = 0.082x + 13.265	0.867
Mg	y = 0.074x - 34.355	0.970
SO_4	y = 0.637x - 226.667	0.982
K	y = 0.0005x + 4.122	0.067
Cl	y = 0.013x - 3.276	0.645

Table 17. Individual salt ion concentration equations calculated using linear regression for the station, PURRCKCO.

Salt Ion	Equation	R^2
Na	y = 0.083 - 24.389	0.974
Ca	y = 0.086x + 11.764	0.953
Mg	y = 0.069x - 27.794	0.976
SO_4	y = 0.623x - 200.501	0.987
K	y = 0.0002x + 5.021	0.017
Cl	y = 0.012x - 2.561	0.870

Historically, 1990 was an unusually rainy year with frequent and intense precipitation events as illustrated in Figure 35. The total annual rainfall reached 19.3 inches (490 mm) in the center of the basin and 17.4 inches (442 mm) near ARKLASCO. Due to the same precipitation event on day 201 as previously discussed, the flow rates at PURTHACO reached 3,250,000 m^3/day and the maximum daily salt load reached 3,990,000 kg/day, accounting for 7% of the total annual salt load dispersed through this site. The flow rate and salt load at PURRCKCO reached maximum quantities two days after the large flow event at 2,470,000 m^3/day and

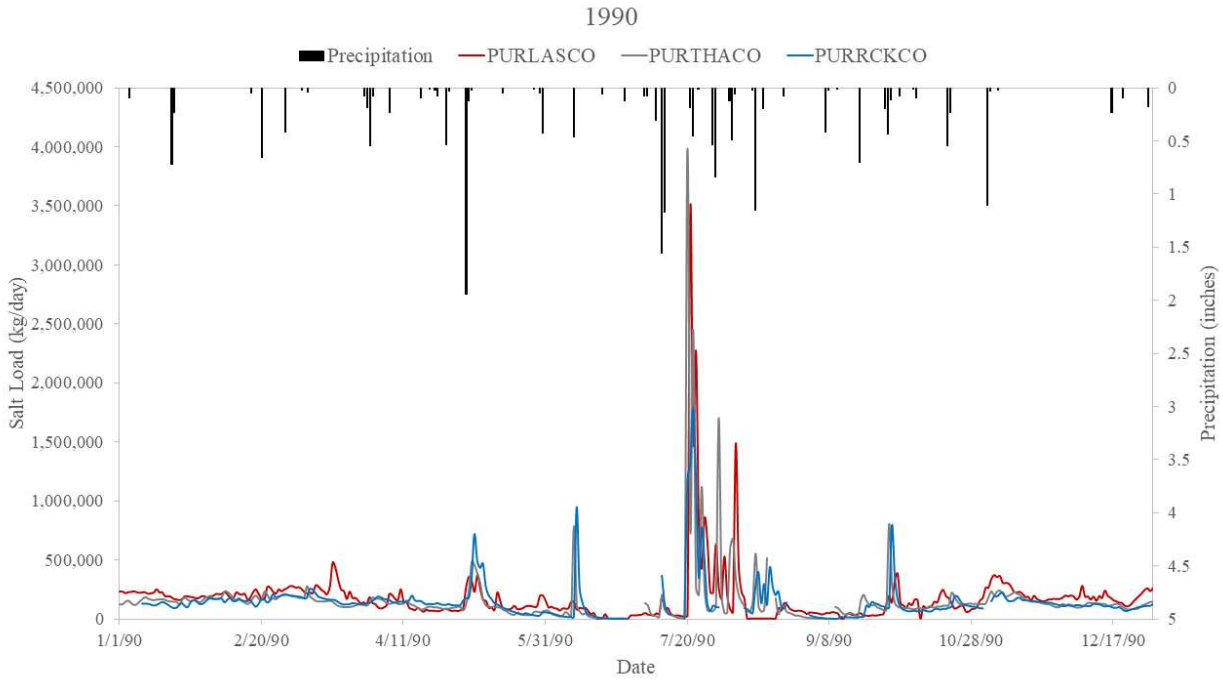

Figure 35. Time series of salt load (TDS) comparison of three different locations along the Purgatoire River with corresponding precipitation quantities (USGS) (NOAA).

1,780,000 kg/day, respectively. The daily loads resulting from the storm event accounted for 15% of the annual salt load at PURRCKCO.

There are roughly 40 kilometers (25 miles) of river between PURTHACO and PURRCKCO with an elevation declination of 230 meters (751 feet). There are approximately 64 kilometers (40 miles) between PURRCKCO and PURLASCO with an elevation difference of -264 meters (866 feet). Numerically, 187,000 kg of salt are transported to the Purgatoire River from either side for every mile between PURRCKCO and PURLASCO. Although different years, considering the decrease in salt load between PURNINCO and PURLASCO over the summer of 2020, it could be broadly hypothesized that some of the salt load in the Purgatoire River is generated in the stretch of upland catchments between PURRCKCO and PURNINCO, approximately 16 kilometers (10 miles) illustrated in Figure 36. With respect to most years, it can be assumed that some of the salt mobilization occurs between PURRCKCO and

PURLASCO as evident by the salt mobilization index map and the spatial variability in the 1990 annual salt loads.

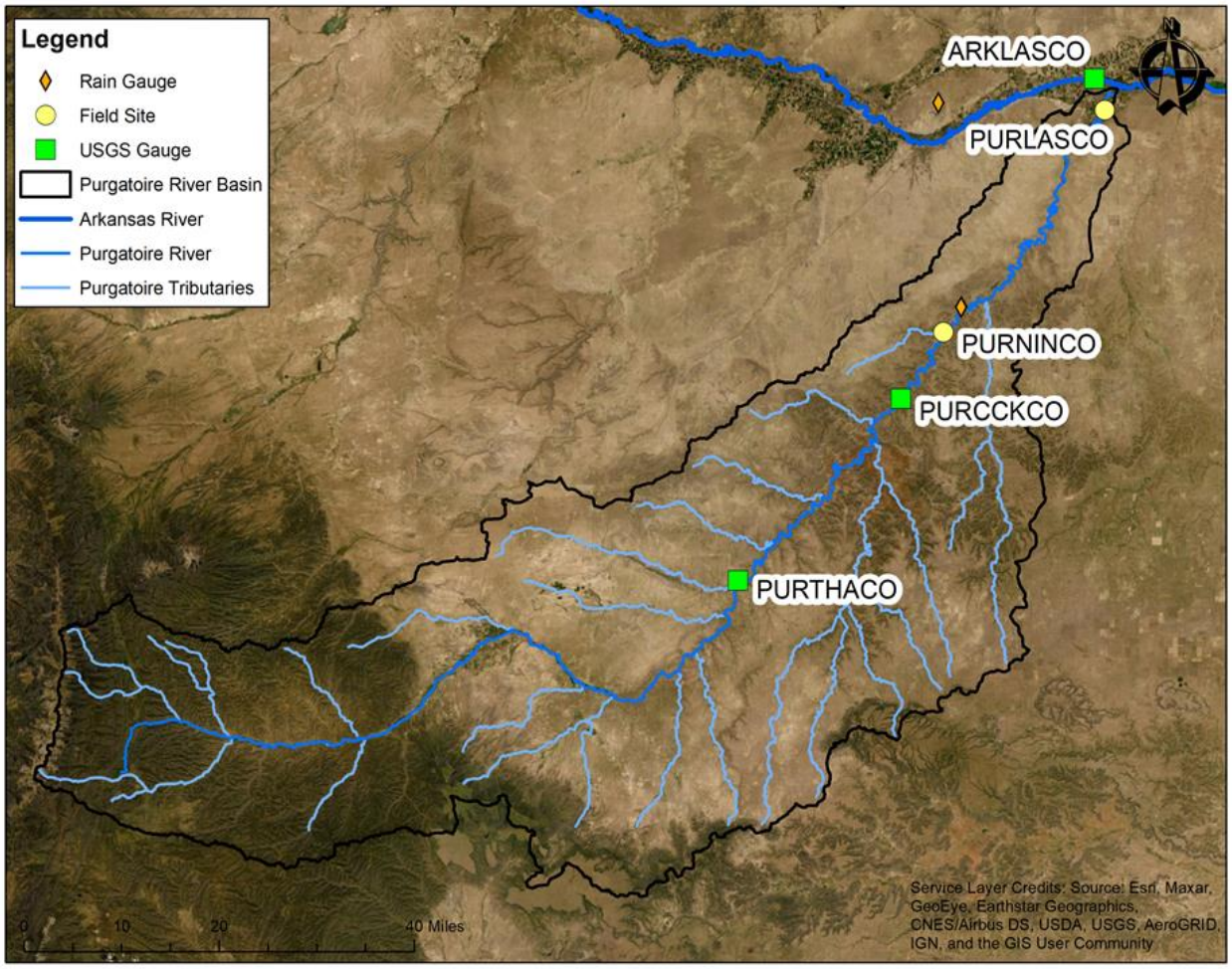

Figure 36. Map of monitoring network within the Purgatoire River Watershed.

Table 18. Annual salt load spatial variability in 1990 with the Purgatoire River Basin.

	PURTHACO	PURRCKCO	PURLASCO
Load (kg)	54,600,000	47,900,000	62,800,000
Annual Discharge (m^3)	32,800,000	35,700,000	30,700,000

A time series of daily loading rates divided into individual salt ions is detailed in Figure 37. Sulfate was the predominant salt ion at both sites, representing over 69% of the total

dissolved solids. This percent is higher than the percent of sulfate in the water at PURLASCO in 1990 of 54% as illustrated in Figure 23. This discrepancy could have been caused by the lack of the bicarbonate ion in the analysis, although it could be hypothesized that the region between PURRCKCO and PURLASCO loads the largest quantity of bicarbonate in the basin.

When reviewing the salt mobilization index map and the inverse association in mass loading values over the summer of 2020, it was concluded that the region between PURRCKCO and PURLASCO may generate most of the salt in the basin as predicted. As flow rate and load are related, it is unusual that flow rate would increase as salt load decreased; this discrepancy is the result of many missing specific conductivity values at PURRCKCO. After quickly reviewing randomly generated specific conductivity values for the null values at PURRCKCO using the Excel function NORM.INV (RAND ()), the total annual salt load jumped from 47,900,000

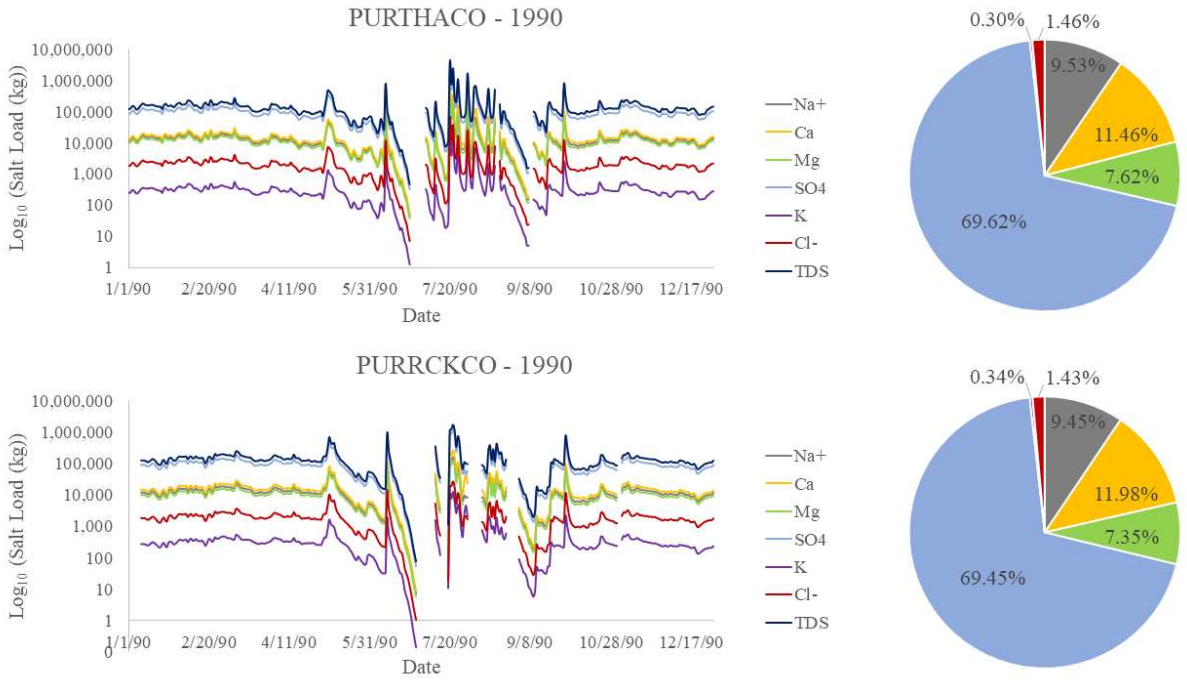

Figure 37. Time series of individual salt ion loading rates for PURTHACO and PURRCKCO in 1990. The analysis of salt ion percentages is illustrated by the pie chart to the right of the corresponding time series.

kg/year to 61,050,000 kg/year. Such analysis emphasizes that interpolation should be performed on all data sets when comparing total annual salt loads to correct for null values. Several other factors must be analyzed to verify this conclusion, such as spatiotemporal precipitation data, geologic formations, groundwater accessions, and antecedent soil moisture data.

CHAPTER 4: CONCLUSIONS AND RECOMMENDATIONS

Salt transport has been a central topic of research for decades; impacting river ecosystems, agriculture productivity and sustainability, and plant growth. The findings of this thesis are summarized in this chapter along with recommendations for future research.

Further research is required to determine the exact correlation between precipitation and salt mobilization in high-desert regions. This study was not able to create a more robust linear relationship between solute concentration and in-stream water quality parameters due to time constraints and site accessibility. Future mobilization research would benefit from incorporating a spatiotemporal precipitation factor into the salt mobilization index, as well as soil moisture content and geological features. The in-stream monitoring network will continue to be monitored by future students. The process and results of this thesis may be used in other regions of the Arkansas River Basin and other high-desert basins worldwide to assess salt contribution of natural upland catchments to river valleys as compared to contributions from largely irrigated basins.

4.1 Key Findings

4.1.1 Objective One

The first objective of this thesis is to quantify the salt load contribution from the Purgatoire River Watershed, a high-desert watershed, to the Arkansas River. The attained results of this objective are outlined below.

- The salt load exported by the Purgatoire River accounted for 11% of the salt load in the Arkansas River in 2020 and 21% in 1990. This difference is thought to be due to annual

precipitation amounts, which is 490 mm in 1990 and 262 mm in 2020. Precipitation and salt load are highly correlated; emphasized by the significant percent difference in salt load from 1990 to 2020 due to differences in precipitation. Total annual precipitation when comparing a wet year to a dry year had a degree of difference of 62% and 47% at ARKLASCO and PURLASCO, respectively, between 1990 and 2020, as the two years received different precipitation quantities. When comparing a wet year (1990) to a dry year (2020), the degree of difference in the percent of salt in the Arkansas River originating from the Purgatoire River was 48%. As a reminder, Figure 38 illustrates a bar chart that shows the annual precipitation amount for the historical record, providing an indication of what salt loading may be in the other years.

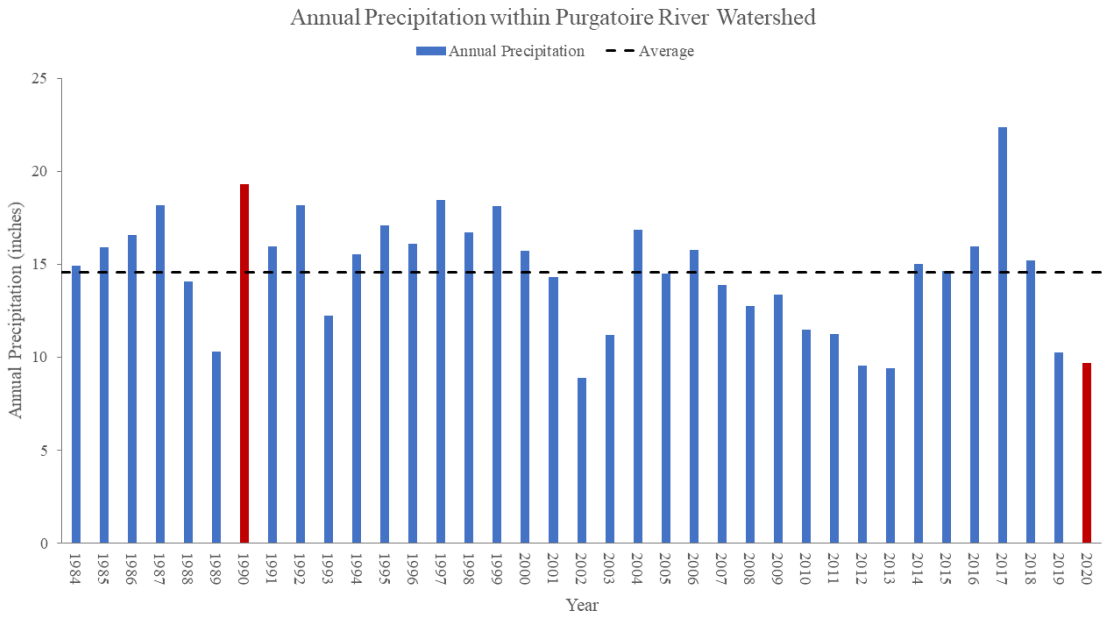

Figure 38. Bar chart of annual precipitation quantities received by the Purgatoire River Basin.

- The overall percentages of Na, Ca, Mg, SO_4, K, HCO_3, and Cl discovered at PURLASCO in 2020 are: 10.92%, 10.87%, 5.59%, 54.39%, 0.38%, 15.22%, 2.63%, respectively. Sulfate and bicarbonate make up the greatest percent of total dissolved solids likely due

to the presence of calcium carbonate and calcium sulfate in the soil throughout the watershed.

- There is an estimated 95% probability that the total annual mass loadings reported in Table 11 lie within a range of 59% to 142% of the temporally averaged ensemble mean load values, depending on the river and year.
- High percentages of total annual load are transported during intense, erosive storm events as evidenced by the transport of 96% of the total load over three months occurring during one storm event at the Purgatoire River at Ninemile Dam near Higbee, Colorado, 48 kilometers upstream of the watershed outlet.
- High-desert watershed streams, such as the Purgatoire River, transport a larger percent of the total annual salt load during large storm events. 8% of the total annual salt load at PURLASCO in 2020 was transported during one large storm event as compared to 0.91% of the total annual salt load at ARKLASCO in 2020.

4.1.2 Objective Two

The second objective of this thesis is to identify possible major environmental factors that control the mobilization of salts in natural upland catchments. The achieved results of this objective are outlined below.

- Overlaying spatial representations of slope gradient, calcium carbonate, gypsum, and land use can provide an understanding of potential locations of high salt generation.
- Bicarbonate and sulfate are the two most prominent salt ions being transported throughout the Purgatoire River Basin with large quantities of sulfate in the riparian soil.
- Salt mobilization likely occurs in the eastern catchments of the watershed, owing to salt-laden soils and steep slopes.

- The stretch of river in the western region of the watershed is heavily loaded with sulfate. Regions further east load larger quantities of bicarbonate in the basin.

Salt loading from naturally occurring basins cannot be regulated as easily as loading generated from irrigated regions. The most beneficial tool in regulating salt loading in naturally occurring basins is identifying the precursory triggers of salt transport.

4.2 Recommendations for Future Work

This study demonstrates a need for further studies to draw more definitive conclusions. Based on results from this thesis, the following recommendations will provide further understanding of salt transport in this and similar semi-arid regions with steep catchments.

- Continue to monitor electric conductivity data loggers and increase the number of water samples taken annually to create a stronger linear correlation between TDS and EC. By continuing to monitor electric conductivity in the basin, stronger conclusions will be drawn regarding salt location and movement.
- For further examination and increased accuracy of salt mobilization zones:
    - Monitor antecedent soil moisture levels before and after large precipitation events to create a stronger relationship between intense precipitation events and runoff.
    - Include a spatiotemporal precipitation map and in-depth atmospheric components such as evaporation.
    - Include geologic information of underlying rocks; emphasized by the Purgatoire Watershed Partnership Report, “watersheds composed of shale created the largest loads, while watersheds composed of sandstone or limestone had the smallest sediment load.”

- Monitor groundwater quality to evaluate groundwater accessions as compared to salt transport via surface runoff.
- Monitor total annual precipitation to create a forecast model for total annual salt load given total annual precipitation.
- Launch electric conductivity data loggers at PURTHACO and PURRCKCO to evaluate current and future salt transport through the basin via salt mass balance. Compare future data to historic data to create a stronger relationship between precipitation and salt mobilization.
- Incorporate residual error into all linear regression equations to improve accuracy.

BIBLIOGRAPHY

Adams, B. (2010, February 20). Creating Confidence Intervals for Linear Regression in EXCEL. Youtube, uploaded by ME4031. Retrieved from youtube.com/watch?v=aSOUQKqlYak&ab_channel=ME4031

Artiola, J., Walworth, J., Musil, S., & Crimmins, M. (2019). Chapter 14 - Soil and Land Pollution. In I. L. Mark L. Brusseau (Ed.), *Environmental and Pollution Science (Third Edition)* (pp. 219-235). Academic Press. doi:https://doi.org/10.1016/B978-0-12-814719-1.00014-8

Bellot, J., Golley, F., & Aguinaco, M. T. (1989). Environmental consequences of salts exports from an irrigated landscape in the ebro river Basin, Spain. *Agriculture, Ecosystems & Environment, 27*(1-4), 131-138. doi:https://doi.org/10.1016/0167-8809(89)90079-0

Bern, C. R., Holmberg, M. J., & Kisfalusi, Z. D. (2020). Salt Flushing, Salt Storage, and Controls on Selenium and Uranium: A 31-Year Mass Balance Analysis of an Irrigated Semiarid Valley. *Journal of the American Water Resources Association*, 647-668. doi:https://doi.org/10.1111/1752-1688.12841

Bhattacharya, A. (2019). Chapter 4 - Nitrogen-Use Efficiency Under Changing Climatic Conditions. In A. Bhattacharya (Ed.), *Changing Climate and Resource Use Efficiency in Plants* (pp. 181-240). Academic Press. doi:https://doi.org/10.1016/B978-0-12-816209-5.00004-0

Biggs, A. (2011). Groundwater salt accessions to land in the Queensland Murray-Darling Basin, Australia. *Hydrogeology Journal, 19*. doi:https://doi.org/10.1007/s10040-011-0714-5

Biggs, A. J., Silburn, D. M., & Power, R. E. (2013). Catchment salt balances in the Queensland Murray-Darling Basin, Australia. *Journal of Hydrology, 500*, 104-113. doi:https://doi.org/10.1016/j.jhydrol.2013.07.027

Butler, B. A., & Ford, R. G. (2018, March 31). Evaluating relationships between total dissolved solids (TDS) and total suspended solids (TSS) in a mining-influenced watershed. *Mine Water Environ., 37*(1), 18-30. doi:10.1007/s10230-017-0484-y

Cadaret, E., Nouwakpo, S., McGwire, K., Weltz, M. A., & Blank, R. R. (2016). Experimental investigation of the effect of vegetation on soil, sediment erosion, and salt transport processes in the Upper Colorado River Basin Mancos Shale formation, Price, Utah, USA. *Catena, 147*, 650-662. doi:https://doi.org/10.1016/j.catena.2016.08.024

de Vente, J., Poesen, J., Verstraeten, G., Govers, G., Vanmaercke, M., Van Rompaey, A., . . . Boix-Fayos, C. (2013). Predicting soil erosion and sediment yield at regional scales: Where do we stand? *Earth-Science Reviews, 127*, 16-29. doi:https://doi.org/10.1016/j.earscirev.2013.08.014

Donald W. Meals, R. P. (2013). *Tech Notes 8: Pollutant Load Estimation for Water Quality Monitoring Projects.* Fairfax, VA: Developed for U.S. Environmental Protection Agency

by Tetra Tech Inc. Retrieved from https://www.epa.gov/polluted-runoff-nonpoint-source-pollution/nonpoint-source-monitoring-technical-notes

Fondriest Environmental, Inc. (2014, March 3). *Conductivity, Salinity and Total Dissolved Solids.* Retrieved from Fundamentals of Environmental Measurements: https://www.fondriest.com/environmental-measurements/parameters/water-quality/conductivity-salinity-tds/

Gates, T. K., Burkhalter, J. P., Labadie, J. W., Valliant, J. C., & Broner, I. (2002). Monitoring and Modeling Flow and Salt Transport in a Salinity-Threatened Irrigated Valley. *Journal of Irrigation and Drainage Engineering, 128*(2), 87-99. doi:https://doi.org/10.1061/(ASCE)0733-9437(2002)128:2(87)

Gates, T., Cox, J., & Morse, K. (2018). Uncertainty in mass-balance estimates of regional irrigation induced return flows and pollutant loads of a river. *Jounral of Hydrology: Regional Studies, 19*, 193-210. doi:https://doi.org/10.1016/j.ejrh.2018.09.004

Gates, T., Garcia, L., & Labadie, J. (2006). *Toward Optimal Water Management in Colorado's Lower Arkansas River Valley: Monitoring and Modeling to Enhance Agriculture and Environment.* Colorado State University.

George, R. J., & Conacher, A. J. (1993). Mechanisms responsible for streamflow generation on a small, salt-affected and deeply weathered hillslope. *Earth Surface Processes & Landforms, 18*, 291-309. doi:https://doi.org/10.1002/esp.3290180402

Goff, K., Lewis, M. E., Person, M. A., & Konikowd, L. F. (1998). Simulated Effects of Irrigation on Salinity in the Arkansas River Valley in Colorado. *Groundwater, 36*(1), 76-86. doi:https://doi.org/10.1111/j.1745-6584.1998.tb01067.x

Harper, R., Dell, B., Ruprecht, J., Sochacki, S., & Smettem, K. (2021). Chapter 7 - Salinity and the reclamation of salinized lands. In M. A. John A. Stanturf (Ed.), *Soils and Landscape Restoration* (pp. 193-208). Academic Press. doi:https://doi.org/10.1016/B978-0-12-813193-0.00007-2

Hayes, A. (2021, April 19). *Confidence Intervals.* (G. Scott, Ed.) Retrieved from Investopedia: investopedia.com/terms/c/confidenceinterval.asp

Helsel, D. R., Hirsch, R. M., Ryberg, K. R., Archfield, S. A., & Gilroy, E. J. (2020). *Statistical Methods in Water Resources: U.S. Geological Survey Techniques and Methods, book 4, chapter A3.* doi:https://doi.org/10.3133/tm4a3

Hoagstrom, C. (2009). Causes and Impacts of Salinization in the Lower Pecos River. *Great Plains Research, 19*(1), 27-44.

Imadi, S. R., Shah, S. W., Kazi, A. G., Azooz, M., & Ahmad, P. (2016). Chapter 18 - Phytoremediation of Saline Soils for Sustainable Agricultural Productivity. In P. Ahmad (Ed.), *Plant Metal Interaction* (pp. 455-468). Elsevier. doi:https://doi.org/10.1016/B978-0-12-803158-2.00018-7

In-Situ. (2016). *Aqua TROLL 600 Multiparameter Sonde Operator's Manual.* Retrieved from https://in-situ.com/pub/media/support/documents/Aqua-TROLL-600-Manual.pdf

Kalev, S. D., & Toor, G. S. (2018). Chapter 3.9 - The Composition of Soils and Sediments. In T. D. Béla Török (Ed.), *Green Chemistry* (pp. 339-357). Elsevier. doi:https://doi.org/10.1016/B978-0-12-809270-5.00014-5

Kennedy, C. M., James, O. R., David, T. M., Sharon, B.-M., & Joseph, K. (2019, March). Managing the middle: A shift in conservation priorities based on the global human modification gradient. *Global Change Biology, 25*(3), 811-826. doi:https://doi.org/10.1111/gcb.14549

Kerr, J. G. (2017). Multiple land use activities drive riverine salinization in a large, semi-arid river basin in western Canada. *Limnology and oceanography, 62*(4), 1331-1345. doi:10.1002/lno.10498

Langbein, W. B., & Schumm, S. A. (1958). Yield of sediment in relation to mean annual precipitation. *EOS, Transactions American Geophysical Union, 39*(6), 1076-1084. doi:https://doi.org/10.1029/TR039i006p01076

Laronne, J. B., & Shen, H. W. (1982). The effect of erosion on solute pickup from Mancos Shale hillslopes, Colorado, U.S.A. *Jounral of Hydrology, 59*(1-2), 189-207. doi:https://doi.org/10.1016/0022-1694(82)90011-7

Maas, E. V., & Grattan, S. (1999). Crop yields as affected by salinity. In R. W. Skaggs, & J. van Schilfgaarde, *Agricultural Drainage* (Vol. 38, pp. 55-108). doi:10.2134/agronmonogr38

Meals, D. W., Richards, R. P., & Dressing, S. A. (April 2013). *Pollutant load estimation for water quality monitoring projects. Tech Notes 8.* Fairfax, VA: Developed for U.S. Environmental Protection Agency by Tetra Tech Inc. Retrieved from https://www.epa.gov/polluted-runoff-nonpoint-source-pollution/nonpoint-source-monitoring-technical-notes

Neely, B., Kettler, S., Horsman, J., Pague, C., Rondeau, R., Smith, R., . . . Klavetter, M. (2006). *Central Shortgrass Prairie Ecoregional Assessment and Partnership Initiative.* The Nature Conservancy of Colorado and the Shortgrass Prairie Partnership.

Nouwakpo, S. K., Weltz, M. A., Arslan, A., Green, C. H., & Al-Hamdan, O. Z. (2018). Process-Based Modeling of Infiltration, Soil Loss, and Dissolved Solids on Saline and Sodic Soils. *Transactions of the ASABE, 61*(3), 1033-1048. doi:https://doi.org/10.13031/trans.12705

Paul, B. K., & Rashid, H. (2017). Chapter Five - Salinity Intrusion and Impacts. In B. K. Paul, & H. Rashid (Eds.), *Climatic Hazards in Coastal Bangladesh* (pp. 153-182). Butterworth-Heinemann. doi:https://doi.org/10.1016/B978-0-12-805276-1.00005-3

Ponce, S. L., & Hawkins, R. H. (1978). SALT PICKUP BY OVERLAND FLOW IN THE PRICE RIVER BASIN, UTAH. *Journal of the American Water Works Association, 14*(5), 1187-1200.

Purgatoire Watershed Partnership. (2014). *Purgatoire River Watershed Plan.* Trinidad, CO: Bureau of Reclamation WaterSMART Cooperative Watershed Management. doi:https://www.usbr.gov/watersmart/cwmp/docs/plans/Spanish-Peaks-Purtgatoire-Conservation-District.pdf

Soil Survey Staff, NRCS, USDA. (n.d.). *Hydologic Soil Group.* Retrieved from Web Soil Survey: http://websoilsurvey.nrcs.esda.gov/

Soil Survey Staff, United States Department of Agriculture, Natural Resources Conservation Service. (n.d.). Web Soil Survey. Retrieved from http://websoilsurvey.sc.egov.esda.gov/

Sparks, D. L. (2003). 10 - The Chemistry of Saline and Sodic Soils. In D. L. Sparks, *Environmental Soil Chemistry (Second Edition)* (pp. 285-300). Academic Press. doi:https://doi.org/10.1016/B978-012656446-4/50010-4

Stenson, M., Littleboy, M., & Gilfedder, M. (2011). Estimation of water and salt generation from unregulated upland catchments. *Environmental Modeling & Software, 26*(11), 1268-1278. doi:https://doi.org/10.1016/j.envsoft.2011.05.013

Stroud, H. B. (2019, September 18). *Arkansas River.* Retrieved from Encyclopedia of Arkansas: https://encyclopediaofarkansas.net/entries/arkansas-river-2225/

Survey, U. G. (2019). National Hydrgraphy Dataset (NHD) (USGS Watershed Boundary Dataset (WBD) for 2-digit Hydrologic Unit - 11 (published 20201002)). Retrieved from https://www.usgs.gov/core-science-systems/ngp/national-hydrography/access-national-hydrography-products

Tanji, K. K. (2002). Salinity in the Soil Environment. In U. L. A. Lauchli, *Salinity: Environment - Plants - Molecules* (pp. 21-51). Springer, Dordrecht. doi:https://doi.org/10.1007/0-306-48155-3_2

United States Environmental Protection Agency. (2020, October). *Polluted Runoff: Nonpoint Source (NPS) Pollution*. Retrieved from EPA: https://www.epa.gov/nps/basic-information-about-nonpoint-source-nps-pollution#facts

United States Geological Survey (USGS). (2016). *National Land Cover Database.* Multi-Resolution Land Characteristics Consortium (MRLC).

Vengosh, A. (2003). Salinization and Saline Environments. In H. D. Holland, & K. K. Turekian (Eds.), *Treatise on Geochemistry* (pp. 1-35). Pergamon. doi:https://doi.org/10.1016/B0-08-043751-6/09051-4

Warburton, J. (2009). Sediment Transfer in Steep Upland Catchments (Northern England, UK): Landform and Sediment Source Coupling. In J.-C. Otto, & R. Dikau, *Landform - Structure, Evolution, Process Control. Lecture Notes in Earth Sciences* (Vol. 115, pp. 165-183). Springer, Berlin, Heidelberg. doi:https://doi.org/10.1007/978-3-540-75761-0_11

Williams, W. (2001). Anthropogenic salinisation of inland waters. In J. M. Melack, R. Jellison, & D. B. Herbst (Eds.), *Saline Lakes* (pp. 329-337). Springer, Dordrecht. doi:https://doi.org/10.1007/978-94-017-2934-5_30

Zaman, M., Shahid, S. A., & Heng, L. (2018). *Guideline for Salinity Assessment, Mitigation and Adaptation Using Nuclear and Related Techniques.* Springer, Cham. doi:https://doi.org/10.1007/978-3-319-96190-3

APPENDICES

APPENDIX A: BAR PLOTS OF SALT CONCENTRATIONS FOR EACH SITE OVER TIME

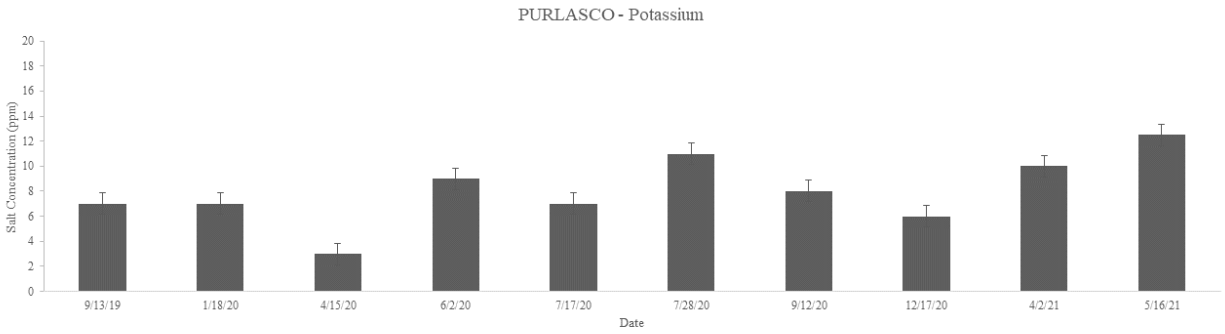

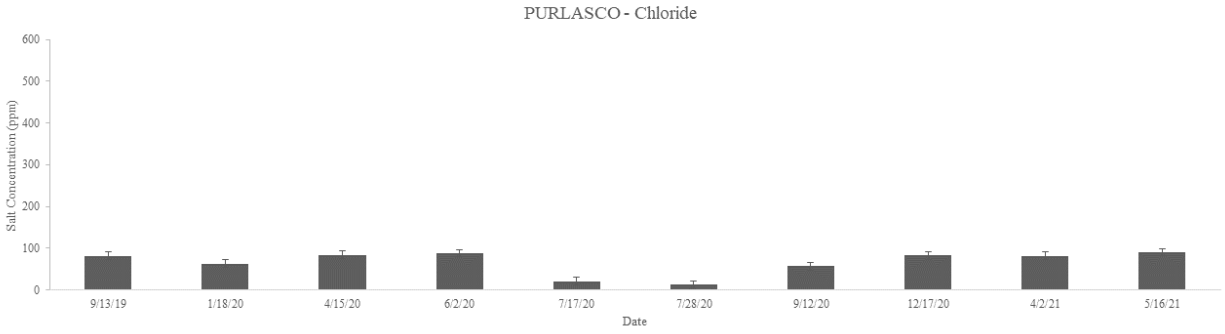

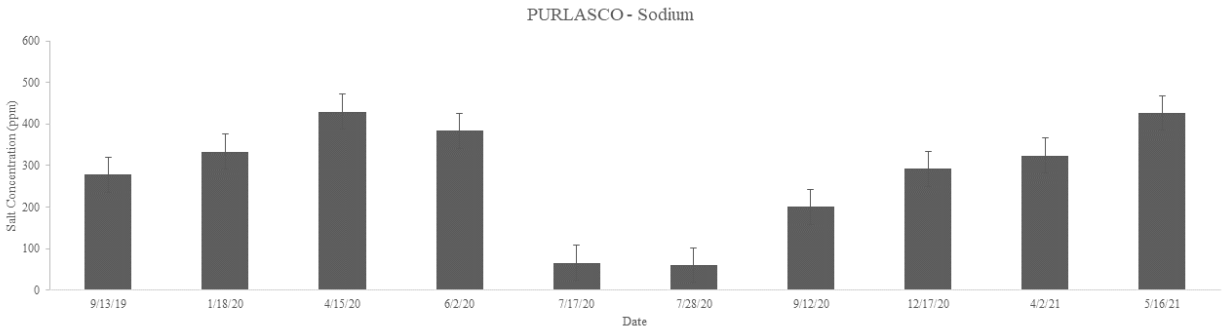

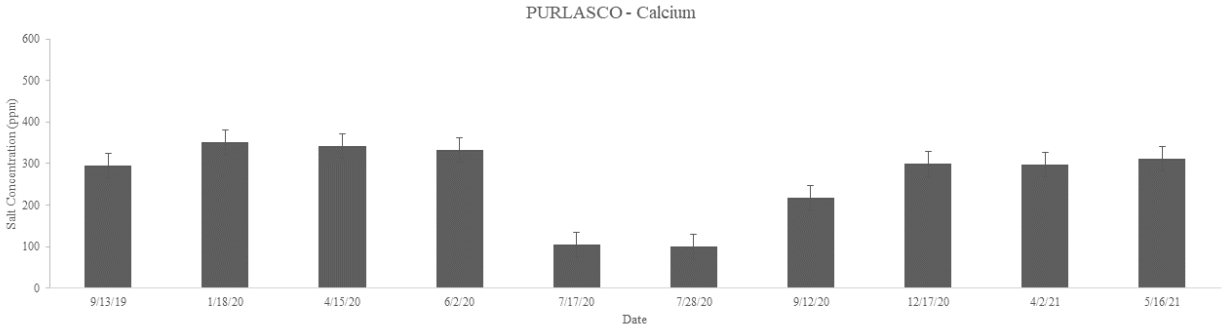

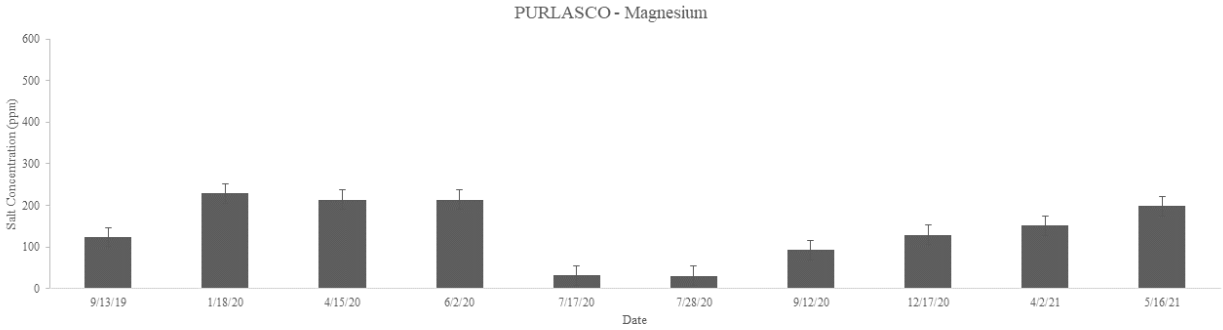
PURLASCO - Magnesium
Salt Concentration (ppm)
600
500
400
300
200
100
0
9/13/19
1/18/20
4/15/20
6/2/20
7/17/20
7/28/20
9/12/20
12/17/20
4/2/21
5/16/21
Date

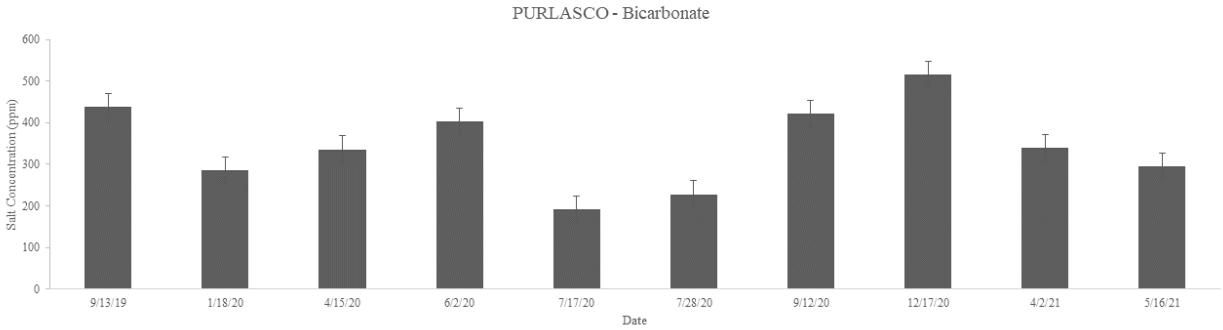
PURLASCO - Bicarbonate
Salt Concentration (ppm)
600
500
400
300
200
100
0
9/13/19
1/18/20
4/15/20
6/2/20
7/17/20
7/28/20
9/12/20
12/17/20
4/2/21
5/16/21
Date

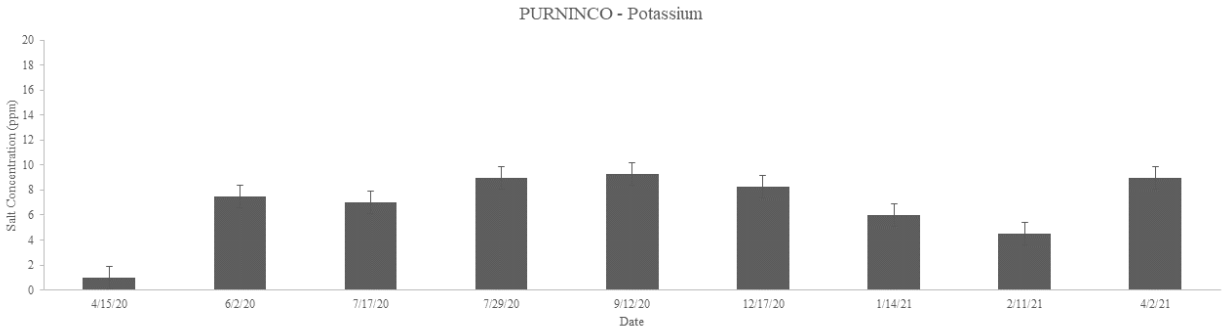
PURNINCO - Potassium
Salt Concentration (ppm)
20
18
16
14
12
10
8
6
4
2
0
4/15/20
6/2/20
7/17/20
7/29/20
9/12/20
12/17/20
1/14/21
2/11/21
4/2/21
Date

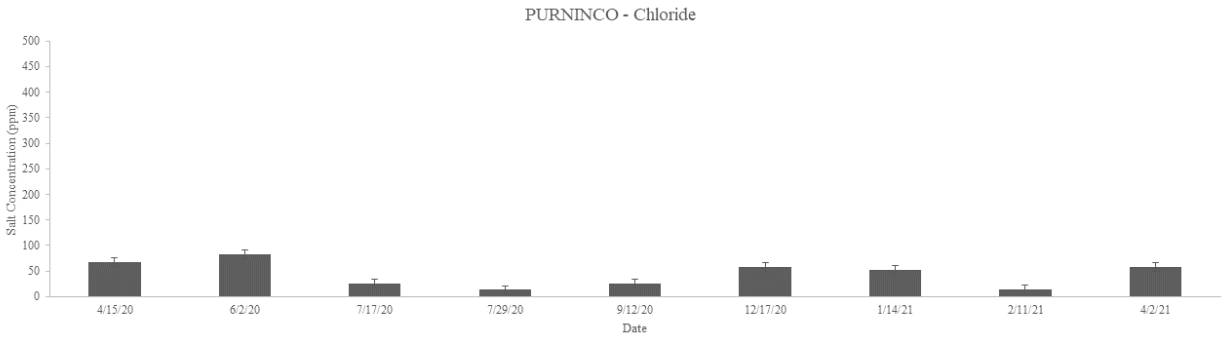
PURNINCO - Chloride
Salt Concentration (ppm)
500
450
400
350
300
250
200
150
100
50
0
4/15/20
6/2/20
7/17/20
7/29/20
9/12/20
12/17/20
1/14/21
2/11/21
4/2/21
Date

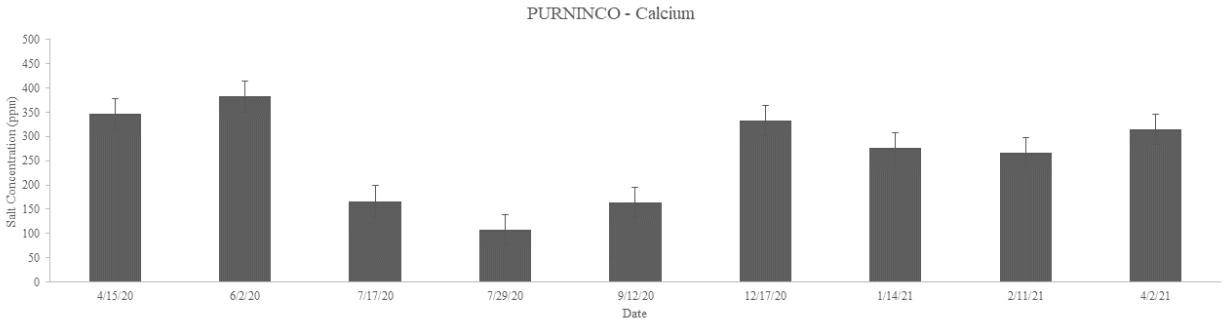
PURNINCO - Calcium
Salt Concentration (ppm)
500
450
400
350
300
250
200
150
100
50
0
4/15/20
6/2/20
7/17/20
7/29/20
9/12/20
12/17/20
1/14/21
2/11/21
4/2/21
Date

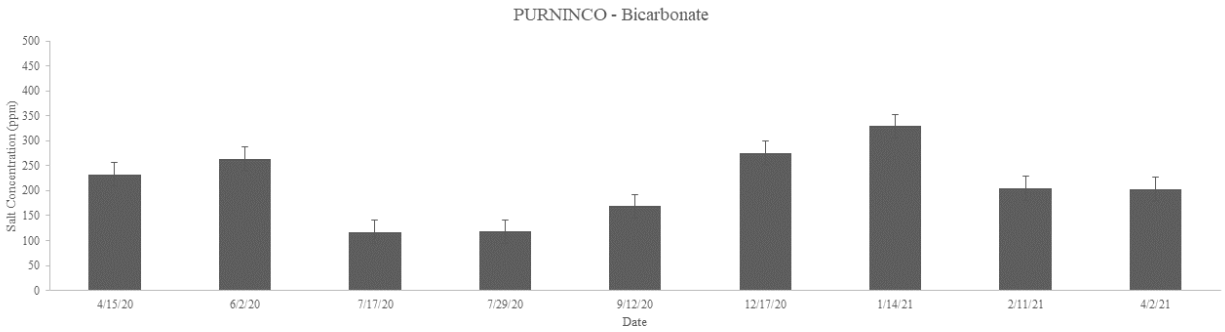
PURNINCO - Bicarbonate
Salt Concentration (ppm)
500
450
400
350
300
250
200
150
100
50
0
4/15/20
6/2/20
7/17/20
7/29/20
9/12/20
12/17/20
1/14/21
2/11/21
4/2/21
Date

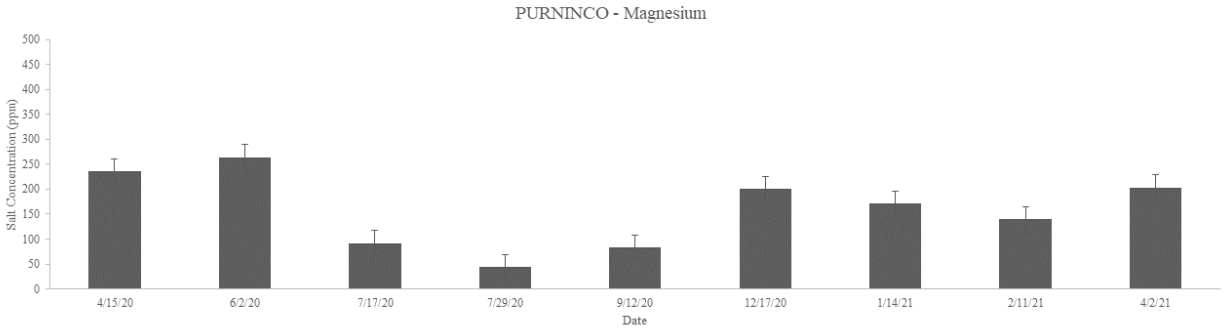
PURNINCO - Magnesium
Salt Concentration (ppm)
500
450
400
350
300
250
200
150
100
50
0
4/15/20
6/2/20
7/17/20
7/29/20
9/12/20
12/17/20
1/14/21
2/11/21
4/2/21
Date

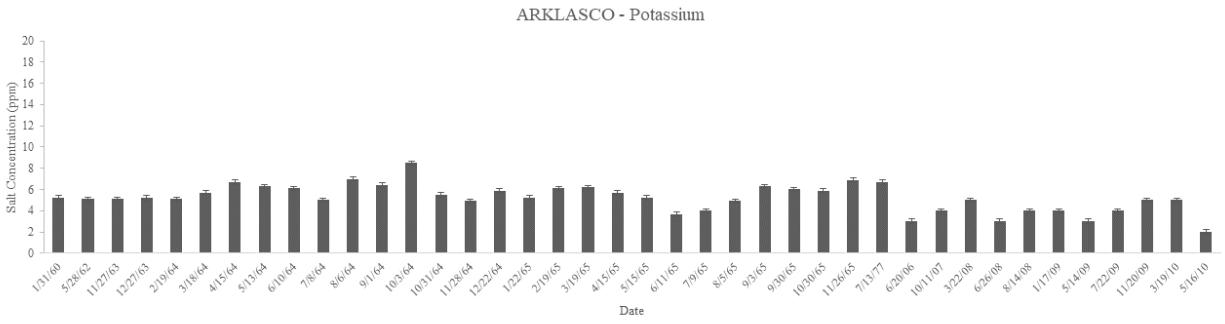
ARKLASCO - Potassium
Salt Concentration (ppm)
Date

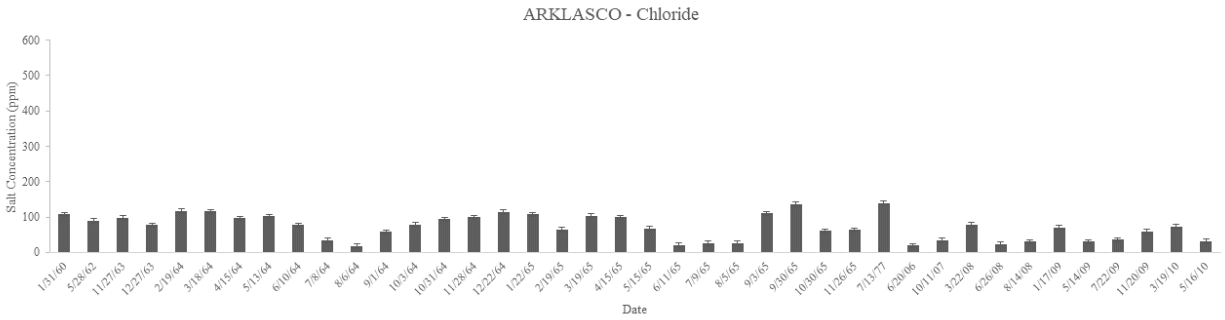
ARKLASCO - Chloride
Salt Concentration (ppm)
Date

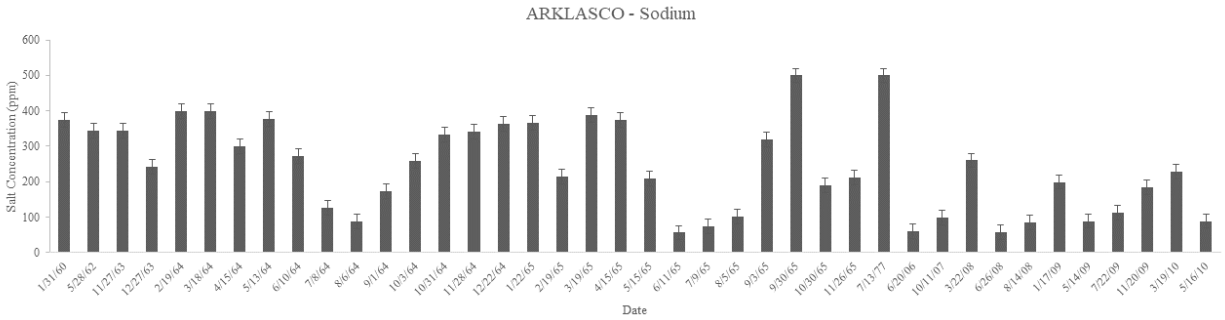
ARKLASCO - Sodium
Salt Concentration (ppm)
Date

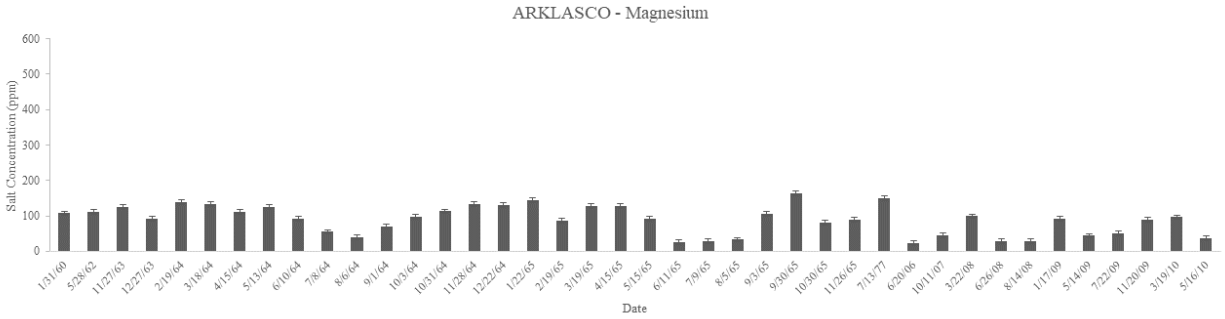
ARKLASCO - Magnesium
Salt Concentration (ppm)
Date

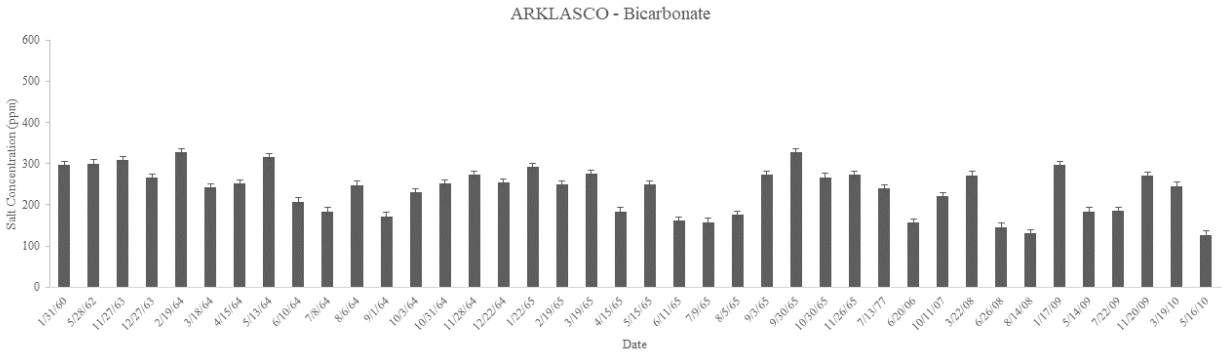
ARKLASCO - Bicarbonate
Salt Concentration (ppm)
600
500
400
300
200
100
0
1/31/60
5/28/62
11/27/63
12/27/63
2/19/64
3/18/64
4/15/64
5/13/64
6/10/64
7/8/64
8/6/64
9/1/64
10/3/64
10/31/64
11/28/64
12/22/64
1/22/65
2/19/65
3/19/65
4/15/65
5/15/65
6/11/65
7/9/65
8/5/65
9/3/65
9/30/65
10/30/65
11/26/65
7/13/77
6/20/06
10/11/07
3/22/08
6/26/08
8/14/08
1/17/09
5/14/09
7/22/09
11/20/09
3/19/10
5/16/10
Date

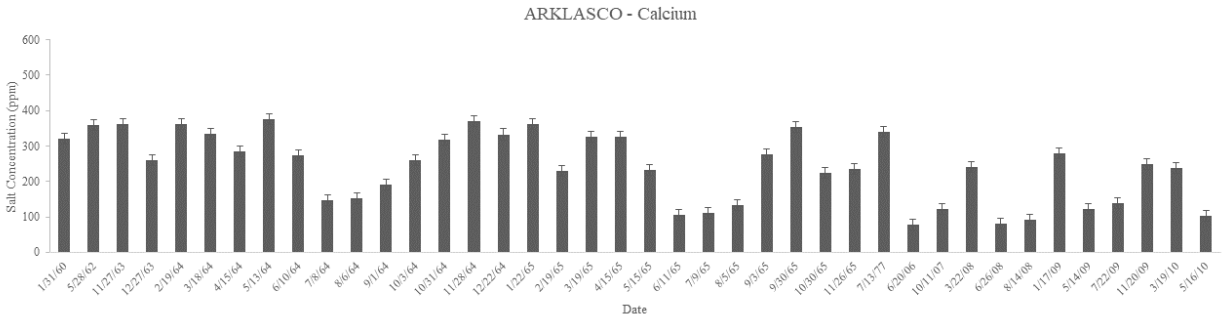
ARKLASCO - Calcium
Salt Concentration (ppm)
600
500
400
300
200
100
0
1/31/60
5/28/62
11/27/63
12/27/63
2/19/64
3/18/64
4/15/64
5/13/64
6/10/64
7/8/64
8/6/64
9/1/64
10/3/64
10/31/64
11/28/64
12/22/64
1/22/65
2/19/65
3/19/65
4/15/65
5/15/65
6/11/65
7/9/65
8/5/65
9/3/65
9/30/65
10/30/65
11/26/65
7/13/77
6/20/06
10/11/07
3/22/08
6/26/08
8/14/08
1/17/09
5/14/09
7/22/09
11/20/09
3/19/10
5/16/10
Date

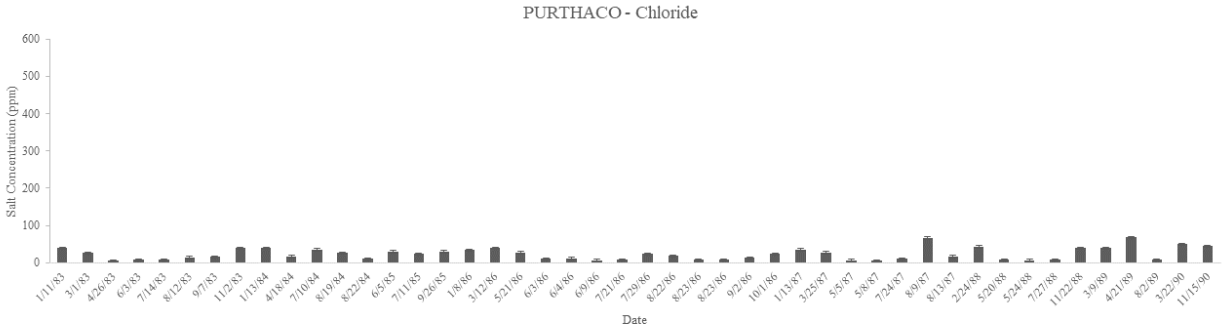
PURTHACO - Chloride
Salt Concentration (ppm)
600
500
400
300
200
100
0
1/11/83
3/1/83
4/26/83
6/3/83
7/14/83
8/12/83
9/7/83
11/2/83
1/13/84
4/18/84
7/10/84
8/19/84
8/22/84
6/5/85
7/11/85
9/26/85
1/8/86
3/12/86
5/21/86
6/3/86
6/4/86
6/9/86
7/21/86
7/29/86
8/22/86
8/23/86
8/23/86
9/2/86
10/1/86
1/13/87
3/25/87
5/5/87
5/8/87
7/24/87
8/9/87
8/13/87
2/24/88
5/20/88
5/24/88
7/27/88
11/22/88
3/9/89
4/21/89
8/2/89
3/22/90
11/15/90
Date

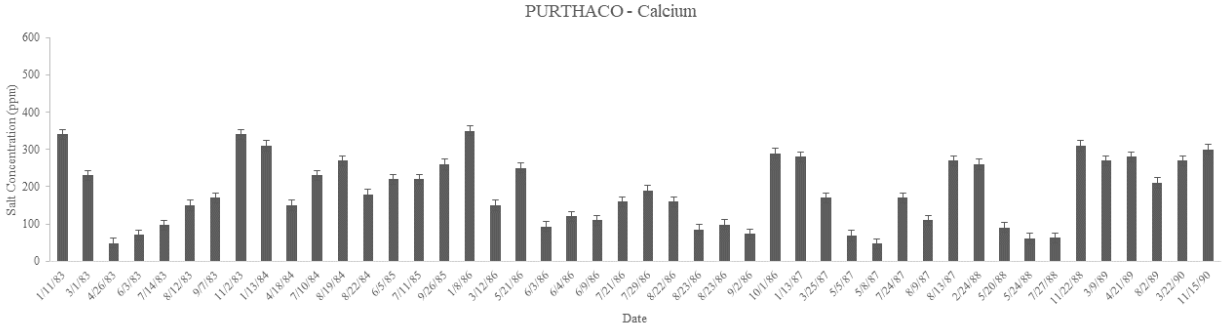
PURTHACO - Calcium
Salt Concentration (ppm)
600
500
400
300
200
100
0
1/11/83
3/1/83
4/26/83
6/3/83
7/14/83
8/12/83
9/7/83
11/2/83
1/13/84
4/18/84
7/10/84
8/19/84
8/22/84
6/5/85
7/11/85
9/26/85
1/8/86
3/12/86
5/21/86
6/3/86
6/4/86
6/9/86
7/21/86
7/29/86
8/22/86
8/23/86
8/23/86
9/2/86
10/1/86
1/13/87
3/25/87
5/5/87
5/8/87
7/24/87
8/9/87
8/13/87
2/24/88
5/20/88
5/24/88
7/27/88
11/22/88
3/9/89
4/21/89
8/2/89
3/22/90
11/15/90
Date

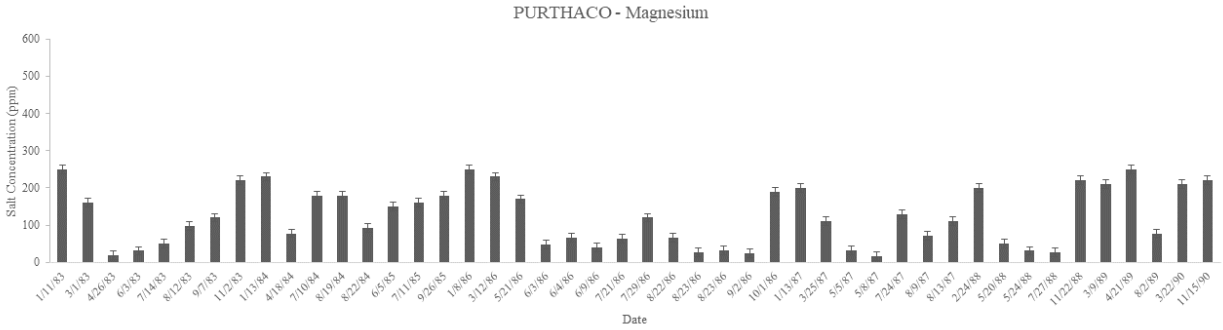
PURTHACO - Magnesium
Salt Concentration (ppm)
Date

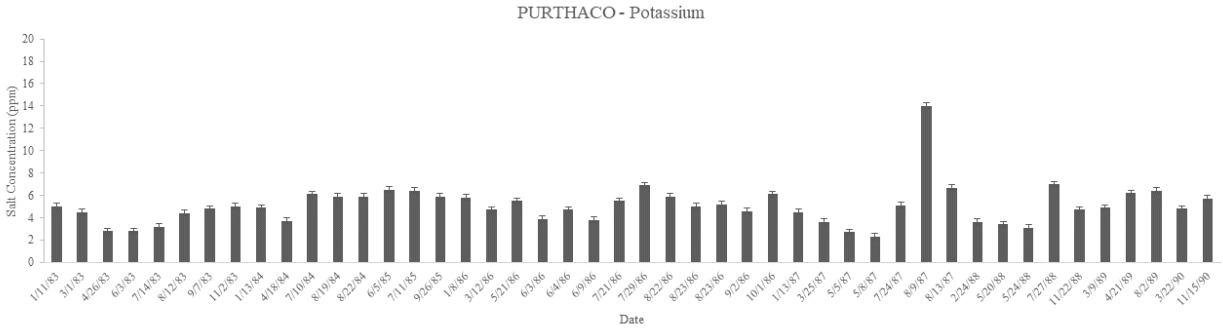
PURTHACO - Potassium
Salt Concentration (ppm)
Date

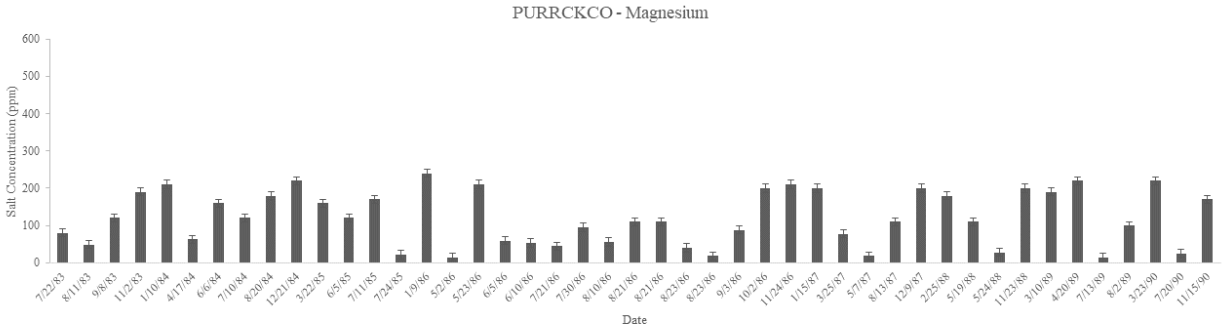
PURRCKCO - Magnesium
Salt Concentration (ppm)
Date

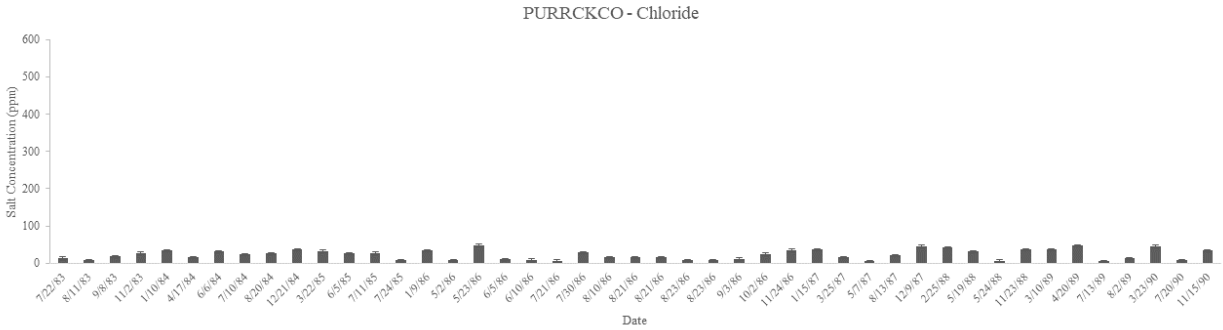
PURRCKCO - Chloride
Salt Concentration (ppm)
Date

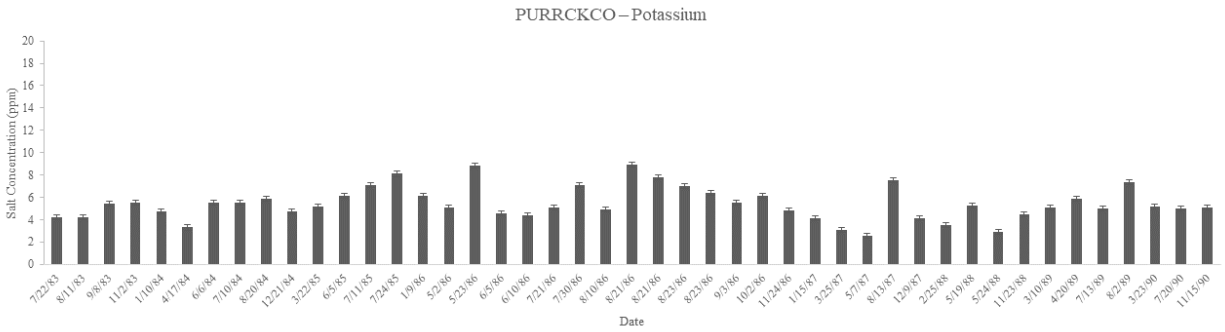
PURRCKCO – Potassium
Salt Concentration (ppm)
20
18
16
14
12
10
8
6
4
2
0
7/22/83
8/11/83
9/8/83
11/2/83
1/10/84
4/17/84
6/6/84
7/10/84
8/20/84
12/21/84
3/22/85
6/5/85
7/11/85
7/24/85
1/9/86
5/2/86
5/23/86
6/5/86
6/10/86
7/21/86
7/30/86
8/10/86
8/21/86
8/21/86
8/23/86
8/23/86
9/3/86
10/2/86
11/24/86
1/15/87
3/25/87
5/7/87
8/13/87
12/9/87
2/25/88
5/19/88
5/24/88
11/23/88
3/10/89
4/20/89
7/13/89
8/2/89
3/23/90
7/20/90
11/15/90
Date

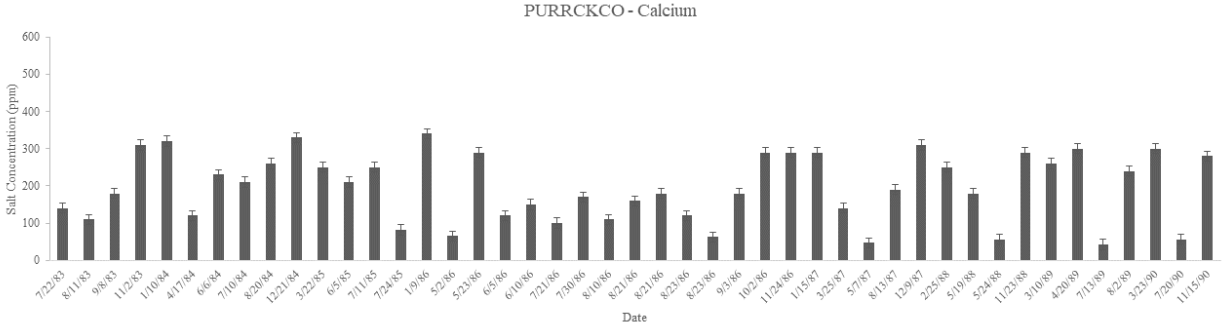
PURRCKCO - Calcium
Salt Concentration (ppm)
600
500
400
300
200
100
0
7/22/83
8/11/83
9/8/83
11/2/83
1/10/84
4/17/84
6/6/84
7/10/84
8/20/84
12/21/84
3/22/85
6/5/85
7/11/85
7/24/85
1/9/86
5/2/86
5/23/86
6/5/86
6/10/86
7/21/86
7/30/86
8/10/86
8/21/86
8/21/86
8/23/86
8/23/86
9/3/86
10/2/86
11/24/86
1/15/87
3/25/87
5/7/87
8/13/87
12/9/87
2/25/88
5/19/88
5/24/88
11/23/88
3/10/89
4/20/89
7/13/89
8/2/89
3/23/90
7/20/90
11/15/90
Date

APPENDIX B: SALT ION CONCENTRATION AND SC GRAPHICAL RELATIONSHIPS

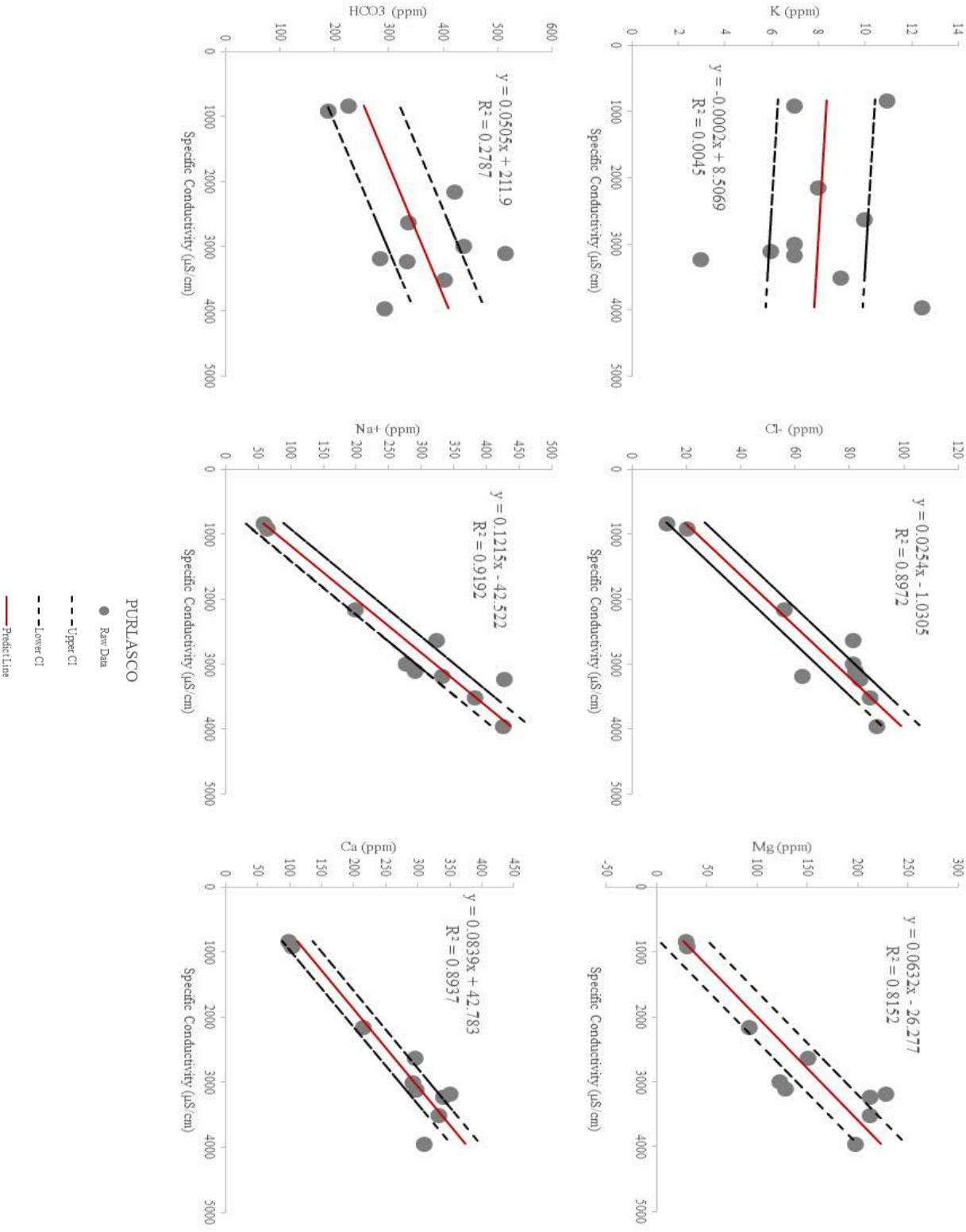

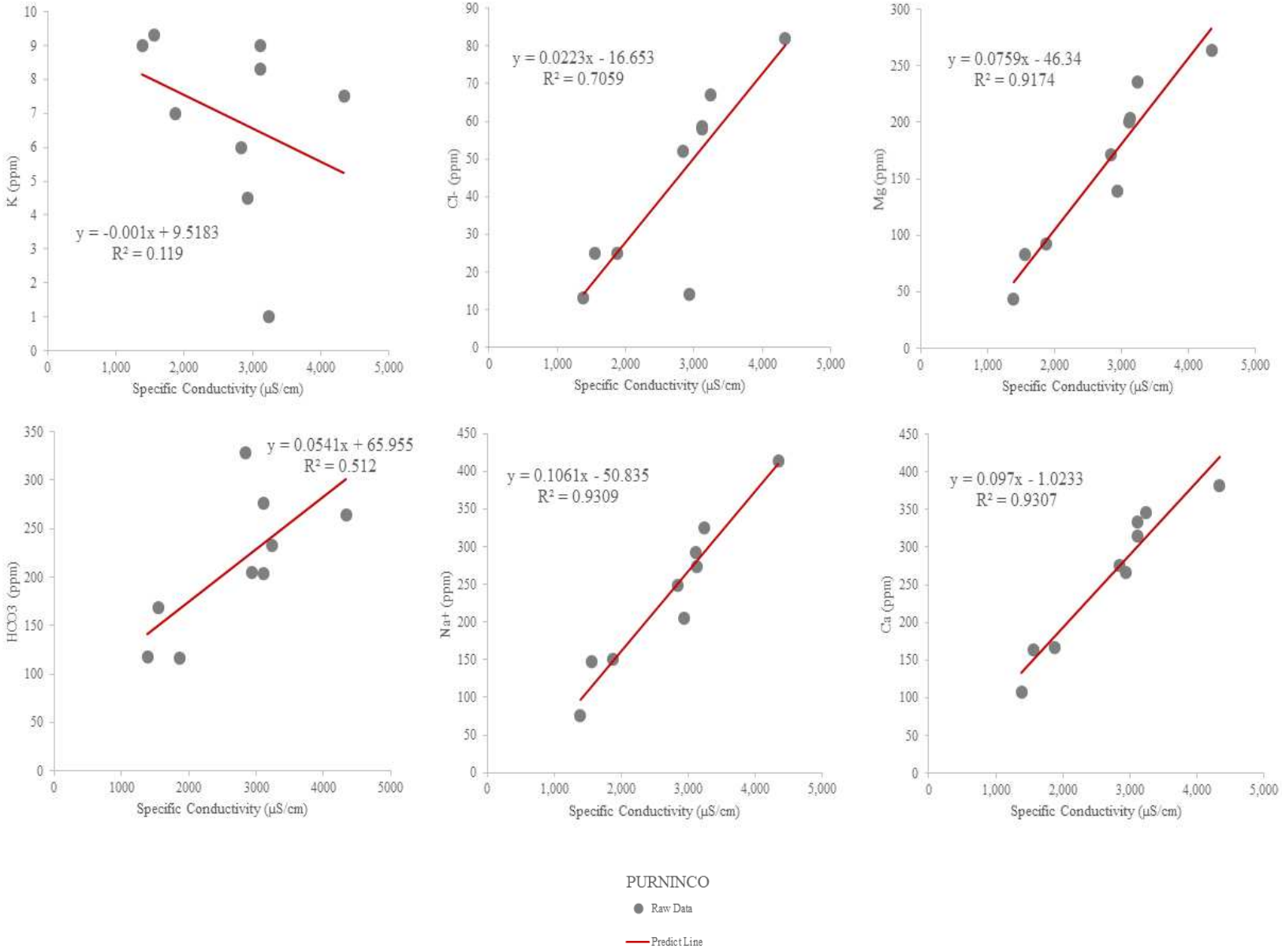
K (ppm)
y = -0.001x + 9.5183
R² = 0.119
Specific Conductivity (µS/cm)
Cl- (ppm)
y = 0.0223x - 16.653
R² = 0.7059
Specific Conductivity (µS/cm)
Mg (ppm)
y = 0.0759x - 46.34
R² = 0.9174
Specific Conductivity (µS/cm)
HCO3 (ppm)
y = 0.0541x + 65.955
R² = 0.512
Specific Conductivity (µS/cm)
Na+ (ppm)
y = 0.1061x - 50.835
R² = 0.9309
Specific Conductivity (µS/cm)
Ca (ppm)
y = 0.097x - 1.0233
R² = 0.9307
Specific Conductivity (µS/cm)
PURNINCO
Raw Data
Predict Line

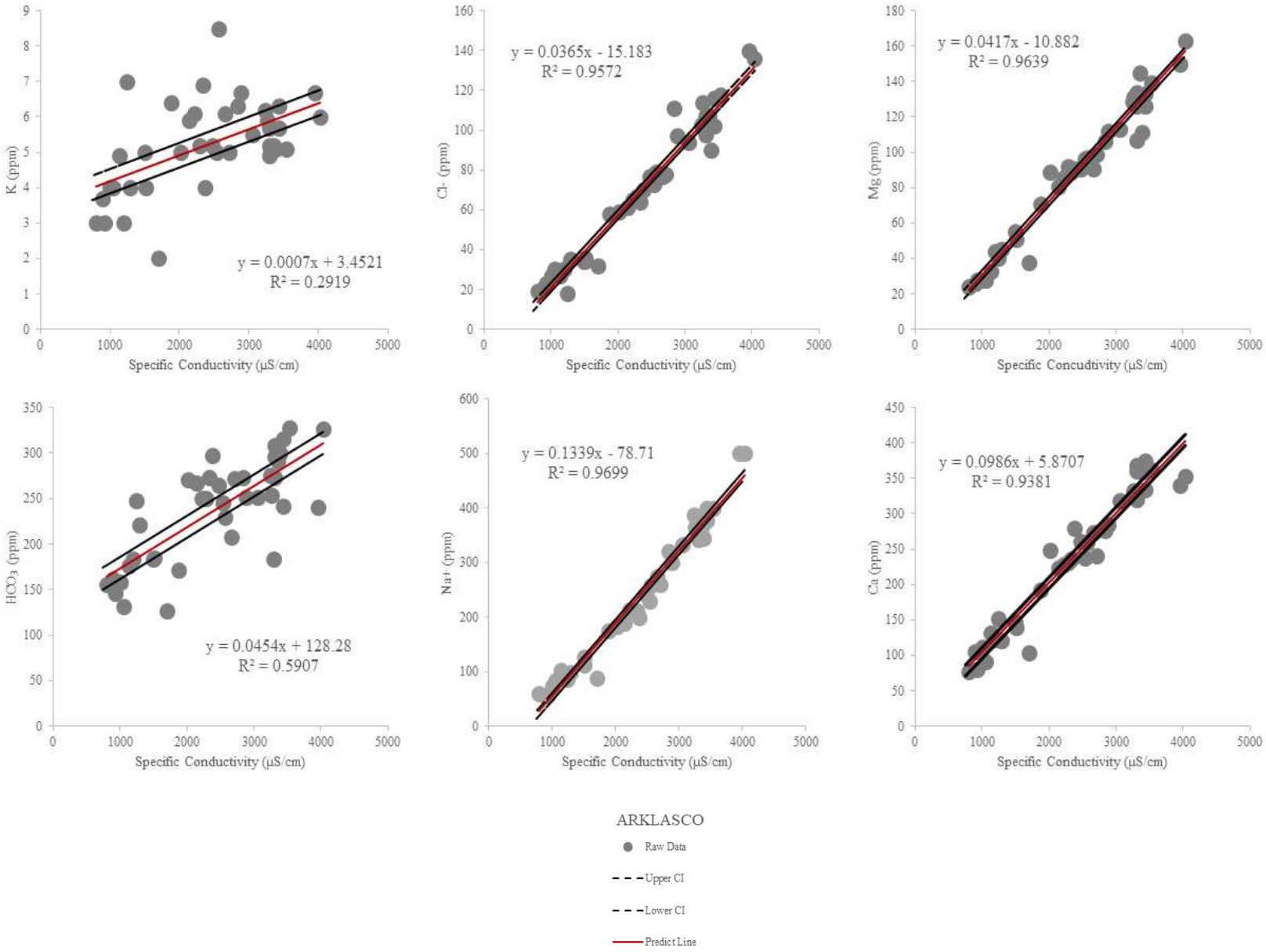
K (ppm)
y = 0.0007x + 3.4521
R² = 0.2919
Specific Conductivity (µS/cm)
Cl- (ppm)
y = 0.0365x - 15.183
R² = 0.9572
Specific Conductivity (µS/cm)
Mg (ppm)
y = 0.0417x - 10.882
R² = 0.9639
Specific Concudtivity (µS/cm)
HCO3 (ppm)
y = 0.0454x + 128.28
R² = 0.5907
Specific Conductivity (µS/cm)
Na+ (ppm)
y = 0.1339x - 78.71
R² = 0.9699
Specific Conductivity (µS/cm)
Ca (ppm)
y = 0.0986x + 5.8707
R² = 0.9381
Specific Conductivity (µS/cm)
ARKLASCO
Raw Data
Upper CI
Lower CI
Predict Line

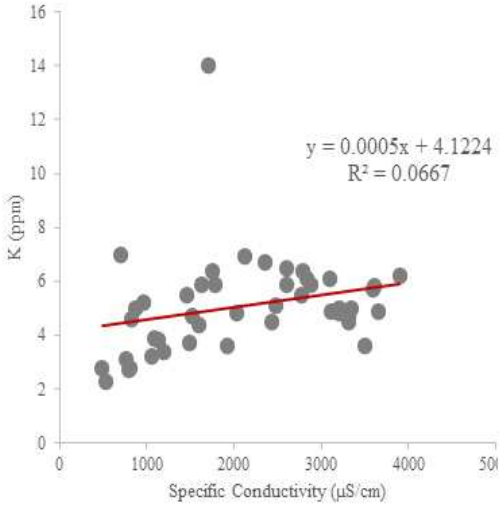

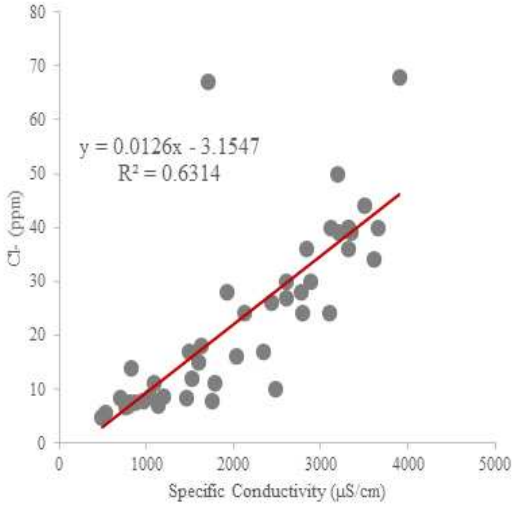

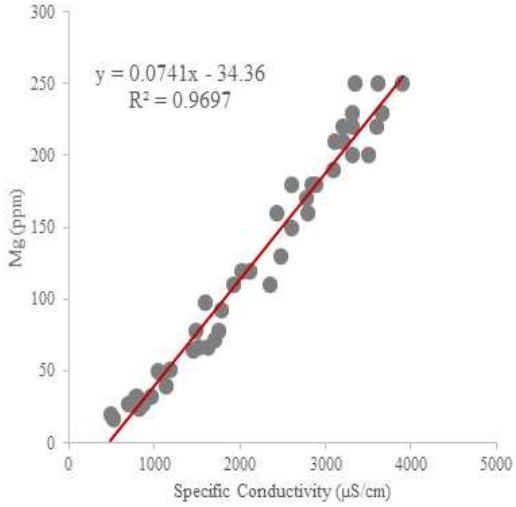

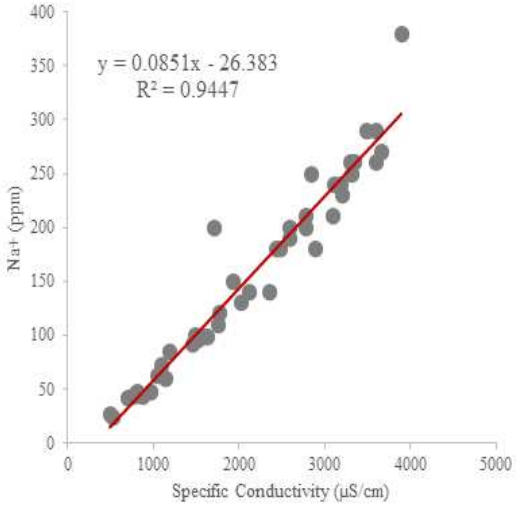

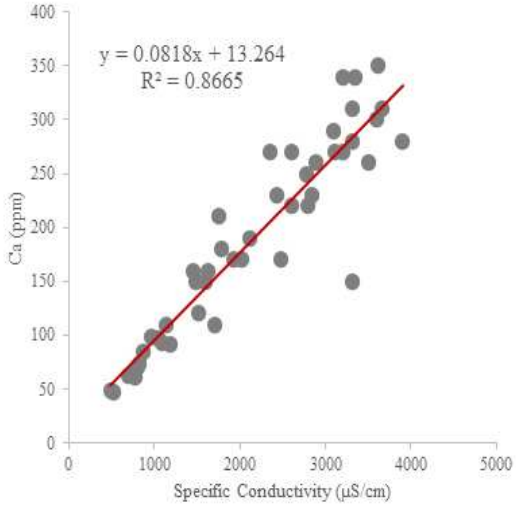

PURTHACO

Raw Data

Predict Line

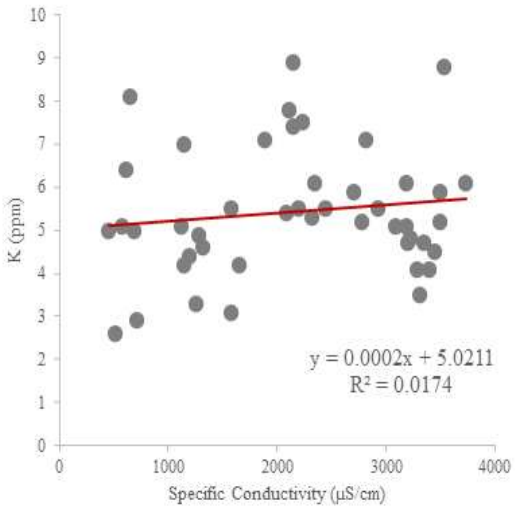
K (ppm)
Specific Conductivity (µS/cm)
y = 0.0002x + 5.0211
R² = 0.0174

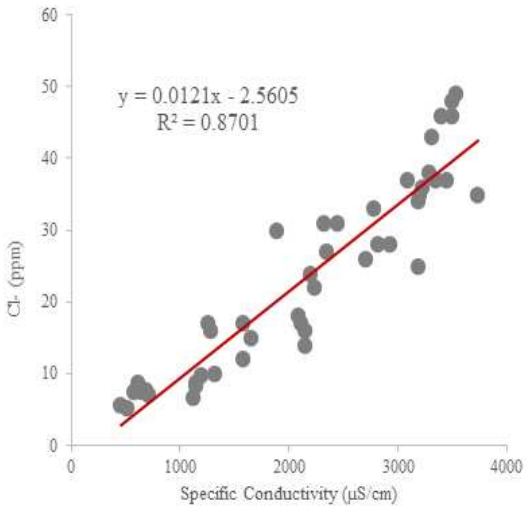
Cl- (ppm)
Specific Conductivity (µS/cm)
y = 0.0121x - 2.5605
R² = 0.8701

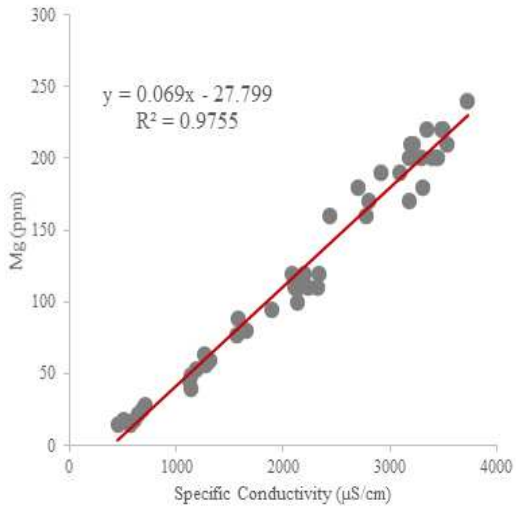
Mg (ppm)
Specific Conductivity (µS/cm)
y = 0.069x - 27.799
R² = 0.9755

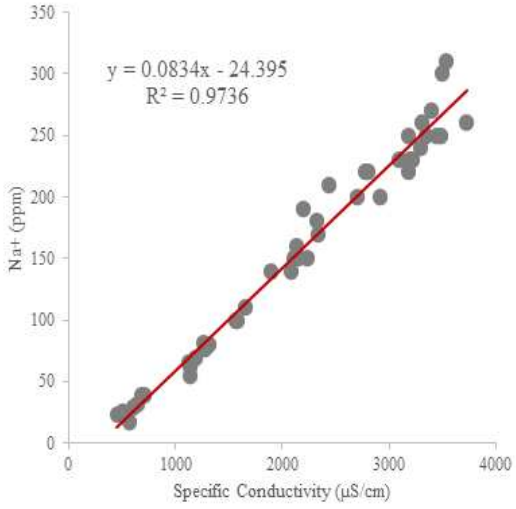
Na+ (ppm)
Specific Conductivity (µS/cm)
y = 0.0834x - 24.395
R² = 0.9736

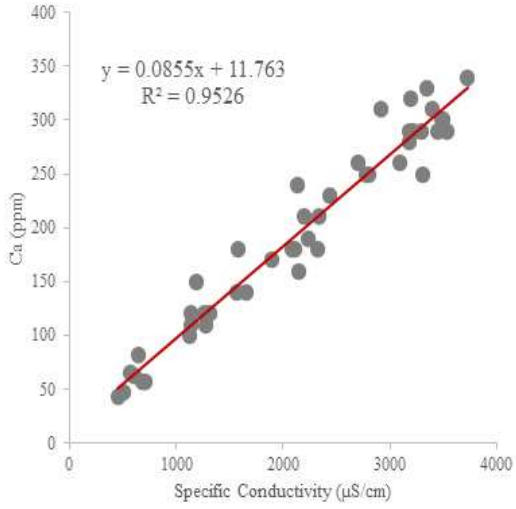
Ca (ppm)
Specific Conductivity (µS/cm)
y = 0.0855x + 11.763
R² = 0.9526


PURCCKCO
Raw Data
Predict Line

APPENDIX C: LIST OF MISSING SPECIFIC CONDUCTIVITY DATA POINTS PER SITE

	PURLASCO		PURNINCO		ARKLASCO		PURTHACO		PURRCKCO	
	1990	2020	1990	2020	1990	2020	1990	2020	1990	2020
1-Jan			X	X				X	X	X
2-Jan			X	X				X	X	X
3-Jan			X	X				X	X	X
4-Jan			X	X				X	X	X
5-Jan			X	X				X	X	X
6-Jan			X	X				X	X	X
7-Jan			X	X				X	X	X
8-Jan			X	X				X	X	X
9-Jan			X	X				X		X
10-Jan			X	X				X		X
11-Jan			X	X				X		X
12-Jan			X	X				X		X
13-Jan			X	X				X		X
14-Jan			X	X				X		X
15-Jan			X	X				X		X
16-Jan			X	X				X		X
17-Jan			X	X				X		X
18-Jan			X	X				X		X
19-Jan			X	X				X		X
20-Jan			X	X				X		X
21-Jan			X	X				X		X
22-Jan			X	X				X		X
23-Jan			X	X				X		X
24-Jan			X	X				X		X
25-Jan			X	X				X		X
26-Jan			X	X				X		X
27-Jan			X	X				X		X
28-Jan			X	X				X		X
29-Jan			X	X				X		X
30-Jan			X	X				X		X
31-Jan			X	X				X		X
1-Feb			X	X				X		X
2-Feb			X	X				X		X
3-Feb			X	X				X		X
4-Feb			X	X				X		X
5-Feb			X	X				X		X
6-Feb			X	X				X		X
7-Feb			X	X				X		X
8-Feb			X	X				X		X
9-Feb			X	X				X		X
10-Feb			X	X	X			X		X
11-Feb			X	X	X			X		X
12-Feb			X	X	X			X		X
13-Feb			X	X				X		X
14-Feb			X	X				X		X
15-Feb			X	X				X		X
16-Feb			X	X				X		X
17-Feb			X	X				X		X
18-Feb			X	X				X		X

19-Feb			X	X				X		X
20-Feb			X	X				X		X
21-Feb			X	X				X		X
22-Feb			X	X				X		X
23-Feb			X	X				X		X
24-Feb			X	X				X		X
25-Feb			X	X				X		X
26-Feb			X	X				X		X
27-Feb			X	X				X		X
28-Feb			X	X				X		X
29-Feb	X		X	X	X		X	X	X	X
1-Mar			X	X				X		X
2-Mar			X	X				X		X
3-Mar			X	X				X		X
4-Mar			X	X				X		X
5-Mar			X	X				X		X
6-Mar			X	X				X		X
7-Mar			X	X				X		X
8-Mar			X	X				X		X
9-Mar			X	X				X		X
10-Mar			X	X				X		X
11-Mar			X	X				X		X
12-Mar			X	X				X		X
13-Mar			X	X				X		X
14-Mar			X	X				X		X
15-Mar			X	X				X		X
16-Mar			X	X				X		X
17-Mar			X	X				X		X
18-Mar			X	X				X		X
19-Mar			X	X				X		X
20-Mar			X	X				X		X
21-Mar			X	X				X		X
22-Mar			X	X				X		X
23-Mar			X	X				X		X
24-Mar			X	X				X		X
25-Mar			X	X				X		X
26-Mar			X	X				X		X
27-Mar			X	X				X		X
28-Mar			X	X				X		X
29-Mar			X	X				X		X
30-Mar			X	X				X		X
31-Mar			X	X				X		X
1-Apr			X	X				X		X
2-Apr			X	X				X		X
3-Apr			X	X				X		X
4-Apr			X	X				X		X
5-Apr			X	X				X		X
6-Apr			X	X				X		X
7-Apr			X	X	X			X		X
8-Apr			X	X	X			X		X
9-Apr			X	X	X			X		X
10-Apr			X	X				X		X
11-Apr			X	X				X		X

12-Apr			X	X				X		X
13-Apr			X	X				X		X
14-Apr			X	X		X		X		X
15-Apr			X	X				X		X
16-Apr			X					X		X
17-Apr			X					X		X
18-Apr			X					X		X
19-Apr			X					X		X
20-Apr			X					X		X
21-Apr			X					X		X
22-Apr			X					X		X
23-Apr			X					X		X
24-Apr			X					X		X
25-Apr			X					X		X
26-Apr			X					X		X
27-Apr			X					X		X
28-Apr			X					X		X
29-Apr			X					X		X
30-Apr			X		X			X		X
1-May			X					X		X
2-May			X					X		X
3-May			X					X		X
4-May			X					X		X
5-May			X					X		X
6-May			X					X		X
7-May			X		X			X		X
8-May			X		X			X		X
9-May			X					X		X
10-May			X					X		X
11-May			X					X		X
12-May			X					X		X
13-May			X					X		X
14-May			X					X		X
15-May			X					X		X
16-May			X					X		X
17-May			X					X		X
18-May			X					X		X
19-May			X			X		X		X
20-May			X			X		X		X
21-May			X					X		X
22-May			X					X		X
23-May			X					X		X
24-May			X					X		X
25-May			X					X		X
26-May			X			X		X		X
27-May			X					X		X
28-May			X		X			X		X
29-May			X		X			X		X
30-May			X					X		X
31-May			X					X		X
1-Jun			X					X		X
2-Jun			X					X		X
3-Jun			X					X		X

4-Jun			X					X		X
5-Jun			X					X		X
6-Jun			X					X		X
7-Jun			X					X		X
8-Jun			X					X		X
9-Jun			X					X		X
10-Jun			X			X		X		X
11-Jun			X			X		X		X
12-Jun			X		X			X		X
13-Jun			X		X			X		X
14-Jun			X					X		X
15-Jun			X					X		X
16-Jun			X					X		X
17-Jun			X					X		X
18-Jun	X		X					X		X
19-Jun	X		X					X		X
20-Jun	X		X			X		X		X
21-Jun			X			X		X		X
22-Jun	X		X			X		X		X
23-Jun	X		X			X		X		X
24-Jun	X		X			X		X		X
25-Jun	X		X					X		X
26-Jun	X		X				X	X		X
27-Jun	X		X				X	X		X
28-Jun	X		X				X	X		X
29-Jun	X		X				X	X		X
30-Jun			X				X	X	X	X
1-Jul			X				X	X	X	X
2-Jul			X				X	X	X	X
3-Jul			X				X	X	X	X
4-Jul			X				X	X	X	X
5-Jul			X					X	X	X
6-Jul			X					X	X	X
7-Jul			X					X	X	X
8-Jul			X					X	X	X
9-Jul			X					X	X	X
10-Jul			X					X	X	X
11-Jul			X					X		X
12-Jul			X					X		X
13-Jul			X					X		X
14-Jul			X					X		X
15-Jul			X					X	X	X
16-Jul			X					X	X	X
17-Jul			X	X				X	X	X
18-Jul			X	X				X	X	X
19-Jul			X	X				X		X
20-Jul			X	X				X		X
21-Jul			X	X				X		X
22-Jul			X	X	X			X		X
23-Jul			X	X	X			X		X
24-Jul			X	X	X			X		X
25-Jul			X	X				X		X
26-Jul			X	X				X		X

27-Jul			X	X				X		X
28-Jul			X	X				X		X
29-Jul			X	X	X			X		X
30-Jul			X	X	X			X		X
31-Jul			X	X	X			X		X
1-Aug			X	X				X	X	X
2-Aug			X	X				X	X	X
3-Aug			X	X				X	X	X
4-Aug			X	X				X		X
5-Aug			X	X				X	X	X
6-Aug			X	X				X	X	X
7-Aug			X	X				X	X	X
8-Aug			X	X				X	X	X
9-Aug			X	X	X			X		X
10-Aug	X		X	X	X			X		X
11-Aug	X		X	X	X			X		X
12-Aug	X		X	X	X			X		X
13-Aug	X		X	X	X			X		X
14-Aug	X		X	X	X			X		X
15-Aug	X		X	X				X		X
16-Aug	X		X	X				X		X
17-Aug	X		X	X				X		X
18-Aug	X		X	X			X	X		X
19-Aug	X		X	X			X	X		X
20-Aug	X		X	X				X		X
21-Aug			X	X				X		X
22-Aug			X	X				X		X
23-Aug			X	X				X		X
24-Aug			X	X				X		X
25-Aug			X	X				X	X	X
26-Aug			X	X				X	X	X
27-Aug			X	X				X	X	X
28-Aug			X	X	X			X	X	X
29-Aug			X	X				X	X	X
30-Aug			X	X				X	X	X
31-Aug			X	X				X	X	X
1-Sep			X	X				X		X
2-Sep			X	X				X		X
3-Sep			X	X				X		X
4-Sep			X	X				X		X
5-Sep			X	X				X		X
6-Sep			X	X				X		X
7-Sep			X	X				X		X
8-Sep			X	X			X	X		X
9-Sep			X	X			X	X		X
10-Sep			X	X				X		X
11-Sep			X	X				X		X
12-Sep	X		X	X				X		X
13-Sep	X		X	X				X		X
14-Sep			X	X				X		X
15-Sep			X	X				X		X
16-Sep			X	X				X		X
17-Sep			X	X				X		X

18-Sep			X	X				X		X
19-Sep			X	X				X		X
20-Sep			X	X				X		X
21-Sep			X	X				X		X
22-Sep			X	X				X		X
23-Sep			X	X				X		X
24-Sep			X	X				X		X
25-Sep			X	X				X		X
26-Sep			X	X				X		X
27-Sep			X	X				X		X
28-Sep			X	X				X		X
29-Sep			X	X				X		X
30-Sep			X	X				X		X
1-Oct			X	X				X		X
2-Oct			X	X				X		X
3-Oct			X	X				X		X
4-Oct			X	X				X		X
5-Oct			X	X				X		X
6-Oct			X	X	X			X		X
7-Oct			X	X	X			X		X
8-Oct			X	X	X			X		X
9-Oct			X	X				X		X
10-Oct	X		X	X				X		X
11-Oct			X	X				X		X
12-Oct			X	X				X		X
13-Oct			X	X				X		X
14-Oct			X	X				X		X
15-Oct			X	X				X		X
16-Oct			X	X				X		X
17-Oct			X	X				X		X
18-Oct			X	X				X		X
19-Oct			X	X				X		X
20-Oct			X	X	X			X		X
21-Oct			X	X	X			X		X
22-Oct			X	X	X			X		X
23-Oct			X	X				X		X
24-Oct			X	X				X		X
25-Oct			X	X				X		X
26-Oct			X	X				X		X
27-Oct			X	X				X		X
28-Oct			X	X				X		X
29-Oct			X	X				X		X
30-Oct			X	X				X		X
31-Oct			X	X				X		X
1-Nov			X	X				X		X
2-Nov			X	X				X	X	X
3-Nov			X	X				X	X	X
4-Nov			X	X				X		X
5-Nov			X	X				X		X
6-Nov			X	X				X		X
7-Nov			X	X	X			X		X
8-Nov			X	X				X		X
9-Nov			X	X				X		X

10-Nov			X	X				X		X
11-Nov			X	X				X		X
12-Nov			X	X				X		X
13-Nov			X	X				X		X
14-Nov			X	X				X		X
15-Nov			X	X				X		X
16-Nov			X	X				X		X
17-Nov			X	X				X		X
18-Nov			X	X				X		X
19-Nov			X	X				X		X
20-Nov			X	X				X		X
21-Nov			X	X				X		X
22-Nov			X	X	X			X		X
23-Nov			X	X				X		X
24-Nov			X	X				X		X
25-Nov			X	X				X		X
26-Nov			X	X				X		X
27-Nov			X	X				X		X
28-Nov			X	X				X		X
29-Nov			X	X				X		X
30-Nov			X	X	X			X		X
1-Dec			X	X				X		X
2-Dec			X	X				X		X
3-Dec			X	X				X		X
4-Dec			X	X				X		X
5-Dec			X	X				X		X
6-Dec			X	X				X		X
7-Dec			X	X				X		X
8-Dec			X	X				X		X
9-Dec			X	X				X		X
10-Dec			X	X				X		X
11-Dec			X	X				X		X
12-Dec			X	X				X		X
13-Dec			X	X				X		X
14-Dec			X	X				X		X
15-Dec			X	X				X		X
16-Dec			X	X		X		X		X
17-Dec			X	X		X		X		X
18-Dec			X	X		X		X		X
19-Dec			X	X		X		X		X
20-Dec			X	X	X			X		X
21-Dec			X	X	X			X		X
22-Dec			X	X	X			X		X
23-Dec			X	X	X			X		X
24-Dec			X	X	X			X		X
25-Dec			X	X	X			X		X
26-Dec			X	X	X			X		X
27-Dec			X	X	X			X		X
28-Dec			X	X	X			X		X
29-Dec			X	X	X			X		X
30-Dec			X	X	X			X		X
31-Dec			X	X	X			X		X